DEPARTMENT OF AEROSPACE ENGINEERING
COLLEGE OF ENGINEERING & TECHNOLOGY
OLD DOMINION UNIVERSITY
NORFOLK, VIRGINIA 23529-0247

RESEARCH RELATED TO MULTI DEGREE OF FREEDOM MAGNETIC SUSPENSIONS

By

Dr. Colin Britcher, Principal Investigator

Progress Report
For the period covering 1/1/97 thru 6/30/97

Prepared for
National Aeronautics and Space Administration
Langley Research Center
Attn.: Joseph Murray, Mail Stop 126
Hampton, Virginia, 23681-0001

Under
Grant NCC-1-248
Nelson Groom, Technical Monitor

August 1997

RESEARCH RELATED TO MULTI DEGREE OF FREEDOM MAGNETIC SUSPENSIONS

by

Yan Yang
B.S. June 1994, Nanjing University of Aeronautics and Astronautics

A Thesis Submitted to the Faculty of
Old Dominion University in Partial Fulfillment of the
Requirement for the Degree of

MASTER OF SCIENCE

ENGINEERING MECHANICS

OLD DOMINION UNIVERSITY
August 1997

Approved by:

Colin P. Britcher (Director)

Brett A. Newman (Member)

Linda L. Vahala (Member)

ABSTRACT

RESEARCH RELATED TO MULTI DEGREE OF FREEDOM MAGNETIC SUSPENSIONS

Yan Yang
Old Dominion University, 1997
Director: Dr. Colin P. Britcher

This thesis covers the activities associated with 1) recommissioning of the 6-inch Magnetic Suspension and Balance System (MSBS) and 2) enhancing the Annular Suspension and Pointing System (ASPS). These activities continue the program of research in the multi degree of freedom magnetic suspension program at Old Dominion University. The 6-inch MSBS is a large gap magnetic suspension system used as a model support and balance system in wind tunnels. The first stage of recommissioning of the 6-inch MSBS for the 6-inch subsonic wind tunnel is performed. Experimental data and computational results for the magnetic field distribution of the MSBS are given and compared with the estimated magnetic field strength. The comparison indicates that the magnet system is still operating as designed. The Electromagnetic Position Sensor used in the 6-inch MSBS is analyzed before its final reinstatement. The ASPS is a small gap magnetic suspension system providing orientation, mechanical isolation and fine pointing of space payloads. The control system of the ASPS is improved by designing a new code to realize real time control over the system. The original Proportional-Derivative controller is upgraded to a Proportional-Integral-Derivative controller. This progress leads to a system which is more stable and robust with less noise. This new controller is generic and can be adapted to the 6-inch MSBS. Finally, future work on these two systems is proposed.

ACKNOWLEDGMENTS

I am very grateful to my advisor Professor Colin P. Britcher, for the opportunity to study here, and for his patience, guidance and encouragement during these two years. I also would like to thank the members of my thesis committee, Professor Brett A. Newman and Professor Linda Vahala, for their input and advice during this work.

Many thanks also go to my parents in China and my friends here, from whom I have gained support and help through all the difficulties.

TABLE OF CONTENTS

Chapter Page

LIST OF TABLES

LIST OF FIGURES

Page

Page

Page

CHAPTER I

INTRODUCTION

I.1 Magnetic Suspension and Levitation

The capability to generate non-contact forces has attracted scientists working in many different fields. Practical magnetic suspension systems first appeared in the early 1950's. Over the last several decades, developments in control theory, innovations in sensing instrumentation, and advancements in digital computer hardware and software technologies have all helped to bring this promising concept to industrial application. Nowadays, magnetic suspensions are used for bearings of gyroscopes, as plasma containers in proposed nuclear fusion electric power generators, as supports for high-speed ground transportation systems, as interference-free model support systems for use with wind tunnels, and many other applications.

Long-term efforts have been made to utilize magnetic suspension concepts in aeronautical and astronautical applications. A series of research projects sponsored by NASA has been conducted since the 1960's [1]. These applications include both small and large gap suspension systems. Small gap magnetic suspension system activities at the NASA Langley Research Center (LaRC) began with the concept of the Annular Momentum Control Device (AMCD) and developed into the Annular Suspension and Pointing System (ASPS), which is designed to provide orientation, mechanical isolation

---

The journal model for this thesis is the *AIAA Journal*.

and fine pointing of space payloads. Large gap magnetic suspension systems have mainly been developed for use in wind tunnel model support systems. The research at LaRC began with the development of a single degree of freedom demonstration system. Since then, several Magnetic Suspension and Balance Systems (MSBS) such as the 6-inch and 13-inch models have been developed under various grants and contracts. Future requirements for systems of this type are associated with test activities such as elimination of aerodynamic support interference in wind tunnel testing, gravity simulation of store jettison testing, etc. [2].

I.2 General Description of the 6-Inch MSBS and ASPS

Two major magnetic suspension systems are available at Old Dominion University (ODU): the 6-inch Magnetic Suspension and Balance System and the Annular Suspension and Pointing System. These two systems will now be described briefly.

In aerodynamic wind tunnel tests, models are normally mounted on mechanical struts or stings. Support interference with wind tunnel models continues to be a serious problem. For example, it is virtually impossible to make steady-state interference-free measurements of wake flow fields without a magnetic support system. MSBS implies systems that can both suspend a model ("suspension") and also measure the forces and moments acting on the model ("balance"). This approach avoids the need for any mechanical support of the model.

The 6-inch MSBS, shown in Figure I.1, is a relatively sophisticated and successful design. The magnetic field is created by electromagnets located around the test section. Measurement of electrical current flowing in each of the electromagnets can be used to

determine the forces and moments acting on the suspended model. These forces include gravitational, aerodynamic, and inertial loads. The position of the suspended body is inherently unstable [3]. Therefore, a closed-loop control system, which includes a position sensing system and feedback logic to adjust the magnetic fields, are applied to stabilize the position of the body. Further details of the 6-inch MSBS are given in Chapter III.

The Annular Suspension and Pointing System, shown in Figure I.2, is a precision payload pointing system designed for the space shuttle. This system consists of several sub-systems. The main sub-system is the Vernier Pointing Assembly (VPA), which utilizes magnetic suspension to provide non-contacting isolation and vernier positioning of the payload. Five Magnetic Bearing Assemblies (MBA) provide control over three translational movements and two transverse rotational movements. Roll control is achieved with a segmented A.C. induction motor. Each magnetic bearing assembly is equipped with two proximity sensors which measure the position and orientation of the rotor. The signals are then fed back to the controller to produce the control signal which will be given to the actuators. Further details of the ASPS are given in Chapter V.

I.3 Hardware History and Current Status

Work on the 6-inch Magnetic Suspension and Balance System was originally supported by the Full Scale Research Division of the NASA Langley Research Station (now Langley Research Center), Virginia, beginning in 1954, and also by the Aerospace Research Laboratories, Wright-Patterson Air Force Base, Ohio, beginning in1957 [4]. The prototype of the 6-inch MSBS was originally designed by Timothy Stephens [5]. Milan Vlajinac [6] designed the subsonic wind tunnel which was compatible with the magnetic

balance test section in 1966. Construction was completed in 1969 at the Massachusetts Institute of Technology (MIT) under contract from NASA Langley Research Center, and the unit was used at MIT for research until 1982 [7]. The 6-inch MSBS was relocated to NASA LaRC in 1984 and resided there for another several years. During these years, the magnetic suspension configuration, as originally conceived, did not prove to be completely satisfactory in terms of convenience in operation and adaptability to a variety of models and test techniques. In September 1989, a program began to restore the system to fully operational status with the wind tunnel. The basic ideas behind the system remained unchanged, but the designs of the various subsystems were refined. The improvements included Electromagnetic Position Sensor (EPS) electronics, control system rewiring and new water-cooled ballast resistors. Reliability problems still existed, and only limited testing was carried out [8]. In 1994, the system was transferred to the Aerospace Engineering Department at ODU and is in the first stage of recommissioning and refurbishing.

The history of the ASPS is somewhat similar. The prototype was developed for NASA LaRC by Honeywell Satellite Systems in the early 1970's and delivered to NASA LaRC in 1983. However, the system was never assembled at LaRC due to a shift in priorities [9]. The device was loaned to ODU in late 1992 in a disassembled condition. Daniel J. Neff [10, 11] carried out the recommissioning. The control electronics rack was updated and software was developed to implement A/D and D/A conversions. A Proportional-Derivative (PD) controller was written to suspend the Vernier Pointing Assembly against gravity in five degrees of freedom.

I.4 Project Goals

The goal of this project is to continue development of various areas of technology in support of the magnetic suspension research program at ODU. The long term focus of this research is the recommissioning of the 6-inch MSBS system. The first goal involves testing the field properties of the MSBS coils and checking against original specifications to verify if operation is as designed, and to permit examination of new hardware configurations. The next goal is to analyze the design of the EPS and eventually bring it back on-line. Finally, a new digital control system must be developed to replace the original analog system. Since the 6-inch system is not operational, the control system of the ASPS has been refined and made somewhat generic through improved software and the addition of some hardware. It is expected that this improved controller will later be modified and applied to the MSBS. The long term goal is to restore the 6-inch MSBS and associated wind tunnel to full operation with a digital controller and a revised magnetic configuration.

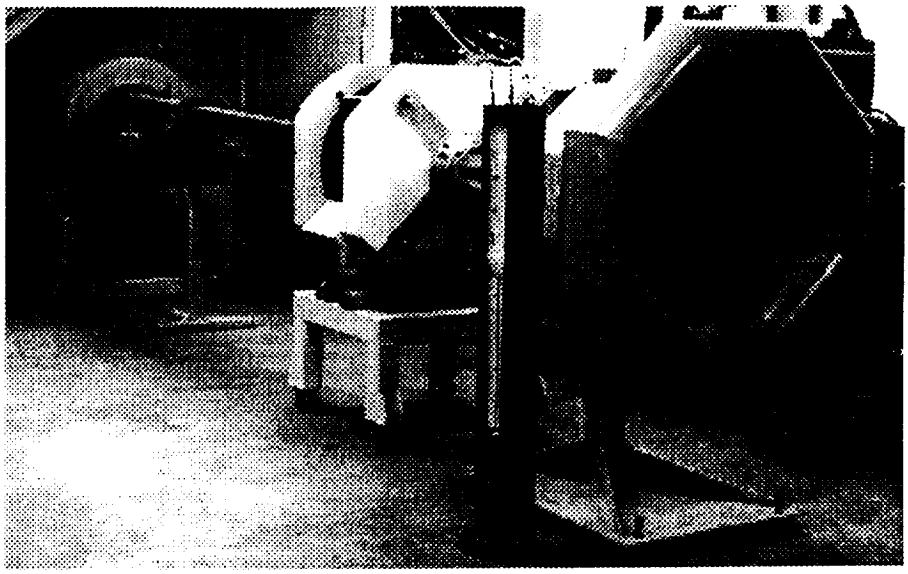

Figure I.1 The 6-Inch MSBS System

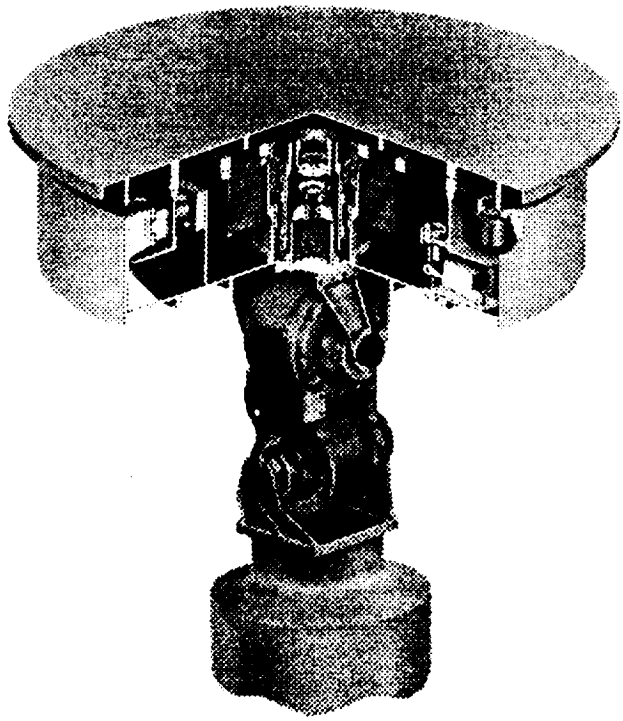

Figure I.2 The ASPS System

CHAPTER II

GENERAL SURVEY

For either a magnetic suspension or a magnetic balance system, an important requirement is determination of the magnitude and direction of the unknown aerodynamic forces and torques by solving for them either implicitly or explicitly. In this chapter, some basic principles from classical magnetostatics are first presented. The equations for the generation of magnetic torques and forces, as well as some special cases, are given. The discussion is then extended to the realization of a generalized system. The analysis for a specific multi degree of freedom system, the ODU 6-inch MSBS, is given later in Chapter IV.

II.1 Basic Magnetostatics

A magnetic field **H** can be generated within a three-dimensional region by some external current I_{ext}. Any ferromagnetic body can be magnetized when immersed in this magnetic field. The magnetization **M** describes the distribution of the magnetic field inside the immersed body. The magnitude and direction of **M** depend upon the shape of the body in comparison to the external magnetic field, the history and the strength of the magnetic field where the body has been immersed, and the constitutive properties of the material from which the body was fabricated. The relationship between the magnetization **M** and the total magnetic flux density **B** ($\mathbf{B} = \mu\mathbf{H}$) of the field around the body may be described as [12]:

$$\mathbf{B} = \mu_0\mathbf{M}+(\mu-\mu_0)[\mathbf{D}]\mathbf{M} = (\mu_0[\mathbf{I}]+(\mu-\mu_0)[\mathbf{D}])\mathbf{M} \qquad \text{(II-1)}$$

$$\mu = \mu_0(1+\chi) \qquad \text{(II-2)}$$

where [**D**] is the demagnetization factor determined by the body geometry, μ_0 is the permeability of free space, μ is the permeability of the actual medium (assuming $\mu_{air} = \mu_0$), and χ is the magnetic susceptibility.

Different materials have different abilities to generate internal magnetic fields. Diamagnetic materials have negative susceptibility and appear to exclude the external magnetic field, while paramagnetic materials have positive susceptibility and appear to "attract" the field. For ferromagnetics, there is a highly non-linear relationship between the induced magnetic field and the applied magnetic field, and the induced field has hysteresis in the sense that the field is non-zero after the applied field is reduced to zero.

For a typical ferromagnetic body $\mu >> \mu_0$ and $\mu D_{ij} >> 1$, therefore Equation (II-1) can be written as:

$$[\mathbf{D}]\mathbf{M} \approx \mathbf{H} \qquad \text{(II-3)}$$

This approximation implies that the magnetization level in the body is essentially independent of μ in the linear range of magnetization. Therefore, **M** is only determined by the material and shape of the body placed inside the field **H** where

$$\mathbf{M} = [\mathbf{D}]^{-1}\mathbf{H}$$

or

$$\begin{bmatrix} M_X \\ M_Y \\ M_Z \end{bmatrix} = \begin{bmatrix} D_{XX} & D_{XY} & D_{XZ} \\ D_{YX} & D_{YY} & D_{YZ} \\ D_{ZX} & D_{ZY} & D_{ZZ} \end{bmatrix}^{-1} \begin{bmatrix} H_X \\ H_Y \\ H_Z \end{bmatrix} \qquad \text{(II-4)}$$

In the application to wind tunnel systems, two sets of axes are in common use. One is the balance axes X, Y, and Z, the other is the principal magnetic axes a, b, and c of a non-axisymmetric body. These two sets of axes are presented in Figure II.1. Notice

these two sets of axes are related by Euler angles of ψ (yaw angle), θ (pitch angle) and φ (roll angle). A transformation matrix [R] ($[\mathbf{a\ b\ c}]^T = [\mathbf{R}][\mathbf{X\ Y\ Z}]^T$) can be defined by these three angles. The development of [R] is given in Appendix A.

In the body coordinates a, b, and c, Equation (II-4) becomes:

$$\begin{bmatrix} M_a \\ M_b \\ M_c \end{bmatrix} = \begin{bmatrix} \frac{1}{D_a} & 0 & 0 \\ 0 & \frac{1}{D_b} & 0 \\ 0 & 0 & \frac{1}{D_c} \end{bmatrix} \begin{bmatrix} H_a \\ H_b \\ H_c \end{bmatrix} \tag{II-5}$$

The demagnetizing factors are related to each other as follows [12]:

$$D_a+D_b+D_c = 1 \tag{II-6}$$

By using wind tunnel coordinates, Equation (II-4) becomes:

$$\begin{bmatrix} M_X \\ M_Y \\ M_Z \end{bmatrix} = [\mathbf{D}]_{(XYZ)}^{-1} \begin{bmatrix} H_X \\ H_Y \\ H_Z \end{bmatrix} \tag{II-7}$$

$$= \left[[\mathbf{R}]^{-1}[\mathbf{D}]_{(abc)}[\mathbf{R}]\right]^{-1} \begin{bmatrix} H_X \\ H_Y \\ H_Z \end{bmatrix}$$

$$= \left[[\mathbf{R}]^{-1}[\mathbf{D}]_{(abc)}^{-1}[\mathbf{R}]\right] \begin{bmatrix} H_X \\ H_Y \\ H_Z \end{bmatrix}$$

$$= [\mathbf{R}]^{-1} \begin{bmatrix} \frac{1}{D_a} & 0 & 0 \\ 0 & \frac{1}{D_b} & 0 \\ 0 & 0 & \frac{1}{D_c} \end{bmatrix} [\mathbf{R}] \begin{bmatrix} H_X \\ H_Y \\ H_Z \end{bmatrix} \tag{II-8}$$

II.2 Force and Torque

When immersed in a uniform magnetic field, an unconstrained magnetized body will experience a torque which turns the body to align its magnetization axis with the direction of the applied field. This behavior is known as the *compass needle phenomenon.* In reverse, a torque can be generated by rotating the body away from its equilibrium position at a certain angle. The torque can be represented as [12]:

$$\mathbf{T} = V\mathbf{M} \times \mathbf{B} \tag{II-9}$$

for a uniform and steady flux density **B**, or

$$\mathbf{T} = \int \mathbf{M} \times \mathbf{B}\, dV \tag{II-10}$$

for a non-uniform steady flux density **B**. Here V is the volume of the levitated body.

Some special cases are discussed when only uniform **B** is involved [5].

Case a. **M** is due to a permanent magnet and $\mathbf{M} = M_a \hat{\mathbf{i}}$.

$$\mathbf{M} \times \mathbf{B} = \begin{bmatrix} M_b B_c - M_c B_b \\ M_c B_a - M_a B_c \\ M_a B_b - M_b B_a \end{bmatrix} = \begin{bmatrix} 0 \\ -M_a B_c \\ M_a B_b \end{bmatrix} \tag{II-11}$$

Case b. An axisymmetric body is magnetized in the linear range along the axis of symmetry. Therefore, $D_b = D_c = D_t = (1-D_a)/2$, where the subscript t indicates the transverse direction.

$$\mathbf{M} = [\mathbf{D}]^{-1}\mathbf{H} = \begin{bmatrix} \frac{H_a}{D_a} \\ \frac{H_b}{D_t} \\ \frac{H_c}{D_t} \end{bmatrix} \tag{II-13}$$

$$\mathbf{M}\times\mathbf{B}=\begin{bmatrix}\hat{\mathbf{i}} & \hat{\mathbf{j}} & \hat{\mathbf{k}}\\ \dfrac{H_a}{D_a} & \dfrac{H_b}{D_t} & \dfrac{H_c}{D_t}\\ \mu H_a & \mu H_b & \mu H_c\end{bmatrix}=\begin{bmatrix}0\\ \dfrac{H_cB_a}{D_t}-\dfrac{H_aB_c}{D_a}\\ \dfrac{H_aB_b}{D_a}-\dfrac{H_bB_a}{D_t}\end{bmatrix} \tag{II-14}$$

Case c. The body has equal demagnetizing factors (a spherical shape) and hysteresis effects are negligible.

$$D_a = D_b = D_c = 1/3 = D$$

$$\mathbf{M}=[\mathbf{D}]^{-1}\mathbf{H}=\begin{bmatrix}\dfrac{H_a}{D}\\ \dfrac{H_b}{D}\\ \dfrac{H_c}{D}\end{bmatrix}=\frac{1}{D}\mathbf{H} \tag{II-15}$$

$$\mathbf{M}\times\mathbf{B}=\frac{\mu}{D}\mathbf{H}\times\mathbf{H}=0 \tag{II-16}$$

Case d. Applied field is parallel to any of the principal magnetic axes. $\mathbf{H} = H_a\,\hat{\mathbf{i}}$ and

$$\mathbf{M}=[\mathbf{D}]^{-1}\mathbf{H}=H_a/D_a\,\hat{\mathbf{i}}$$

$$\mathbf{M}\times\mathbf{B}=\begin{bmatrix}\hat{\mathbf{i}} & \hat{\mathbf{j}} & \hat{\mathbf{k}}\\ \dfrac{H_a}{D_a} & 0 & 0\\ \mu H_a & 0 & 0\end{bmatrix}=0 \tag{II-17}$$

In cases **a** and **b** only pitching and yawing moment can be generated ($T_a = 0$). In cases **c** and **d**, torque can not be generated along any axis ($\mathbf{T} = 0$).

The generation of rolling moment has always been difficult in wind tunnel magnetic suspension systems. Stephens [12, 13] suggests three concepts of roll moment generation: a) Interaction between a transverse or non-symmetrical model magnetization and

transverse D.C. field components, b) Interaction between a controlled single phase transverse A.C. field with a model supporting a conduction plane or loop, which perhaps can be located inside the wing area, and c) Interaction between a rotation 2-phase transverse A.C. field and a copper plated or other conducting model.

The only way to generate a net force on a magnetized body in steady fields is by applying a non-uniform **B**. In a Cartesian coordinate system [12],

$$\mathbf{F} = \int (\mathbf{M} \bullet \nabla)\mathbf{B}\, dV \qquad \text{(for magnetized body)} \qquad \text{(II-18)}$$

$$\mathbf{F} = V\mathbf{M} \bullet \nabla\mathbf{B} \qquad \text{(for permanent magnet)} \qquad \text{(II-19)}$$

Notice that because $\nabla \times \mathbf{B} = 0$ (Maxwell's Equations),

$$\mathbf{F} = \begin{bmatrix} M_X \frac{\partial B_X}{\partial x} + M_Y \frac{\partial B_X}{\partial y} + M_Z \frac{\partial B_X}{\partial z} \\ M_X \frac{\partial B_Y}{\partial x} + M_Y \frac{\partial B_Y}{\partial y} + M_Z \frac{\partial B_Y}{\partial z} \\ M_X \frac{\partial B_Z}{\partial x} + M_Y \frac{\partial B_Z}{\partial y} + M_Z \frac{\partial B_Z}{\partial z} \end{bmatrix}$$

$$= \begin{bmatrix} M_X \frac{\partial B_X}{\partial x} + M_Y \frac{\partial B_Y}{\partial x} + M_Z \frac{\partial B_Z}{\partial x} \\ M_X \frac{\partial B_X}{\partial y} + M_Y \frac{\partial B_Y}{\partial y} + M_Z \frac{\partial B_Z}{\partial y} \\ M_X \frac{\partial B_X}{\partial z} + M_Y \frac{\partial B_Y}{\partial z} + M_Z \frac{\partial B_Z}{\partial z} \end{bmatrix} \qquad \text{(II-20)}$$

If magnetization only exists along the X direction, which is also the body's axis of symmetry, the force equation can be simplified and forces can be controlled independently by adjustment of the gradient of **B**:

$$\mathbf{F} = \begin{bmatrix} M_x \dfrac{\partial B_x}{\partial x} \\ M_x \dfrac{\partial B_x}{\partial y} \\ M_x \dfrac{\partial B_x}{\partial z} \end{bmatrix} \qquad \text{(II-21)}$$

II.3 System Analysis

In general, forces and moments will be generated on the model. Therefore, in a real system, application of the above concepts relies upon the ability to independently control and compensate the individual force and torque components. A successful system not only includes features such as a source of magnetization and a source of field gradients, but also needs several subsystems to complete the suspension task. These subsystems include power supplies, a cooling system, and a sensing and control system to maintain the stability of the suspended object and overcome couplings among multiple degrees of freedom. The more degrees of freedom the system has, the more complicated the problem becomes. In this section, force and torque generation, and the corresponding control law for a one degree of freedom system analysis, is given first as a microcosm of a complete system. General descriptions of sensing units, power supplies and cooling systems for multi degree of freedom systems are also given.

II.3.1 Force and Torque

The one degree of freedom system to be discussed consists of a single N-turn circular coil of radius a which is shown in Figure II.2. The magnetic field on axis is given by

$$H_z = \frac{NIa^2}{4\pi(z^2+a^2)^{3/2}} \int_0^{2\pi} d\theta = \frac{NIa^2}{2(z^2+a^2)^{3/2}} = \frac{H_0}{(z^2/a^2+1)^{3/2}} \qquad \text{(II-22)}$$

where H_0=NI/2a

$$\frac{\partial H_Z}{\partial z} = -\frac{3z}{a^2}\frac{H_0}{(1+z^2/a^2)^{5/2}} \tag{II-23}$$

$$\begin{aligned} F_Z &= \int M_Z \frac{\partial B_Z}{\partial z} dV = \int \mu M_Z \frac{\partial H_Z}{\partial z} dV \\ &= -\int \frac{3\mu z}{a^2}\frac{M_Z H_0}{(1+z^2/a^2)^{5/2}} dV \end{aligned} \tag{II-24}$$

If M_Z is generated by a permanent magnet, it can be assumed to be a constant. Therefore

$$F_Z = -\frac{3\mu M_Z V}{a^2}\frac{zH_0}{(1+z^2/a^2)^{5/2}} \tag{II-25}$$

is zero at $z = 0$ and is maximum at $z = \frac{1}{5}a$. If M_Z is generated by magnetizing a ferromagnetic material in the linear range, then $M_Z = H_Z/D$, where $D = D_a = D_b = D_c = 1/3$. Hence, the force component is given by:

$$\begin{aligned} F_Z &= \int \mathbf{M} \bullet \nabla B_Z dV = \int \mu \frac{H_Z}{D}\frac{\partial B_Z}{\partial z} dV \\ &= -(H_0)^2 \left(\frac{3\mu}{aD}\right)\frac{z}{a}\frac{V}{(1+z^2/a^2)^4} \end{aligned} \tag{II-26}$$

is zero at $z = 0$ and is maximum at $z = \frac{1}{7}a$.

II.3.2 Control Law

To study the possibility of achieving a stable system, it is necessary to study the motion of the sphere from Newton's second law:

$$\ddot{z} = g + F_M / m \tag{II-27}$$

z_0 is defined as the equilibrium position when $v = \dot{z} = 0$, $\ddot{z} = 0$ and $mg = -F_0$.

The control law requires that F increase when the sphere falls and vice versa. A Proportional-Derivative controller is defined by:

$$H = H(z,v) = H_0 + K_1 Z + K_2 \dot{Z} \tag{II-28}$$

Notice that in Equation (II-28), Z (= z-z_0) is the displacement from the equilibrium point and $\dot{Z}$ is the time derivative of Z which is equal to the velocity.

$$m\ddot{Z} = -F_Z + F_M = \Delta F \tag{II-29}$$

Substituting (II-25) into the Equation (II-29),

$$dF = (-\frac{3\mu M_Z V}{a^2})(d\frac{zH}{(1+z^2/a^2)^{5/2}})$$

$$= (-\frac{3\mu M_Z V}{a^2})[(H_0)(d\frac{z}{(1+z^2/a^2)^{5/2}}) + (\frac{z}{(1+z^2/a^2)^{5/2}})(dH)]$$

and hence

$$\ddot{Z} = (-\frac{3\mu M_Z V}{ma^2})[H_0 \frac{1+\frac{z_0^2}{a^2}-\frac{5z_0^2}{a^2}}{(1+z_0^2/a^2)^{7/2}}(z-z_0) + (\frac{z}{(1+z^2/a^2)^{5/2}})(H-H_0)]$$

$$= (-\frac{3\mu M_Z V}{ma^2})[H_0 Z \frac{1-\frac{4z_0^2}{a^2}}{(1+z_0^2/a^2)^{7/2}} + (\frac{z}{(1+z^2/a^2)^{5/2}})(K_1 Z + K_2 \dot{Z})]$$

Therefore, the equation of motion for the system can be written as

$$\begin{bmatrix}\dot{Z}\\ \ddot{Z}\end{bmatrix} = \begin{bmatrix}0 & 1\\ \frac{L_2 - K_1 L_1}{m} & -\frac{L_1 K_2}{m}\end{bmatrix}\begin{bmatrix}Z\\ \dot{Z}\end{bmatrix} \tag{II-30}$$

where $L_1 = kz_0$,

$$L_2 = kH_0(\frac{\frac{5z_0^2}{a^2}}{1+z^2/a^2} - 1),$$

$$k = \frac{3}{a^2}\frac{\mu M_Z V}{(1+z_0^2/a^2)^{5/2}}$$

The system dynamics are uniquely determined by the eigenvalues of the matrix on the right-hand side of Equation (II-30).

$$\ddot{Z} + \frac{L_1 K_2}{m}\dot{Z} + \frac{K_1 L_1 - L_2}{m} Z = 0 \qquad \text{(II-31)}$$

The natural frequency is then

$$\omega_n = \sqrt{\frac{K_1 L_1 - L_2}{m}} \qquad \text{(II-32)}$$

and the damping factor is

$$\zeta = \frac{K_2 L_1}{2}\sqrt{\frac{1}{m(K_1 L_1 - L_2)}} \qquad \text{(II-33)}$$

The control law given by Equation (II-28) is adequate for a pure suspension system, but not for the case where a drag load is applied. With a drag load, Equation (II-31) becomes:

$$\ddot{Z} = -\frac{L_1 K_2}{m}\dot{Z} + \frac{L_2 - K_1 L_1}{m} Z + \frac{D}{m} \qquad \text{(II-34)}$$

where $Z_0' = -\dfrac{D}{L_2 - K_1 L_1}$ at $\dot{Z} = \ddot{Z} = 0$.

This new equilibrium position is determined by the magnitude of drag, and the steady state error caused by this additional force cannot be compensated for by using a PD controller. To eliminate this unfavorable displacement and hold the model at a fixed position, the control law is modified by adding a new state variable u which is defined as $u = \int Z dt$ to get a Proportional-Integral-Derivative controller [12] such that

$$\begin{bmatrix} \dot{u} \\ \ddot{u} \\ \dddot{u} \end{bmatrix} = \begin{bmatrix} 0 & 1 & 0 \\ 0 & 0 & 1 \\ -\frac{K_3'}{m} & \frac{L_2'-L_1'K_1'}{m} & -\frac{K_2'L_1'}{m} \end{bmatrix} \begin{bmatrix} u \\ \dot{u} \\ \ddot{u} \end{bmatrix} \qquad \text{(II-35)}$$

II.3.3 Position Sensor

To use an automatic control system, position sensing equipment is necessary. The desired characteristics for a position sensing system are [12]:

(a) No mechanical contact with the body exists.

(b) Translational displacements of the model parallel to the orthogonal wind tunnel axes will be transformed into three independent high-level electrical signals proportional to the translational displacements over a suitable range.

(c) Angular displacements of the model about the wind tunnel axes will be transformed into three or more independent, high-level electrical signals proportional to or strong functions of the angular displacements, over a suitable range.

(d) Resolution, repeatability, and frequency response must be compatible with desired accuracy of static and dynamic wind tunnel results.

(e) The system must be easily adaptable to a broad range of model geometries.

(f) The system must be compact, and must not interfere with access to the test section or prevent visual contact with the model.

(g) The system must operate without interference from the magnetic fields used to support the model.

Two methods have been applied to detect the model positions. One is optical sensing, another is electromagnetic position sensing. Optical systems meet most of the

above requirements and are dominant at the present time. A basic system, shown in Figure II.3, is needed for each degree of freedom being controlled. The large beam system [12] permits the model to be controlled over a large distance. This system is shown in Figure II.4. The use of triangular mirrors can double the sensitivity of the system.

The Electromagnetic Position Sensor (EPS) is believed to have low sensitivity due to the large air gap and relatively small model size. However, a well-designed, compact EPS system, of which only one exists so far, has been demonstrated. The advantage of the EPS is its capability to accommodate a wide range of geometry with minor adjustment. The system is based upon differential transformer action. The idea is that in an A.C. magnetic field, the model's displacement changes the coupling between excitation windings and secondary coils. This signal can be picked up, demodulated and decoupled to resolve the model's movement. The details of the hardware arrangement and analysis of this system are discussed in Chapter III.

II.2.4 Power and Cooling

The power supplies are usually the most expensive component of the entire magnetic suspension and balance system. Also, many of the reliability problems and performance limitations are directly related to the power supply system. A fast response is required which means the power unit must have the ability to absorb the regenerated energy when inverting the output. Safety and reliability are also considered to be of prime importance. If using an EPS, there is an additional task of minimizing high-frequency noise to prevent interferences between two magnetic fields. Two passive filter configurations are

shown in Figure II.5. These low-pass or band-pass filters can be connected after the power supplies to limit the output frequency.

The suspension coils must be designed to handle large ohmic power dissipation. Three schemes have been used for heat removal purposes. They are an air-cooled system with fans added, a conduction cooling system (shown in Figure II.6), and a liquid cooling system. The liquid used in a liquid cooling system could be either water or oil. The liquid usually runs in a closed loop to minimize the requirement for filtering, dechlorination and other liquid treatment. If water is used, it must be demineralized and deaerated. Some attached subsystems such as pressure, temperature and flow indicators are needed to protect the system from overheating. A complete description of a water cooling system used in the 6-inch MSBS is introduced in Chapter III.

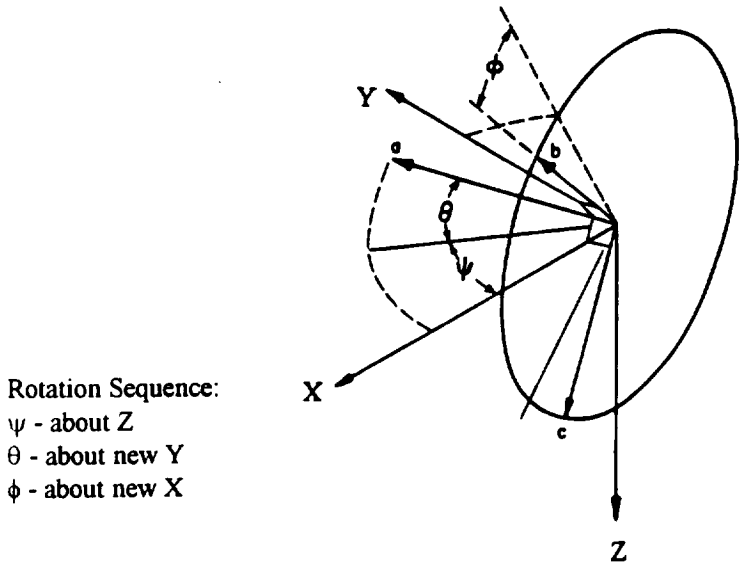

Figure II.1 Model and Wind Tunnel Axis System

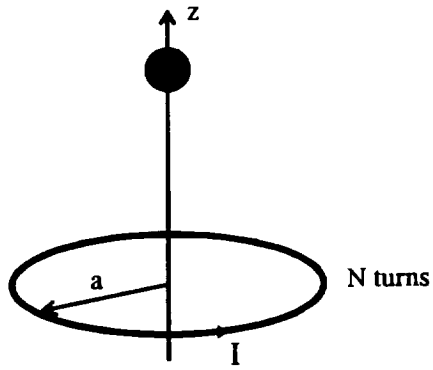

Figure II.2 One Degree of Freedom System

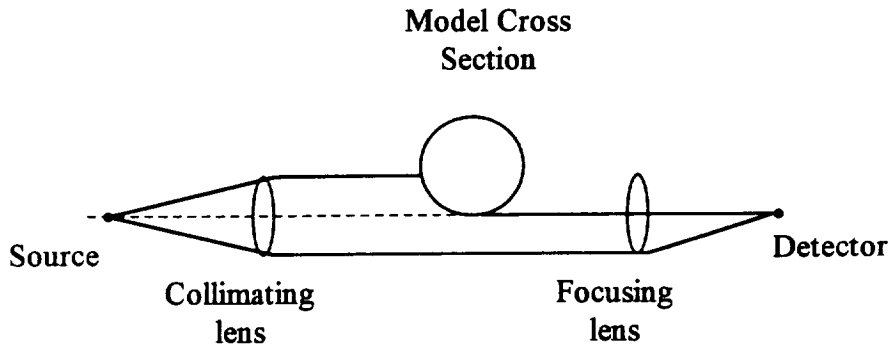

Figure II.3 Narrow Light Beam Position Sensor

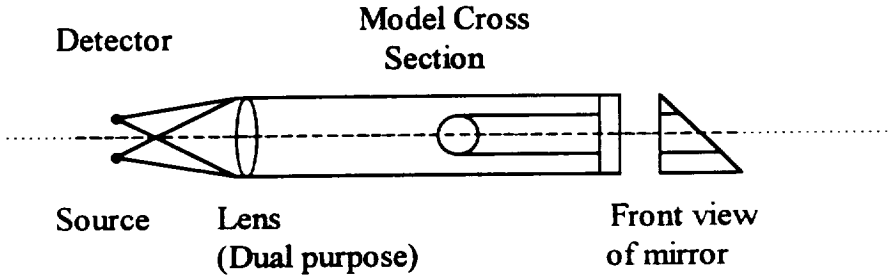

Figure II.4 Large Beam Position Sensor

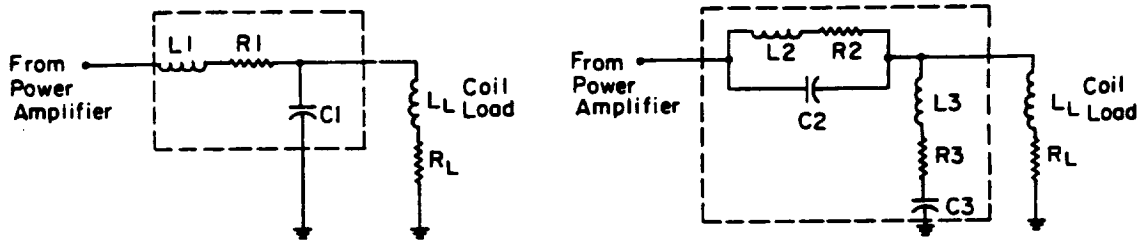

Low-pass Filter

Band-pass Filter

Figure II.5 Filter Configurations

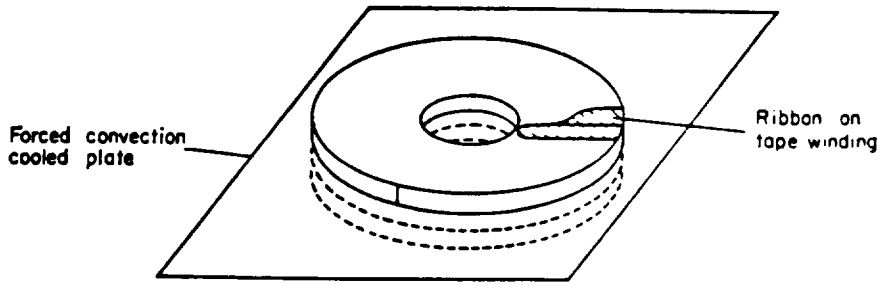

Figure II.6 Conduction Cooled Coil

CHAPTER III

HARDWARE DESCRIPTION OF THE 6-INCH MSBS

A detailed description of the 6-inch Magnetic Suspension and Balance System is given in this chapter. The configuration of the electromagnetic coils, which generate controlled magnetic fields in the test section, is introduced first. The general features of the model position sensing system, compensation system, and power and cooling systems are then outlined. Current status of the 6-inch MSBS system is presented at the end of this chapter.

III.1 Magnet System

Although a variety of magnet configurations can be conceived, the design should be as compact as possible for reasons of power economy. The geometric constraints imposed by the wind tunnel, the position of the EPS, the accessibility to the test section, and the view path for a Schlieren system must also be considered. Further requirements include providing access for installation of instrumentation probes and injection of the model.

The prototype magnet system hardware is comprised of several elements and subelements. The magnetic fields are generated by the Helmholtz coils, saddle coils and iron core magnet assemblies. Other structures such as end plates, tie rods, and safety shrouds are also necessary to support the coils, to provide the structure, and to protect other devices. These subsystems are now introduced in turn.

III.1.1 Helmholtz Coils

Helmholtz coils provide an axial magnetization field and drag force control. A "Helmholtz configuration" is defined as a pair of identical circular solenoid coils between which the axial spacing is approximately one mean coil radius. The Helmholtz coil system used in the 6-inch MSBS has two subelements: magnetization windings to provide a steady state magnetic field, B_X, and drag windings to provide a gradient of the axial field, B_{XX}.

Figure III.1a shows the arrangement of the Helmholtz coil system. Each coil is wound in three parts which are separated by insulating layers. The middle sections of the two coils are arranged in series to generate uniform B_X over an appreciable volume of the central region of the test section. The inner and outer sections are connected in series, with the current in the two coils circulating in the opposite sense. Therefore, at the centroid of the test section, the axial field strength is zero, and a uniform gradient B_{XX} is produced along the axis.

The coils are wound of hollow copper conductors in layers of constant radius. Joints between layers occur at the beginning and end of each layer, and they incorporate hydraulic fittings which allow cooling water to be circulated. Figure III.1b shows the coils before installation [5].

III.1.2 Saddle Coils

The transverse magnetic field components B_Y and B_Z are produced by two pairs of saddle shaped coils. The arrangement and a photo are shown in Figure III.2a and III.2b. These coils consist of an inner pair and an outer pair which are orthogonal to each other.

B_Y and B_Z are then composed of components from both pairs of coils to provide pitch and yaw moments. The apertures in the inner coils overlap the apertures in the outer coils in order to provide a horizontal viewing and Schlieren path, and a vertical path for additional access to the test section is available.

The coils are wound of hollow copper conductor in double layer pancakes, bent to shape and encapsulated. Cooling manifolds are attached to the ends of coils [5].

III.1.3 Lift and Side Force Coil Assemblies

Control of lift and side force is affected by a pair of iron core magnet assemblies, shown in Figure III.3a. Each assembly consists of octagonal laminated silicon steel core structures having four symmetric tapered poles which point toward each other and are canted at 45° to the plane of the octagon. The iron core is used to enhance the magnetic field strength by an appreciable factor thereby reducing the power consumption, which is a highly desirable characteristic. On the other hand, the iron places a limit on the range of linear operation of the magnet system, due to saturation effects. Furthermore, the inductance of the coil system will increase due to the presence of the iron cores. This increment will generate more reactive power in the circuit and nearly offset the power saved by the merit of strength enhancement [4].

Four identical magnet coils are mounted on the joints of the poles vertically and horizontally. The coils are constructed of hollow copper conductor, which is water-cooled. The four coils with vertical axes (two coils per assembly) are connected in series and control the lift force, shown in Figure III.3b. The four coils with horizontal axes (two coils per assembly) are connected in series to control side force. A picture of these

assemblies before installation is shown in Figure III.3c.

III.1.4 Roll Control System

A complete roll control system compatible with the 6-inch MSBS system was originally suggested by Stephens [5] to provide control of the sixth degree of freedom, roll. This system will not be introduced here since it relies on A.C. fields to provide separation from the other five degrees of freedom. The development of this system, which includes the drive circuit, the Roll Position Sensor (RPS), and the compensation circuit, was completed in 1982 [14, 15].

III.1.5 Mechanical Considerations

All magnet coils are provided with thermal sensor switches and coolant flow switches to prevent thermal overload. The various coils in the magnet system are interconnected and connect to terminal boxes on top of the assembly. The magnet assembly is sandwiched between two fabricated cruciform aluminum end plates which are held together by longitudinal tie rods. Lateral alignment of the subsystem is provided by inserting dowels into structural elements. Figure III.4a shows the structure of the magnet system, and Figure III.4b shows a photo of the structure before assembly. The complete system is then covered by safety shrouds which prevent personnel from contacting high voltages in the magnet coils and to prevent magnetic objects from being attracted into the magnet system which might cause short-circuits. A support structure is also designed to distribute the weight of the system uniformly to the floor. Finally, the entire system is connected to the 6-inch wind tunnel with an octagonal test section, shown in Figure III.5.

III.1.6 Wind Tunnel

The wind tunnel compatible with the magnetic balance system is an open circuit, closed-jet tunnel. The contraction is constructed of molded plywood. Two settling chambers and a honeycomb are located upstream of the contraction to improve flow quality. The octagonal test section is located within the magnetic assembly. It is made of transparent acrylic, measures 6.25 inches across flats and is 36 inches long. A two-piece diffuser with access doors is located between the magnetic assembly and the squirrel cage fan. A maximum dynamic pressure of 2.5 psi, a Mach number of 0.6, and a freestream unit Reynolds number of 3.5×10^6/ft are attainable [6].

III.2 Electromagnetic Position Sensor

Although optical model sensing systems have been used extensively because of their linearity and low noise, the most obvious drawback of this approach is that the design of an optical system must be tailored to the size and configuration of the wind tunnel model. The Electromagnetic Position Sensor is an alternative, which employs the principle of the differential transformer with the model forming the core to resolve five components of the model position and orientation.

An EPS compatible with the 6-inch magnet system was originally designed by Stephens [16]. The simplified schematic of the EPS system is shown in Figure III.6. The sensor subsystem, which is a transducer coil assembly, and the electronics subsystem, which is used to actuate the coil system and resolve the output signal, are introduced respectively. A qualitative description of the system's operation is also given.

III.2.1 EPS Coil System

The key part of the overall system, (e.g. a coil assembly with excitation and pickup coils) is shown in more detail in Figures III.7a, III.7b and III.7c. The excitation and pickup coils are arranged to provide a viewing window into the test section. The windings are potted with epoxy for mechanical strength and painted black outside and white inside to enhance the model visibility during operation.

The excitation windings consist of a pair of Helmholtz coils, designated as EXC A and EXC B, which terminate at the end of the assembly at a 2-pin socket. These coils generate a uniform axial magnetic field which oscillates at f = 20 kHz when driven by a suitable power amplifier.

The pickup coils consist of seven pairs of No. 30 Teflon-covered stranded small gage wire, all having an equal number of turns (thirty turns on each coil) and terminating at a multiple-pin socket at the end of the assembly. Axial pickup coils, designated as AX A and AX B, are also in a Helmholtz configuration and are coaxial with the excitation coils but are connected in opposition. These coils are used to pick up the model's axial signal. The remaining six pairs of pickup coils are in four rows of saddle-shaped coils, from which signals are resolved to derive the model's horizontal and vertical translation, as well as pitch and yaw orientation. The parameters of the pickup coils are given in Table III.1 [15] and compared with the data obtained from the pickup socket.

A small electrical box, connected directly behind the excitation signal cable, is used to minimize the reactive power. The circuit is shown in Figure III.8. The required

Table III.1 ODU 6-Inch MSBS, EPS Coil Parameters

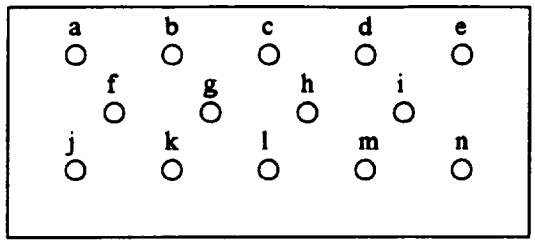

$R_{af} = 6.2\ \Omega$
$R_{bi} = 11.7\ \Omega$
$R_{cl} = 14.0\ \Omega$
$R_{dm} = 9.5\ \Omega$
$R_{en} = 8.5\ \Omega$
$R_{gj} = 6.6\ \Omega$
$R_{hk} = 6.2\ \Omega$

Pickup Socket

EPS Coil Circuit	DC Resistance[1] (Ω)	Inductance[2] (mH)	Self-capacitances[3] (mF)
Axial	14.76	0.919	0.00141
Lateral I	7.57	0.468	0.00156
Lateral II	10.41	0.517	0.00143
Lateral III	7.18	0.416	0.00126
Vertical I	12.42	0.509	0.00144
Vertical II	9.49	0.502	0.00146
Vertical III	12.47	0.488	0.00152

1. Measured with Fluke digital VOM.

2. Calculated from resonance frequency with 0.25 μf mica transmitting capacitor.

3. Calculated from self-resonant frequency.

capacitance to offset the inductance of excitation coils can be estimated as follows:

$$R_{\text{Operation impedance}} = \frac{\frac{1}{Cs}(sL+R)}{(sL+R)+\frac{1}{Cs}} = \frac{sL+R}{s^2LC+RCs+1} \qquad \text{(III-1)}$$

$$s \rightarrow j\omega$$

$$R_{\text{Operation impedance}} = \frac{(R+j\omega L)(1-LC\omega^2-RC\omega j)}{(1-LC\omega^2)^2+(RC\omega)^2} = \frac{R+j(\omega L-L^2C\omega^3-R^2C\omega)}{(1-LC\omega^2)^2+(RC\omega)^2} \qquad \text{(III-2)}$$

To minimize reactive power,

$$\omega L - L^2C\omega^3 - R^2C\omega \rightarrow 0$$

Therefore,

$$C = \frac{L}{\omega^2L^2+R^2} \qquad \text{(III-3)}$$

For L = 404 μH, R = 0.7 Ω, and $\omega = 2\pi f = 4\pi\times10^4$, Equation (III-3) gives $C = 0.1567\times10^{-6}$ F. The capacitance actually used is 0.2×10^{-6} F.

The working principle of the coil assembly is briefly introduced here. Once the excitation coils are actuated, they produce a uniform magnetic field over a region surrounding the centroid of the test section, oscillating axially at 20 kHz. When a slender ferromagnetic model is aligned with the axis of the coil assembly, it will be magnetized at the same frequency with the excitation field. Figure III.9 shows the induced fields when the model is at different locations in the frame. From the diagrams, it follows that the drag signals are measured by AX without first-order coupling with the other four motions. A general statement can be made that linear motions are detected by subtracting coil outputs

and rotations are detected by summing coil outputs. For example, vertical motion can be resolved by subtracting the output of pick-up coils V3 from the output of V1, and pitch motion can be resolved by summing V1, V2 and V3 together. The results apply equally well to lateral translation and yaw rotation by symmetry.

III.2.2 Electronics System

Figure III.10 shows the block diagram of the electronics associated with the EPS coil system. However, this original system provided poor sensitivity, high noise and correlated interference, some of which is due to the weak points in the signal processing circuit design, and some due to the unreliable analog elements.

A new design was developed in the late 1980s and the old data reduction circuit was replaced by a new compact electronic system providing output with less noise, drift, and higher sensitivity and repeatability [17]. EPS circuit diagrams are given in Appendix B. Unfortunately, system documentation was never completed. Therefore, some efforts to analyze the circuits were made and the comments are given in Appendix B. The compensation system consists of several stages in cascade, and each of them has several elements in common. Figure III.11 is a block diagram of one channel, and it will be used to illustrate the operation of the whole system. Other channels are similar.

III.2.2.1 EPS Oscillator and Power Amplifier

The 20 kHz, 2.5 V peak-to-peak carrier sinewave for primary coil excitation, input stage nulling, and demodulation is supplied by a crystal-controlled IC oscillator with $\pm 0.05\%$ stability and $\leq 5\%$ total harmonic distortion. The original vacuum tube amplifier was replaced by a new solid state power amplifier. This item did not arrive at ODU with

other EPS hardware. According to the documentation [17], this amplifier should be an audio frequency amplifier with output amplitude about 210 volts peak-to-peak.

III.2.2.2 Reference Phase Adjustment

The output of the amplifier is sent to both the position sensor coil assembly and the nulling system as the null-reference used in the demodulation stage. Signals pass through amplifiers driving bipolar balanced output transformers to provide seven pairs of active summing networks and five demodulator references.

III.2.2.3 Summation and Demodulation

The seven differential coil voltages are sent to band-pass filters and amplified before arriving at summing circuits, in order to attenuate higher order harmonics. Five AD630 demodulator integrated circuits combined with low-pass filters are applied to obtain continuous DC outputs which should be approximately proportional to the movements of the model relative to the axes of the transducer assembly.

III.3 Compensation System

Since the suspension system is a position control servo, designed to maintain the suspended model at some commanded position, a superior compensator should accomplish at least three things: 1) Stabilization of the loop, 2) Minimization of static position errors for given disturbance inputs, and 3) Minimization of static position errors for given position command inputs.

A functional block diagram of the suspension system is shown in Figure III.12. The position of the model is translated into electrical signals by means of the position sensing device, and these signals are compared with the position command signals. The resulting

position error signals are modified by passing through a set of feedback compensation networks, and then amplified and applied to the actuators. The magnetic forces and moments, which are functions of the coil currents, act on the model to cause changes to its position and orientation. These operations adjust continuously to counteract the aerodynamic and gravity loads.

The feasibility of applying digital information processing to the magnetic suspension system was proposed in the mid-1970s [18, 19]. Establishment of the overall system model and calibration procedures for discrete subsystems were accomplished during this period. Although a more advanced controller might increase operating performance levels for this non-linear control problem, the control method outlined in References [18, 19] provides a framework for further recommissioning work.

A simple and effective form of the controller consists of three paths: proportional, integral and third-order lead-lag network, shown in Figure III.13. The main purpose of using the integrator is to improve the system's low frequency response, in other words, maintain zero position error with a steady disturbance input. The application of a proportional controller helps reduce rise time, and the lead-lag path helps reduce overshoot. From a practical point of view, experiments are necessary to determine acceptable combinations of settings for the gains and poles and zeros of the compensator. These settings are dependent on the model used.

III.4 Power and Cooling System

The power system is the most expensive part of the 6-inch MSBS. This subsystem was modified several times to increase drive current capability [4, 5, and 20]. A schematic

of this old power supply system is given in Figure III.14. Seven power amplifiers are needed for this six degree of freedom system, i.e., five D.C. amplifiers for drag, lift, side force, pitch and yaw respectively, and two additional A.C. amplifiers for rolling moment control. The D.C. amplifiers are required to operate in all four quadrants. Therefore, they could provide a continuously variable current output which is linearly proportional to the input voltage control signal. The repeatability and stability of the output current is of the order of 0.1% of the operating output current for day-to-day operation. The maximum output power level is approximately 1,000 amps into a 0.34 (±20%) ohm load. The L/R time-constant of this load was about one second. The power at maximum resistance is approximately 400 kW.

The magnet coils, and the conductors which form the interconnections between coils, must be provided with a means of removing the heat which is generated due to ohmic losses. The cooling system must be reliable and of moderately high power-density capability. The most suitable choice of cooling media appears to be water, and in order to avoid electrolysis and silting of the conductors, the cooling water needs to be demineralized and deaerated.

Figure III.15 gives the cooling as well as electrical paths in the conductor coils. The brass adapters fit nylon tubing (d = 0.25 inches), which is used to connect the coils to the inlet and outlet coolant manifolds. The cooling water actually circulates through the magnet coils and is contained in a closed loop, as shown in Figure III.16. Heat is removed from this water with a heat exchanger, which transfers the heat to unpurified water. This unpurified water is then circulated through a cooling tower. The "inner" cooling loop

(purified water loop) is provided with a high-pressure circulating pump to force the purified water through the magnet coils. A reservoir is used to accommodate changes in volume of the coolant due to expansion, and a portion of the cooling fluid flow is circulated through a small demineralizer and deaerator to maintain the required purity. Notice that pressure, temperature and flow indicators are also necessary to prevent coolant failure which will result in magnet coil burnout.

III.5 Current Status of the 6-Inch MSBS

The 6-inch Magnetic Suspension and Balance System was transferred to the Aerospace Engineering Department of Old Dominion University in 1994 and is in the first stage of recommissioning work.

The magnet system was checked and tested to verify the magnetic field distribution. Results are given and discussed in the next chapter. A new amplifier is needed to complete the EPS hardware. Further, schematics of the printed circuit boards, which are very helpful to recover the EPS electronics, are sought, but have not been found at this time. The original power supply and compensation systems have been totally abandoned due to their out-of-date condition. These two systems need to be redesigned or replaced according to new performance requirements. New technology in digital electronics should bring a more compact and advanced control system. The aged cooling system needs to be either repaired or replaced. Restoring the whole wind tunnel is the last task of the reassembly work.

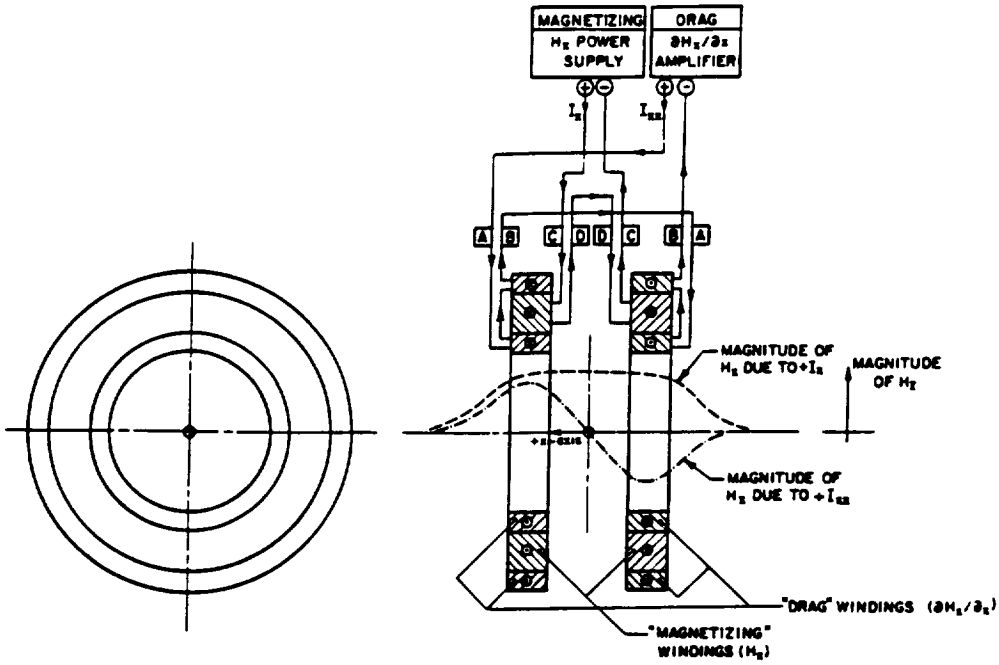

Figure III.1a Helmholtz Coils: System Arrangement

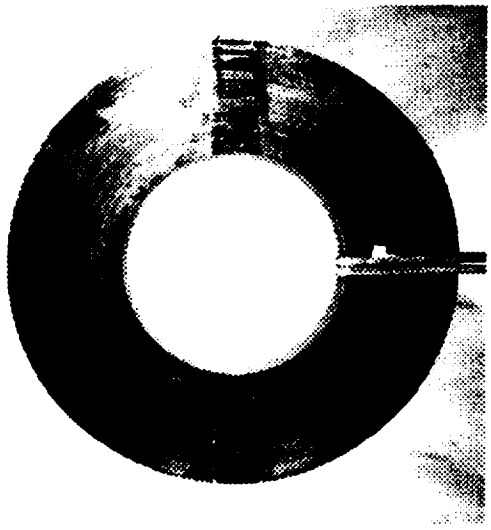

Figure III.1b Helmholtz Coils: Prior to Installation

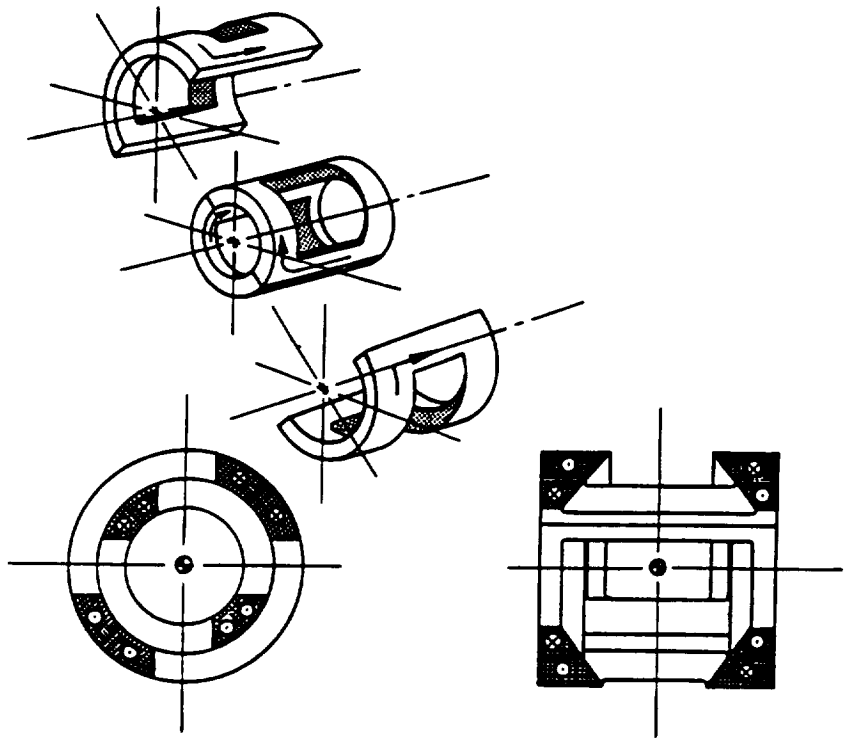

Figure III.2a Saddle Coils: System Arrangement

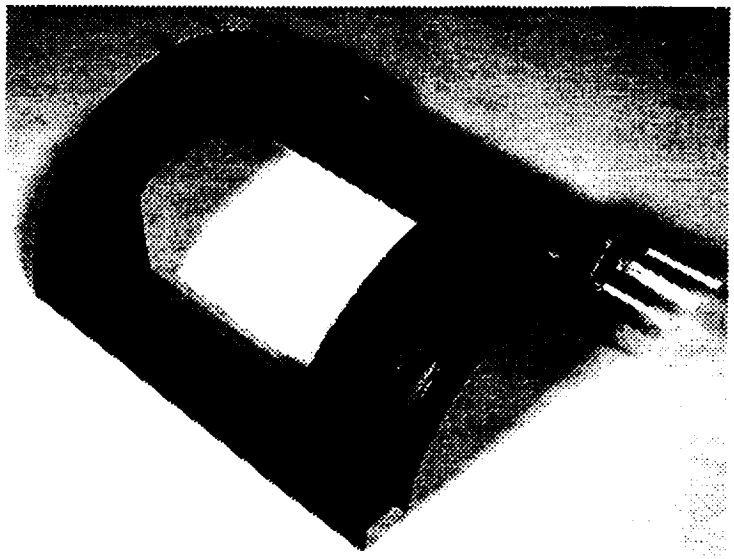

Figure III.2b Saddle Coils: Prior to Installation

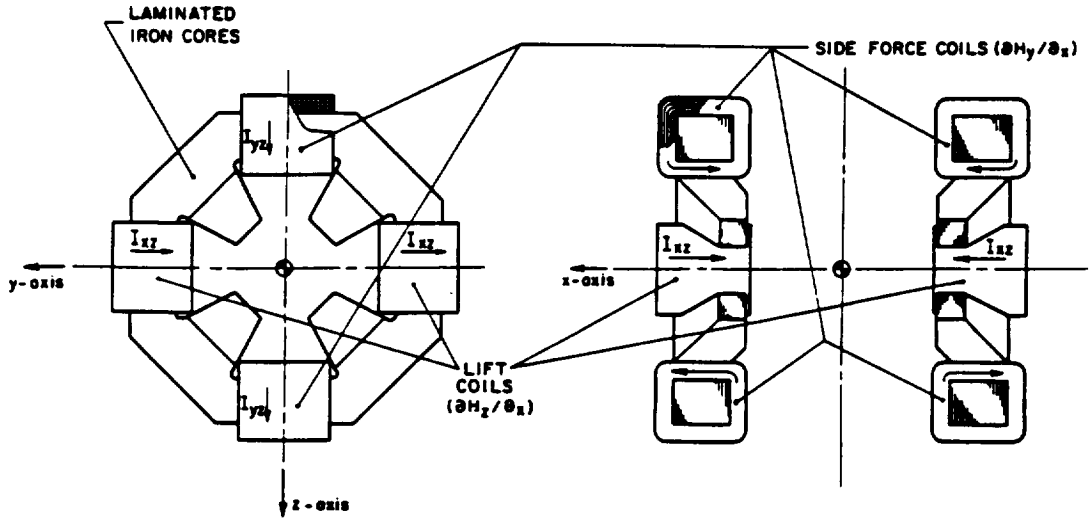

Figure III.3a Lift and Side Force Coils: System Arrangement

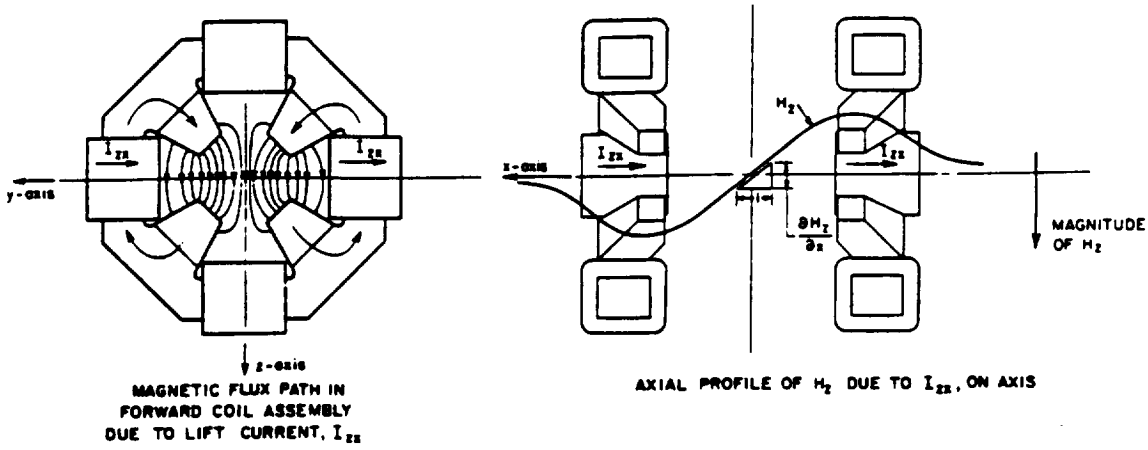

Figure III.3b Lift and Side Force Coils: Flux Paths in Lift Force System

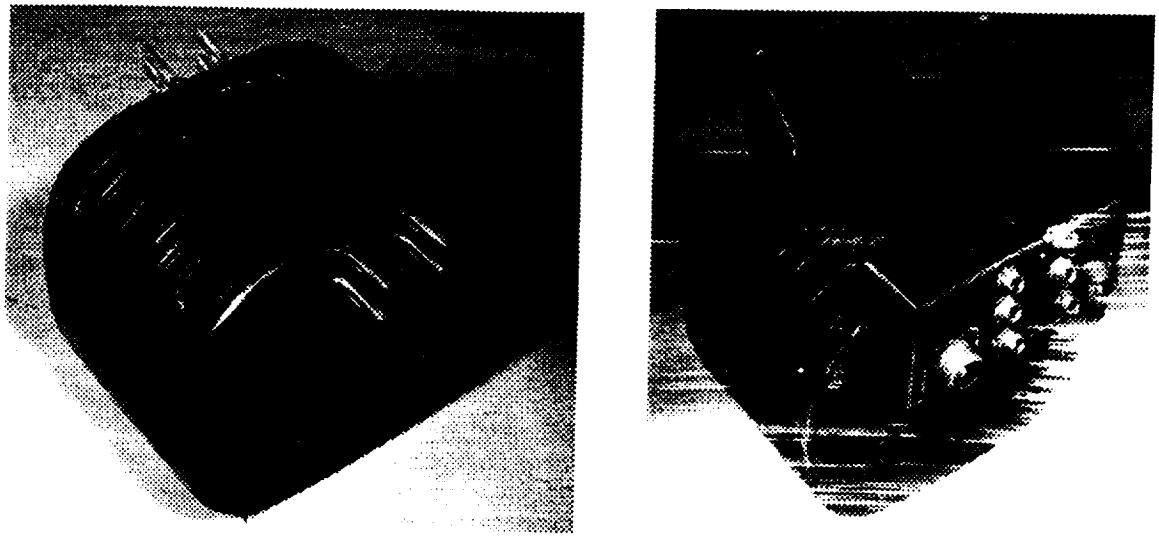

Figure III.3c Lift and Side Force Coils: Prior to Installation

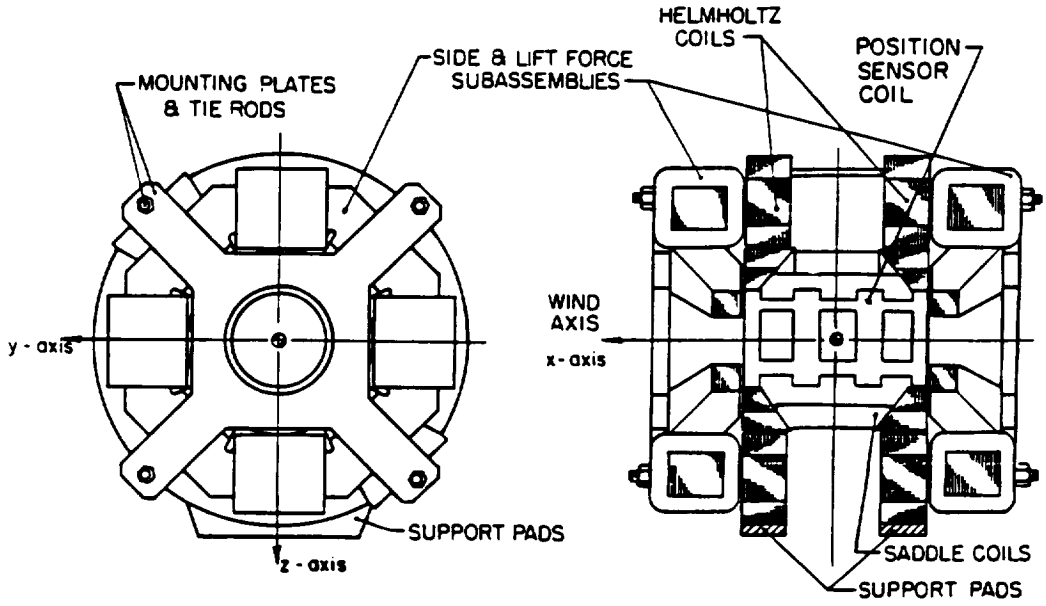

Figure III.4a Magnet System Assembly: System Arrangement

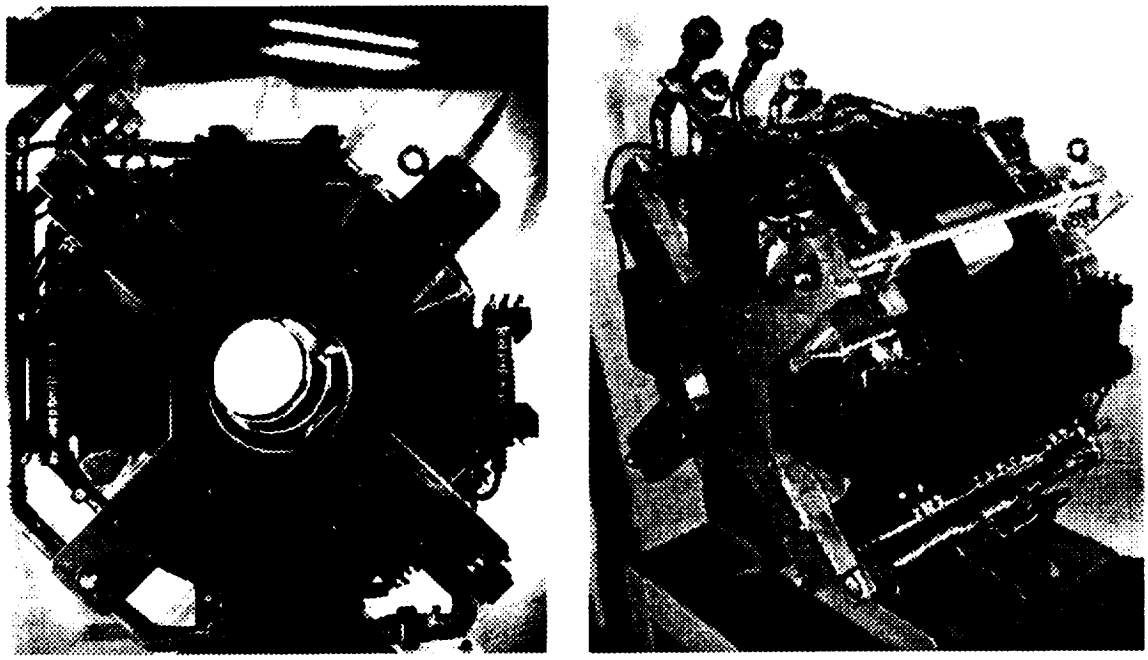

Figure III.4b Magnet System Assembly: Prior to Installation

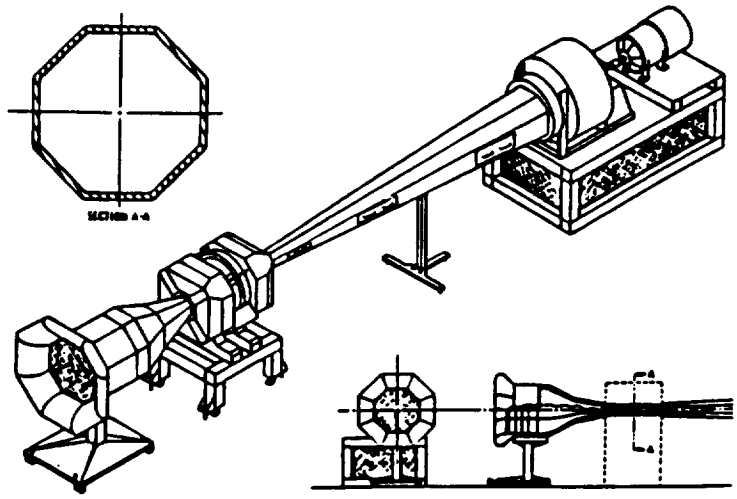

Figure III.5 A Schematic of the 6-Inch MSBS Wind Tunnel

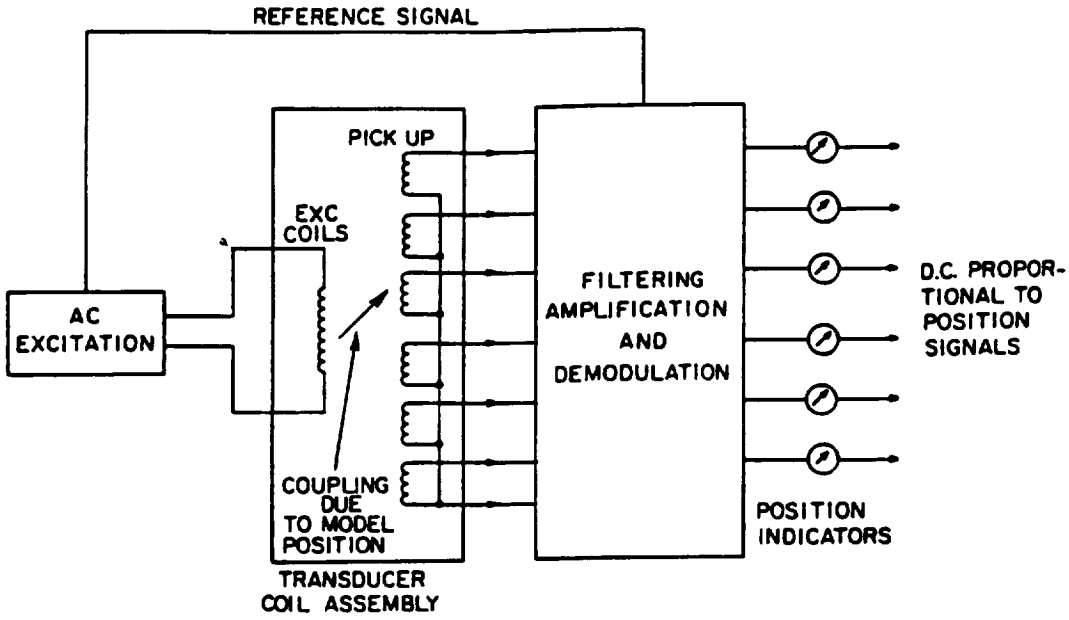

Figure III.6 A Simplified Schematic of the EPS Sensor

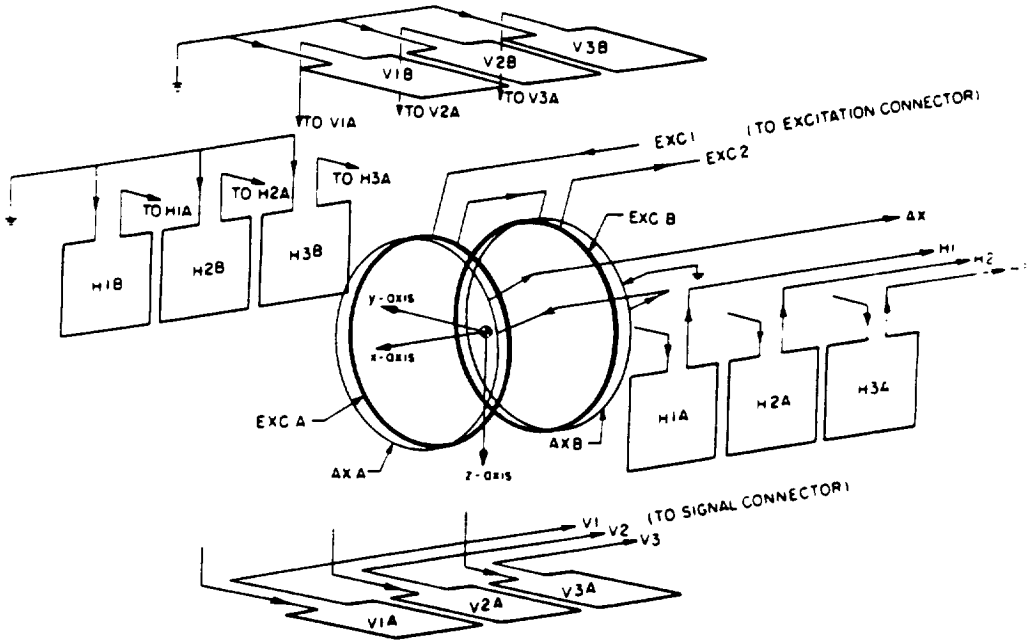

Figure III.7a EPS Coil Assembly: Pictorial of Windings

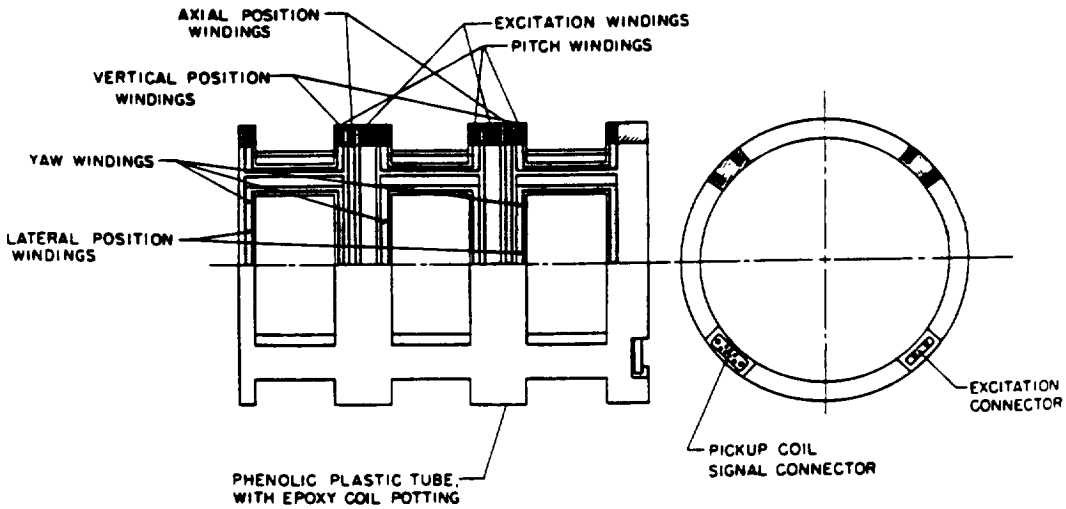

Figure III.7b EPS Coil Assembly: Section View of Windings

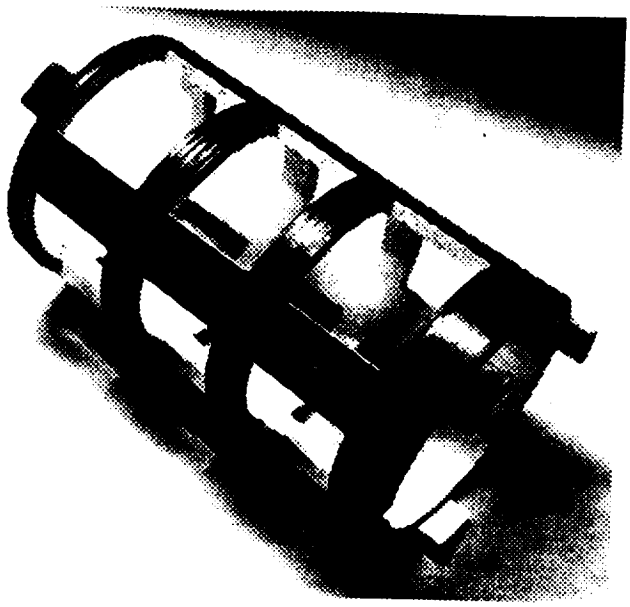

Figure III.7c EPS Coil Assembly: Prior to Installation

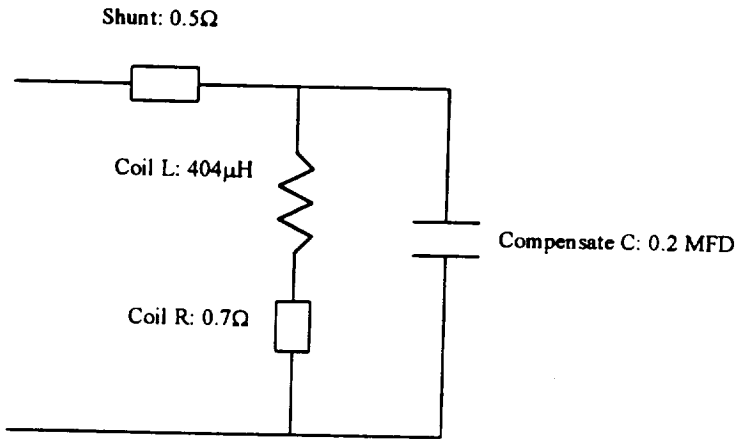

Figure III.8 Circuit Used to Minimize the Reactive Power in EPS Coil Assembly

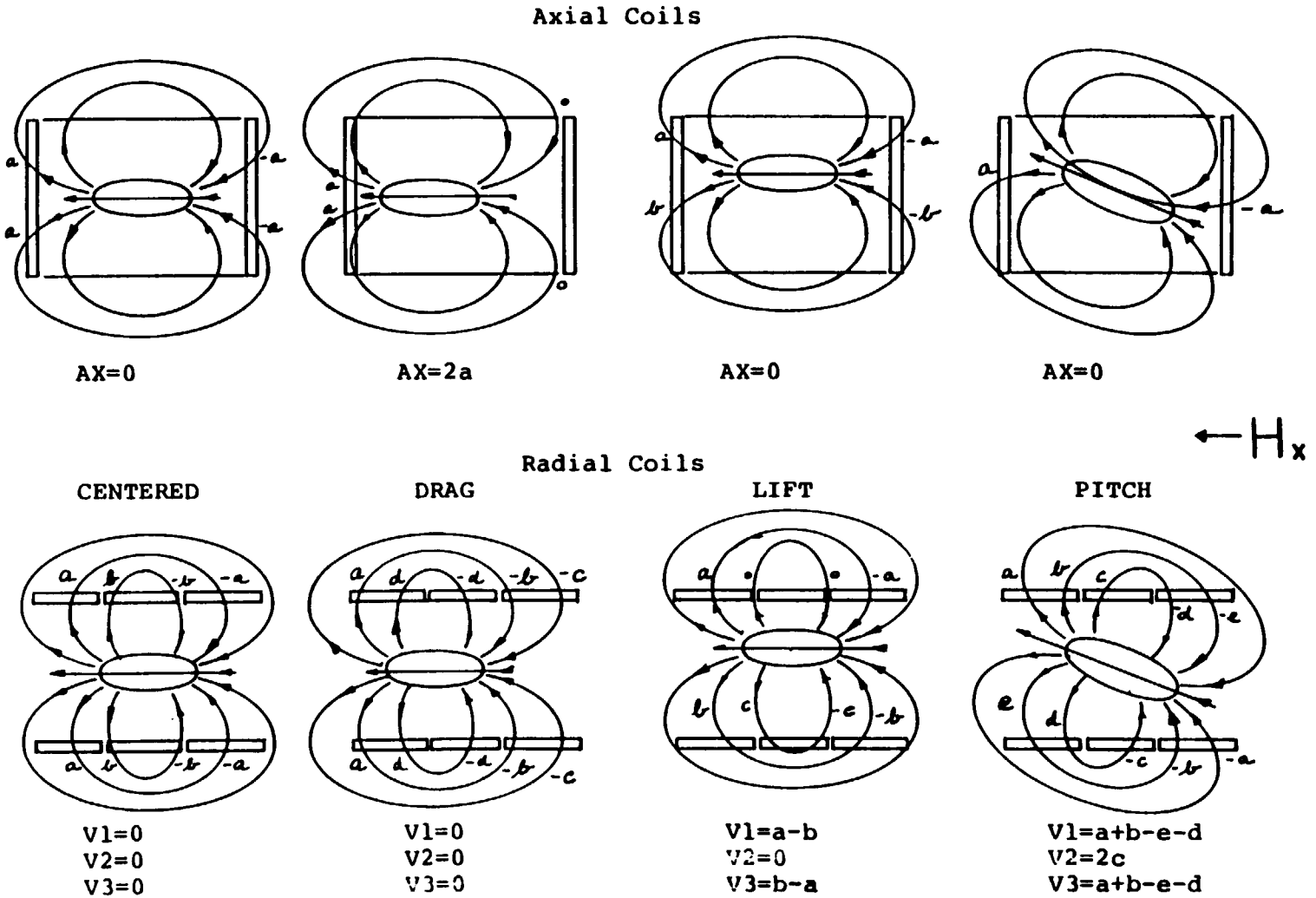

Figure III.9 EPS Signal Contributions from Single Flux Lines

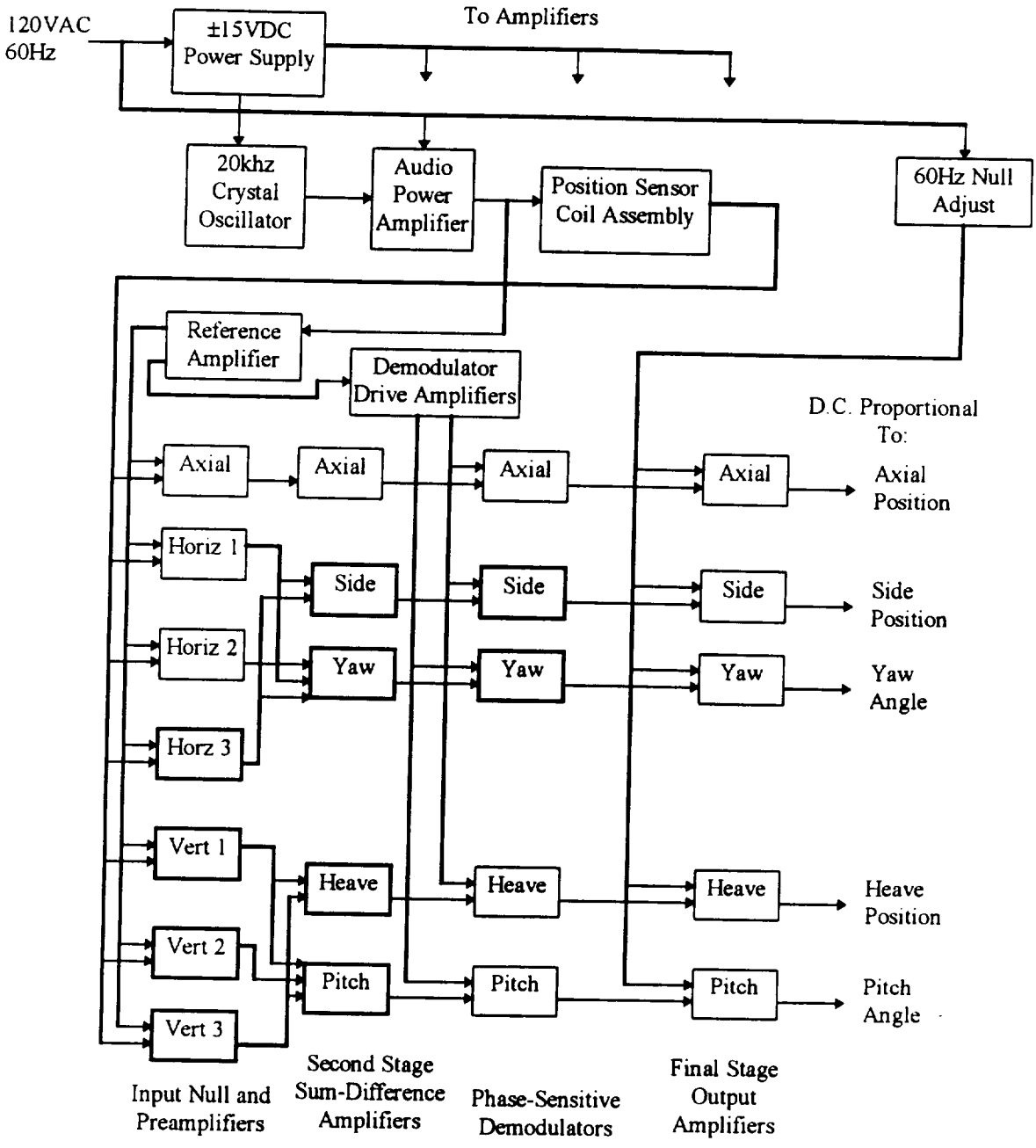

Figure III.10 EPS Electronics System Block Diagram

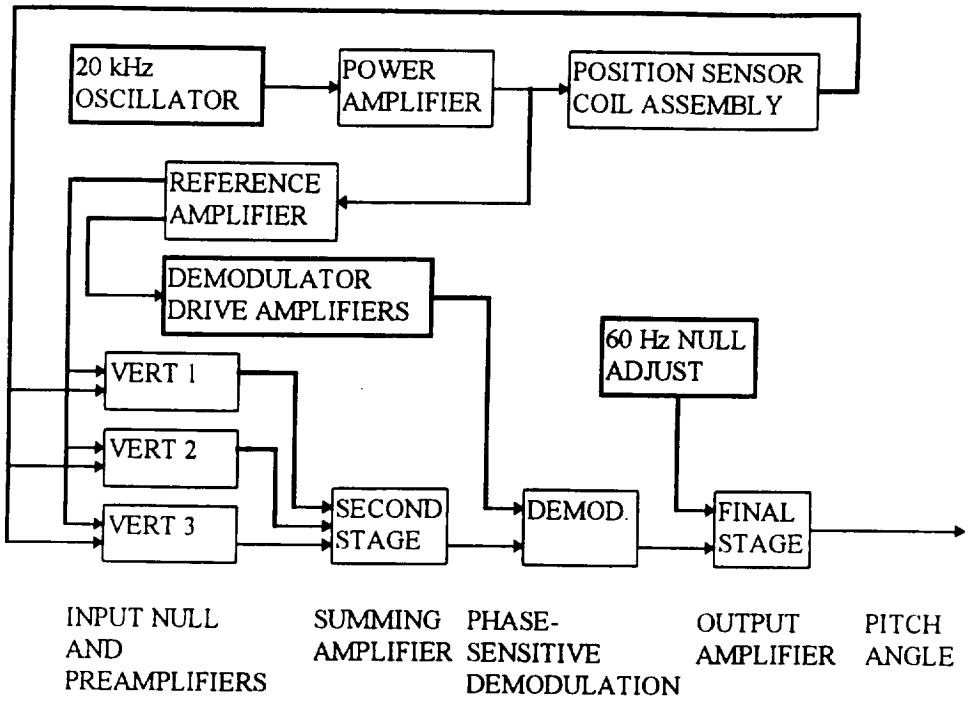

Old System

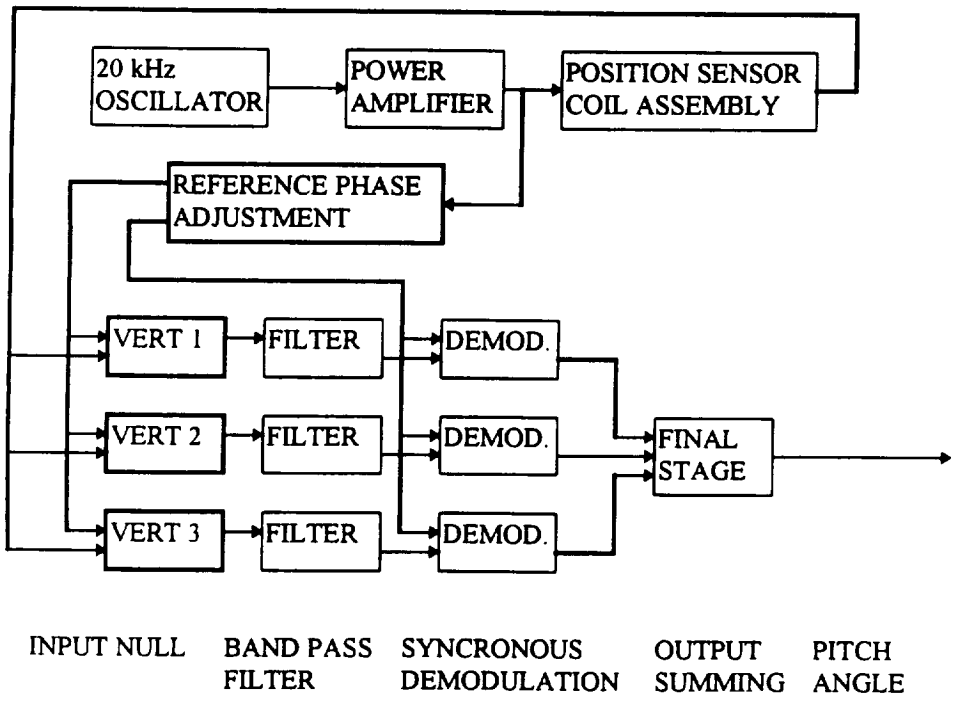

New System

Figure III.11 Block Diagram Comparison of Pitch Channel

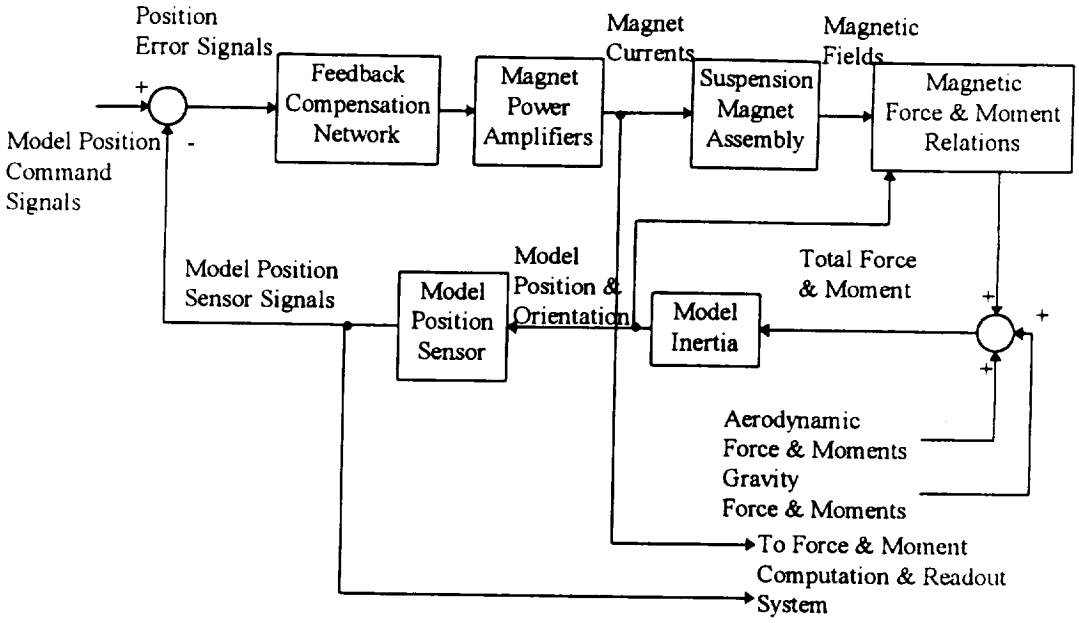

Figure III.12 Functional Block Diagram of System

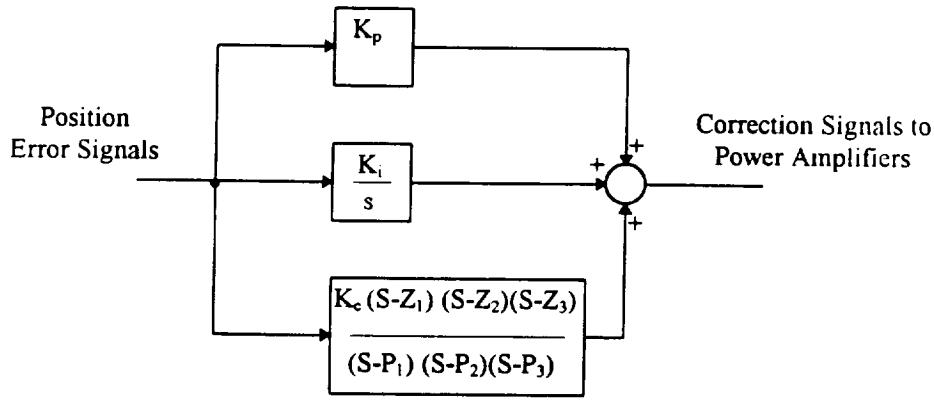

Figure III.13 Schematic of Compensator

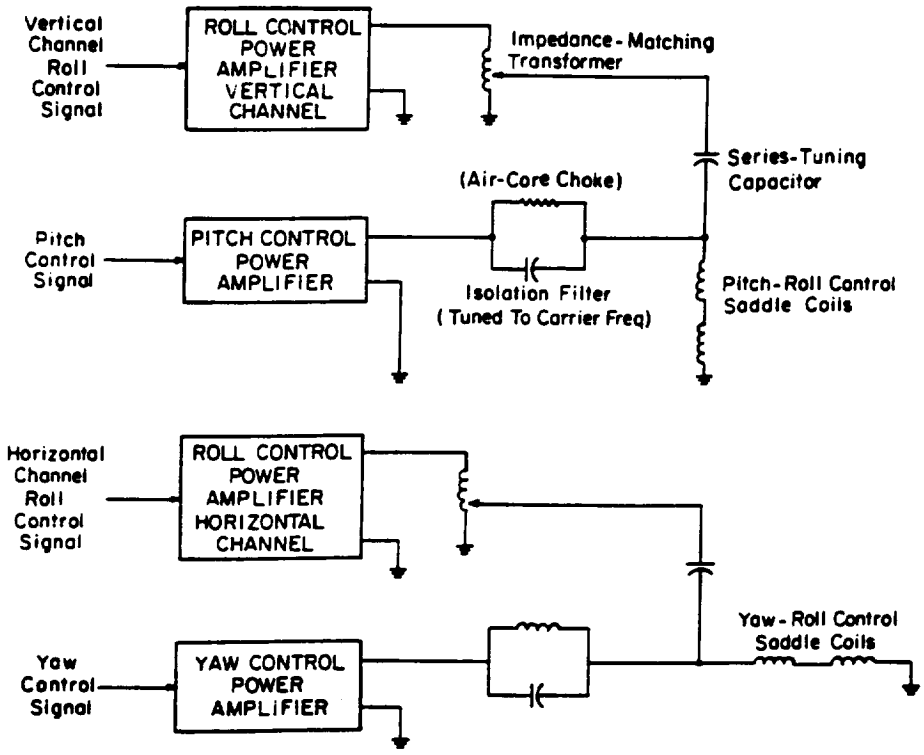

Figure III.14 Power Supply System Schematic

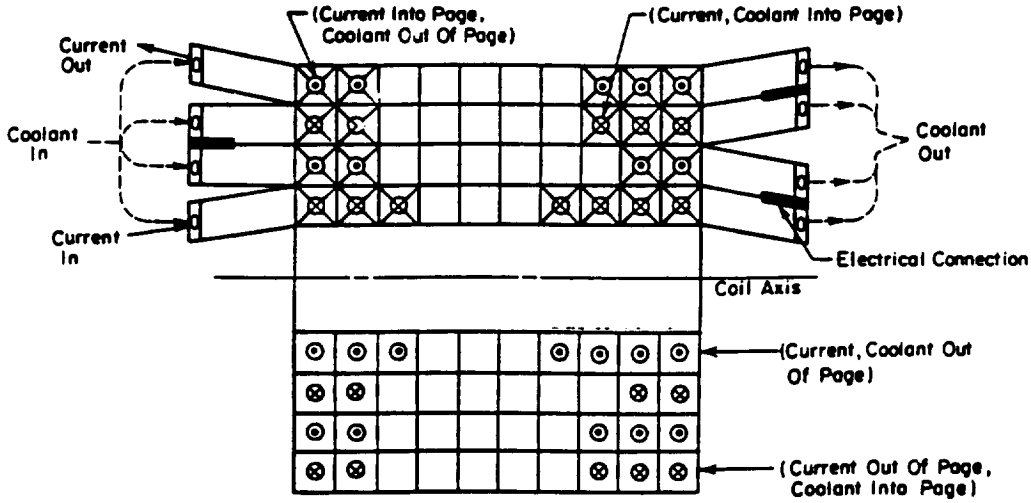

Figure III.15 Layer-wound Hollow Conductor Coil Cooling and Electrical Paths

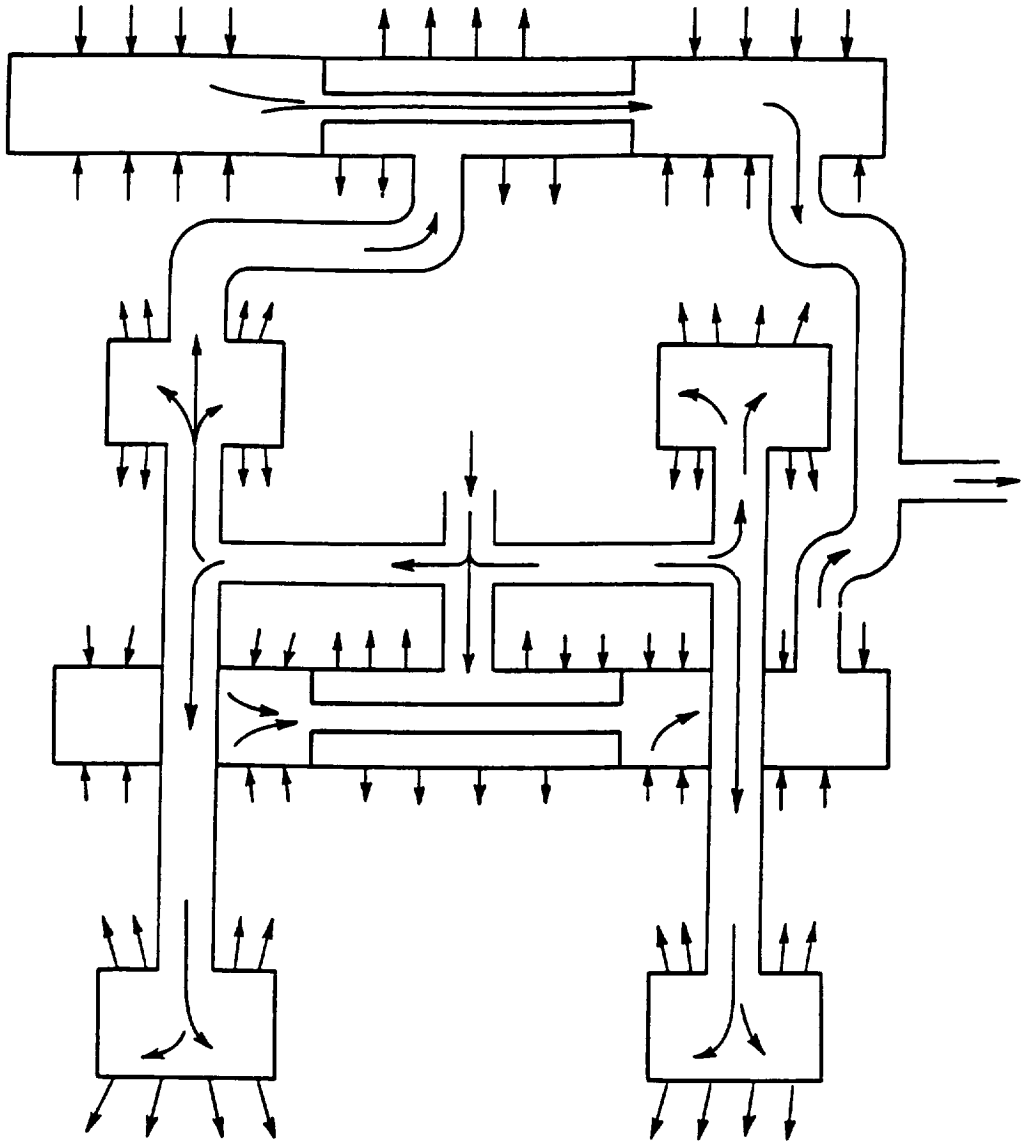

Figure III.16 Coolant Manifold: Schematic

CHAPTER IV

THE MAGNETIC FIELD OF THE 6-INCH MSBS

In this chapter, the magnetic field generated by the magnetic assembly of the 6-inch MSBS is estimated by analyzing the individual subsystems. Measurements and computational results are also given and compared with each other.

IV.1 Performance Estimation

In the design of a large-scale magnet system, it is desirable that the magnetic performance be estimated accurately. Two classical approaches for estimation are commonly used: 1) the use of a small scale model and 2) the analytical calculation of the magnetic fields. The former is more accurate and more reliable for a complicated system, but it also more expensive. The latter is much cheaper, although the simplification of the systems' geometry, saturation effects and the absence of the iron cores may cause large errors. Modern computational techniques are available and are superior to both of these approaches, but require the use of sophisticated computer codes.

The basic formula used to calculate the magnetic field generated by coils with different geometries is the Biot-Savart Law, which states that the magnetic field **B** at a distance **r** from a line current element Idl is:

$$\mathbf{B} = \int_L d\mathbf{B} = \int_L \frac{\mu I d\mathbf{l}}{2\pi r^2} \times \frac{\mathbf{r}}{r} \qquad \text{(IV-1)}$$

IV.1.1 Helmholtz Coils

The calculation begins with a single loop shown in Figure IV.1. The magnetic field generated along the Z axis is B_Z.

$$B_Z = \frac{\mu_0 I a^2}{4\pi(z^2+a^2)^{3/2}} \int_0^{2\pi} d\phi = \frac{\mu_0 I a^2}{2(z^2+a^2)^{3/2}} \qquad \text{(IV-2)}$$

For the Helmholtz coils in Figure IV.2, the magnetic field at the center of the axis of symmetry is the superposition of the fields generated by the drag windings and magnetizing windings. The fore-and-aft pair is used to improve field uniformity.

The symmetrical part B_X, generated by the middle sections of the Helmholtz coils, is the main axial magnetization, called the *"bias"* field. The current per unit area in the windings is

$$K_0 = \frac{NI}{(x_2 - x_1)(r_3 - r_2)}$$

$$\begin{aligned} B_X(0,0,0) &= B_{X\text{left}}(0,0,0) + B_{X\text{right}}(0,0,0) = 2B_{X\text{left}}(0,0,0) \\ &= \oiint_S \frac{\mu_0 r^2 K_0}{(x^2+r^2)^{3/2}} dS = \int_{r_2}^{r_3}\int_{x_1}^{x_2} \frac{\mu_0 r^2 K_0}{(x^2+r^2)^{3/2}} dx dr \\ &= \int_{r_2}^{r_3} \left(\frac{x}{r^2\sqrt{x^2+r^2}}\right)\Bigg|_{x_1}^{x_2} \mu_0 r^2 K_0 dr = \int_{r_2}^{r_3} \left(\frac{x_2}{\sqrt{x_2^2+r^2}} - \frac{x_1}{\sqrt{x_1^2+r^2}}\right)\mu_0 K_0 dr \\ &= \mu_0 K_0 \left\{ \left[x_2 \ln\left(r+\sqrt{r^2+x_2^2}\right)\right]_{r_2}^{r_3} - \left[x_1 \ln\left(r+\sqrt{r^2+x_1^2}\right)\right]_{r_2}^{r_3} \right\} \\ &= \mu_0 \frac{NI}{(x_2-x_1)(r_3-r_2)} \left(x_2 \ln \frac{r_3+\sqrt{r_3^2+x_2^2}}{r_2+\sqrt{r_2^2+x_2^2}} - x_1 \ln \frac{r_3+\sqrt{r_3^2+x_1^2}}{r_2+\sqrt{r_2^2+x_1^2}} \right) \end{aligned} \qquad \text{(IV-3)}$$

where $\mu_0 = 4\pi\times10^{-7}$ henrys/meter, r_3 = 14 inches, x_2 = 8 inches

N = 400, r_2 =10 inches, x_1 = 4 inches

Substituting these numerical values into Equation (IV-3) and converting to meters (multiply by κ = 39.37 inches/meter) to get the correlation between current and magnetic field yields

$$\boxed{B_X/I = 11.78 \text{ gausses/amp} = 1.178\times10^{-3} \text{ teslas/amp}} \qquad \text{(IV-4)}$$

The drag force is produced by the axial gradient field B_{XX} ($= \frac{\partial B_{drag}}{\partial x}$) which is the anti-symmetric contribution. Defining

$$NI = K_0(r_4-r_3) = K_0'(r_2-r_1)$$

$$x_0=(x_1+x_2)/2$$

$$B_{drag} = \int_{r_3}^{r_4}\frac{\mu_0 K_0 r^2}{(x_0^2+r^2)^{3/2}}dr + \int_{r_1}^{r_2}\frac{\mu_0 K_0' r^2}{(x_0^2+r^2)^{3/2}}dr \qquad \text{(IV-5)}$$

$$\begin{aligned}
B_{XX} &= \int_{r_3}^{r_4} -\frac{3\mu_0 K_0 r^2 x_0}{(x_0^2+r^2)^{5/2}}dr + \int_{r_1}^{r_2} -\frac{\mu_0 K_0' r^2 x_0}{(x_0^2+r^2)^{5/2}}dr \\
&= -3\mu_0 x_0\left[\left(\frac{N_1 I}{r_4-r_3}\right)\left(\frac{r^3}{3x_0^2(x_0^2+r^2)^{3/2}}\right)\Bigg|_{r_4}^{r_3} + \left(\frac{N_2 I}{r_2-r_1}\right)\left(\frac{r^3}{3x_0^2(x_0^2+r^2)^{3/2}}\right)\Bigg|_{r_1}^{r_2}\right] \\
&= -\mu_0 x_0\left[\left(\frac{N_1 I}{r_4-r_3}\right)\left(\frac{r_4^3}{x_0^2(x_0^2+r_4^2)^{3/2}} - \frac{r_3^3}{x_0^2(x_0^2+r_3^2)^{3/2}}\right)\right. \\
&\qquad \left. + \left(\frac{N_2 I}{r_2-r_1}\right)\left(\frac{r_2^3}{x_0^2(x_0^2+r_2^2)^{3/2}} - \frac{r_1^3}{x_0^2(x_0^2+r_1^2)^{3/2}}\right)\right]
\end{aligned} \qquad \text{(IV-6)}$$

where $N_1 = 200$, $r_1 = 8$ inches, $r_3 = 14$ inches, $x_1 = 4$ inches

$N_2 = 200$, $r_2 = 10$ inches, $r_4 = 16$ inches, $x_2 = 8$ inches

$$\boxed{B_{XX}/I = 1.34 \text{ gausses/inch/amp} = 5.27\times10^{-3} \text{ teslas/m/amp}} \qquad \text{(IV-7)}$$

IV.1.2 Saddle Coils

Using the Biot-Savart Law for the geometry shown in Figure IV.3, the magnetic field at point P is

$$\mathbf{B} = \frac{\mu I}{4\pi a}\int_{\beta_2}^{\beta_1}\cos\beta d\beta \mathbf{e}_\theta = \frac{\mu I}{4\pi a}(\sin\beta_2 - \sin\beta_1)\mathbf{e}_\theta. \qquad \text{(IV-8)}$$

For the geometry shown in Figure IV.4, the magnetic field generated by a current element at point O is

$$B_Z = -\int_{\phi_1}^{\pi-\phi_2} \frac{\mu a I}{4\pi(a^2+L^2)} \sin\phi \sin\beta d\phi$$

$$= \frac{\mu I}{4\pi a} \cos^2\beta \sin\beta(\cos\phi_2 + \cos\phi_1) \qquad \text{(IV-9)}$$

The field strength of the saddle coil is complicated to calculate due to its geometry. However, an approximation can be given by using a "mean turn", corresponding to the centroid of the winding, as shown in Figure IV.5. The transverse field B_t, at the origin, can been seen as the contribution from the straight line currents B_{t1} and the contribution from the current in the segment of the loops B_{t2}.

Applying Equations (IV-8) and (IV-9) to calculate B_{t1} and B_{t2}, and noting that $\phi_1 = \phi_2$, $\sin\beta_1 = -\sin\beta_2 = \frac{\frac{L}{2}}{[(\frac{L}{2})^2 + r^2]^{1/2}}$, and that each coil consists of two saddles, yields

$$B_t = \frac{\mu N I}{4\pi r} \frac{1}{[1+\frac{r^2}{(L/2)^2}]^{1/2}} (1 + \frac{1}{1+(\frac{L/2}{r})^2}) \times 4 \times 2\cos\phi \qquad \text{(IV-10)}$$

For the inner saddle coil,

$$\boxed{B_{t(in)}/I = 5.5 \text{ gausses/amp} = 0.00055 \text{ teslas/amp}} \qquad \text{(IV-11)}$$

where N = 88, r = 5.2 inches, L/2 = 5.5 inches, $\phi = 15°$

For the outer saddle coil,

$$\boxed{B_{t(out)}/I = 5.58 \text{ gausses/amp} = 0.000558 \text{ teslas/amp}} \qquad \text{(IV-12)}$$

where N = 133, r = 7 inches, L/2 = 5 inches, $\phi = 15°$

IV.1.3 Lift and Side Force Coil Assemblies

A lift coil model is shown in Figure IV.6 to calculate the magnetic field strength in the Z direction along the wind tunnel axis. Using the Biot-Savart Law, the field is

$$\mathbf{B} = \frac{\mu NI}{2\pi}\int_0^{2\pi}\frac{\mathbf{dl}\times\mathbf{s}}{\mathbf{s}^3}$$

Noting that

$$\mathbf{s} = \mathbf{r} - \mathbf{a}$$
$$= r\hat{i} - a\cos\theta\hat{i} - a\sin\theta\hat{j}$$

$$s^3 = [(r - a\cos\theta)^2 + (a\sin\theta)^2]^{3/2}$$

$$\mathbf{dl} = ad\theta(-\sin\theta\hat{i} + \cos\theta\hat{j})$$

$$\mathbf{dl}\times\mathbf{s} = a(a - r\cos\theta)\hat{k}$$

the Z component of the field is

$$B_Z = \frac{\mu NI}{2\pi}\int_0^{2\pi}\frac{a(a - r\cos\theta)d\theta}{(r^2 + a^2 - 2ar\cos\theta)^{3/2}} \qquad \text{(IV-13)}$$

where N = 290, a = 3 inches, r = 11.5 inches

For a pair of coils, arranged as shown in Figure IV.7a, B_Z along the X axis of the tunnel is calculated and shown in Figure IV.7b. The slope of the magnetic field per amp is:

$$\boxed{B_{XZ}/I = 0.1314 \text{ gausses/inch/amp} = 0.5173\times10^{-3} \text{ teslas/m/amp}} \qquad \text{(IV-14)}$$

IV.2 Measured Data

Coil resistances are measured to check the system characteristics before the magnetic field measurement. The results are given in Table IV.1. The field intensities of various coils are measured using a BELL640 Incremental Gaussmeter. For all tests, the

Table IV.1 Coil Resistances

Coil Name	R (Ω)
Helmholtz Coil (H_X - Bias field)	1.5
Drag Coil (H_{XX} -Gradient Field)	2.1
Inner Saddle ($H_{t(in)}$)	0.3
Outer Saddle ($H_{t(out)}$)	0.5
Lift Coil (H_{ZX})	1.0
Side Force Coil (H_{YX})	1.0

Table IV.2 Bias Field Strength at I = 3 amps, y = 0, z = 0
(Plotted in Figure VI.8)

Position x (inches)	-3	-2	-1	0	1	2	3
Field Strength B (gausses)	43	43	43	43	43	43	43

Table IV.3 Gradient Field Strength at I = 3 amps, y = 0, z = 0
(Plotted in Figure IV.8)

Position x (inches)	-3	-2	-1	0	1	2	3
Field Strength B (gausses)	15.6	10.5	5.9	0	-6	-10.2	-15.6

current applied to the coil is 3 amps. The direction of the vector **B** is found by rotating the probe until the output reaches a maximum.

IV.2.1 Helmholtz Coils

For the Helmholtz coil system, the bias and gradient fields were tested separately. Experimental data are listed in Table IV.2 and IV.3, and plotted in Figure IV.8. Comparison with the computational results given by Equations IV.4 and IV.7 shows the performance of the Helmholtz coil system is satisfactory.

$$\boxed{B_X / I = 14.33 \text{ gausses/amp} = 1.433\times10^{-3} \text{ teslas/amp}} \quad \text{(IV-15)}$$

$$\boxed{B_{XX} / I = 1.67 \text{ gausses/inch/amp} = 6.57\times10^{-3} \text{ teslas/m/amp}} \quad \text{(IV-16)}$$

IV.2.2 Saddle Coils

One of the inner saddle coils was tested, and the results were assumed to represent the performance of the entire coil system. Experimental data are listed in Table IV.4 and plotted in Figure IV.9. The magnetic field per amp generated by the half inner saddle coil is

$$\boxed{B_{t(in)} / I = 3.1 \text{ gausses/amp} = 0.31\times10^{-3} \text{ teslas/amp}} \quad \text{(IV-17)}$$

Note that this value is very close to the estimated value given in Equation (IV-11).

IV.2.3 Lift and Side Force Coil Assemblies

Only one of the eight coils which comprise the lift and side force assembly is tested. The data are given in Table IV.5. The performance of a pair of coils and the whole lift system (four coils total) are plotted in Figure IV.10a and b by superimposing the fields generated by the other three coils assuming the same characteristics. The slope of B_Z in the test section is quite uniform, which is shown in detail in Figure IV.10c.

$$\boxed{B_{xz}/I = 0.987 \text{ gausses/inch/amp} = 3.886\times10^{-3} \text{ teslas/m/amp}} \qquad \text{(IV-18)}$$

This value corresponds to the estimated value given in Equation (IV-14). The significant discrepancy between this measured value and the estimated value is discussed in Section IV.4.

Table IV.4 Half Inner Saddle Coil Field Strength at I = 3 amps, y = 0, z = 0 (Plotted in Figure IV.8)

x (inches)	-7.5	-2.5	0	2.5	7.5
Field Strength B (gausses)	2.7	9.3	9.3	9.3	2.25

Table IV.5 One Lift Coil Field Strength at I = 3 amps, y = 0, z = 0 (Plotted in Figure IV.9)

x (inches)	-17.5	-12.5	-10	-7.5	-2.5	0	2.5	7.5	12.5	17.5
Field Strength B (gausses)	12	22.2	24	19.8	8.6	4.9	3	1.14	0.5	0.36

IV.3 Computational Results

A finite element method of computing the magnetic flux density is developed to provide designers with a good reference. This method can also properly represent the iron core effect which should explain the discrepancy between the estimated values and experimental data. The finite element code used to compute the magnetic fields is TOSCA, by Vector Fields Incorporated. This software is a commercial product which has

been used by NASA for several years. By inputting the geometries of the coils as well as the positions and geometries of the iron cores, the code gives the magnetic flux intensity distribution in a three-dimensional space. The three-dimensional stationary electromagnetic fields B_X, B_{XX}, and B_{XZ} are computed. Results for the transverse field $B_{t(in)}$ and $B_{t(out)}$ have not been calculated at this time. Figure IV.11 shows the model of the Helmholtz coils as well as the bias field density. Figure IV.12 gives the gradient field created by the anti-symmetric coil windings; note that the variation of the magnetic field in the test section (-0.0768 m to 0.0768 m) is approximately linear. The field intensity, per amp, of a pair of coils in the lift and side force assembly is computed using a model which includes both the coil and the iron core (Figure IV-13). The model assumes a simplified geometry which neglects the effects of fillets in the corners and the copper plating of the iron core poles. The computed fields are given in Equations (IV-19, 20 and 21) below:

$$\boxed{B_X / I = 11.78 \text{ gausses/amp} = 1.178\times10^{-3} \text{ teslas/amp}} \quad \text{(IV-19)}$$

$$\boxed{B_{XX} / I = 1.31 \text{ gausses/inch/amp} = 5.1558\times10^{-3} \text{ teslas/m/amp}} \quad \text{(IV-20)}$$

$$\boxed{B_{XZ} / I = 1.52 \text{ gausses/inch/amp} = 5.98\times10^{-3} \text{ teslas/m/amp}} \quad \text{(IV-21)}$$

IV.4 Discussion

The three sets of results are compiled in Table IV.6. Note that the computational and test values are all found to be within 44% of the estimated values except for B_{XY}. However, the computational result, which includes the iron core effect, is very close to the test value. Thus one conclusion is that the magnet system still works as it was originally designed. Another conclusion is that the iron cores can greatly increase the magnetic field strength, in this case about 7.5 times.

For B_x, it is not unusual to find that the estimated value exactly matches the computational value, since the simple geometry of the Helmholtz coils allows the flux density to be estimated using the same exact integral which is used to obtain the computational value. However, these two sets of data do not take into account the iron core effect brought on by the coil assemblies located adjacent to the Helmholtz coils. The same effect can be seen in B_{xx}, although the estimated and computational values differ slightly due to the simplified geometry used for the estimated value. The relatively large discrepancy between the estimated and measured values of B_t can be attributed to the greatly simplified geometry (using coils of infinitesimal cross-section) assumed for the estimation. Note that a simplified geometry, which neglects the influence of the copper plating of the iron core poles, is also used to obtain computational values for B_{xy}. This assumption could result in the systematic error of the computed value.

Table IV.6 Comparison of Three Sets of Results for Magnetic Flux Density

	Estimation	Measurement	Computation
B_X /I (teslas/amp)	1.178×10^{-3}	1.433×10^{-3}	1.178×10^{-3}
B_{XX} /I (teslas/m/amp)	5.27×10^{-3}	6.57×10^{-3}	5.1558×10^{-3}
$B_{t(in)}$ /I (teslas/amp)	0.55×10^{-3}	0.31×10^{-3}	
$B_{t(out)}$ /I (teslas/amp)	0.558×10^{-3}		
B_{XZ} /I (teslas/m/amp)	0.5173×10^{-3}	3.886×10^{-3}	5.98×10^{-3}

Two other tests are performed in order to illustrate the effect of the iron cores. The first is a measurement of the magnetic flux through the test section created by one left coil at I = 3 amps. The result of this test is shown in Figure IV.14. Note that the measurement is identical to the design requirement shown in Figure III.3b. The next test involves measurement of the magnetic field strength distribution around the coil with the iron core. The results are shown in Figure IV.15. Again, note the magnitude of the field strength on the side toward the tunnel (zero-degree direction) is much higher than on the other side due to the iron core effect.

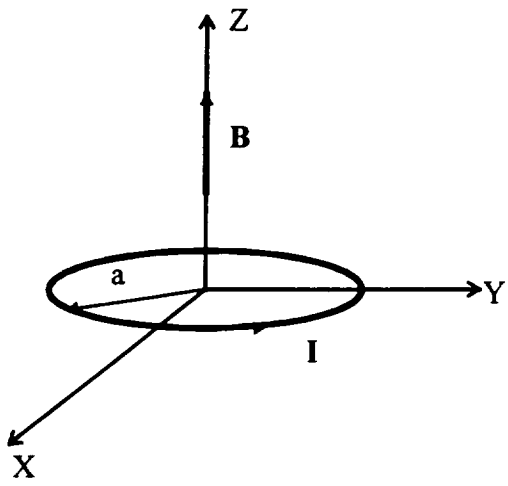

Figure IV.1 Magnetic Field Generated by a Single Loop

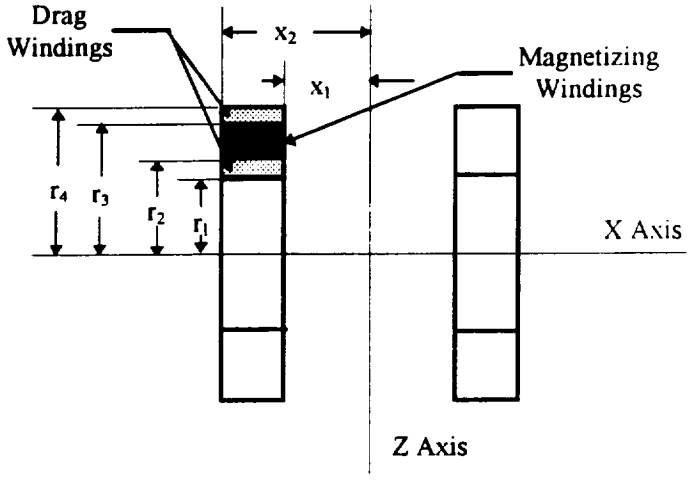

Figure IV.2 Helmholtz Coil Model

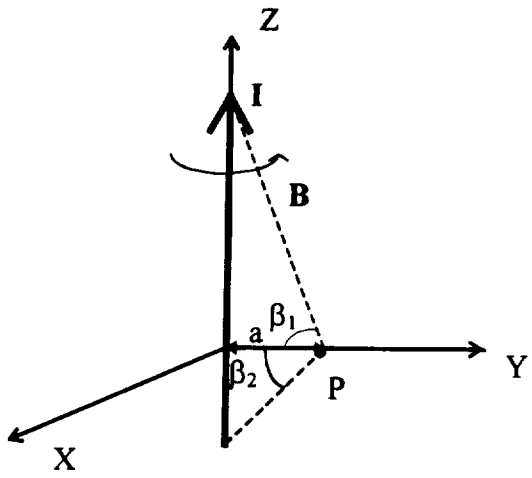

Figure IV.3 A Current Element

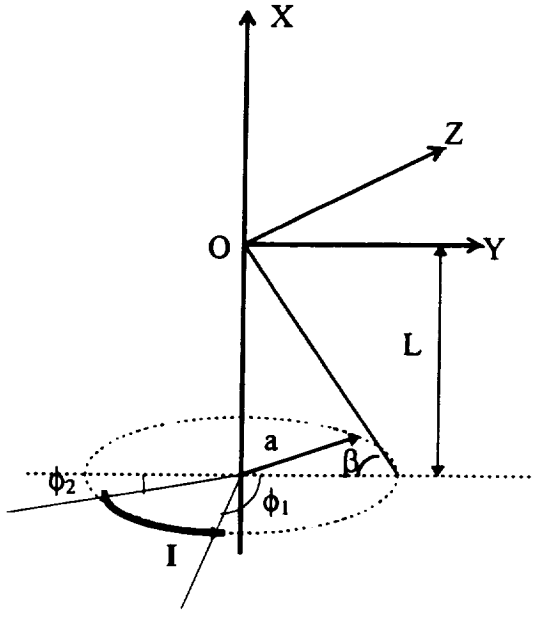

Figure IV.4 A Segment of Current Loop

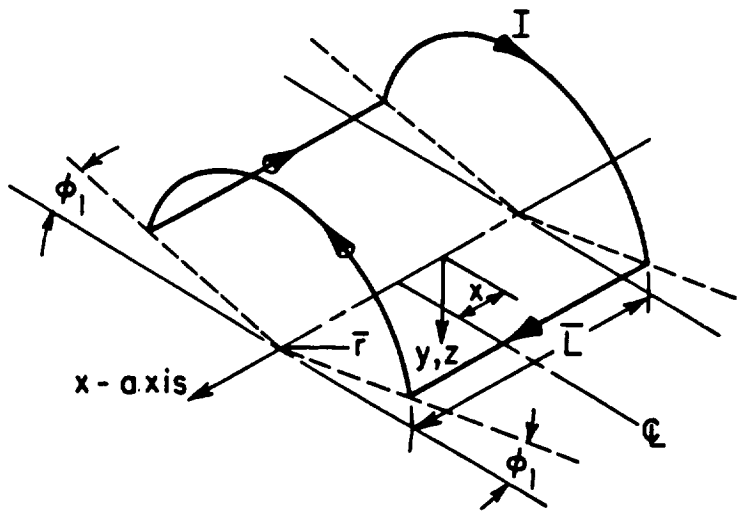

Figure IV.5 Saddle Coil Model

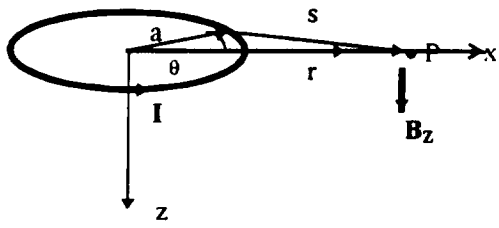

Figure IV.6 Lift Coil Model

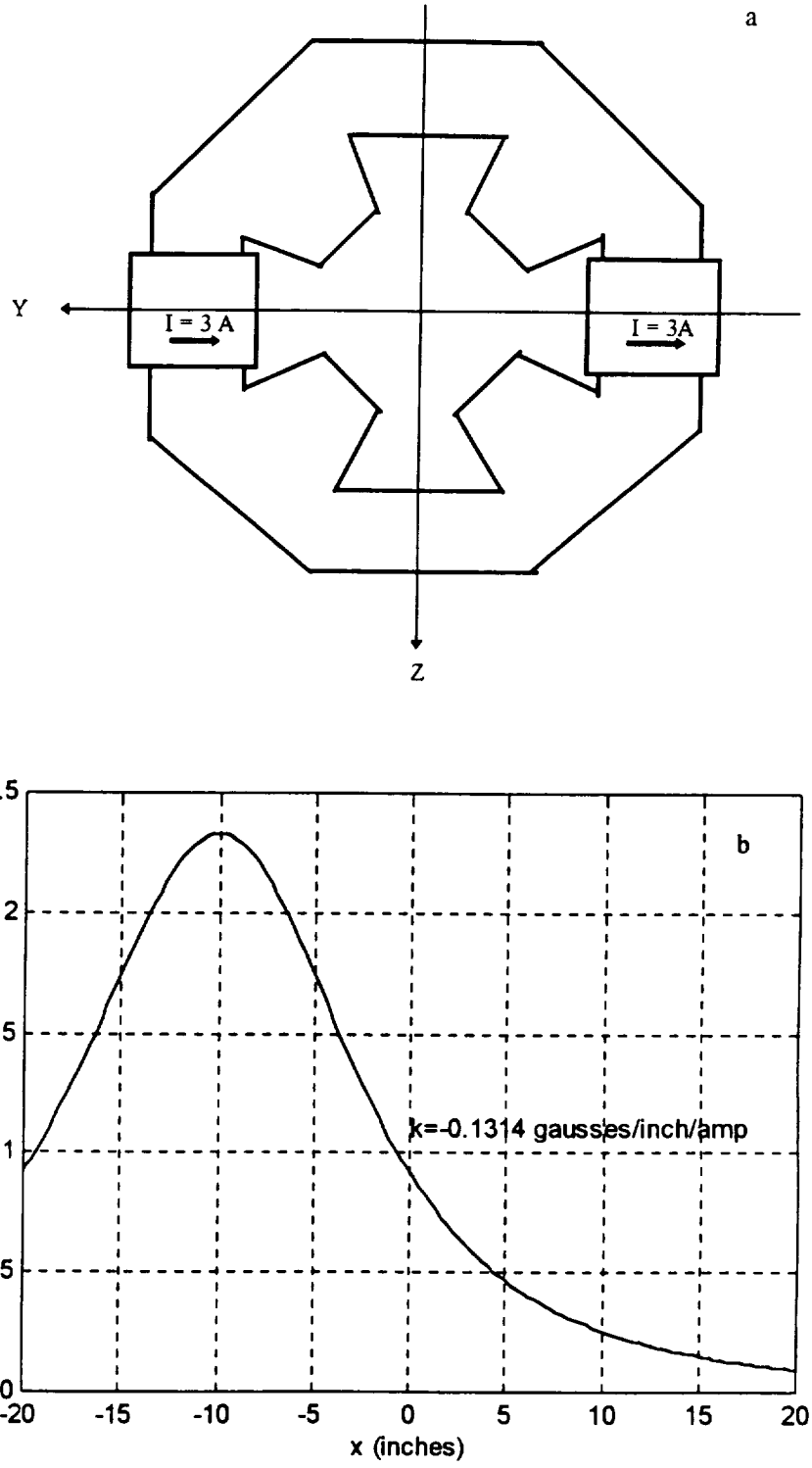

Figure IV.7 a. A Pair of Lift Coils
b. Estimation: Magnetic Field by Lift Coil at I = 3 A

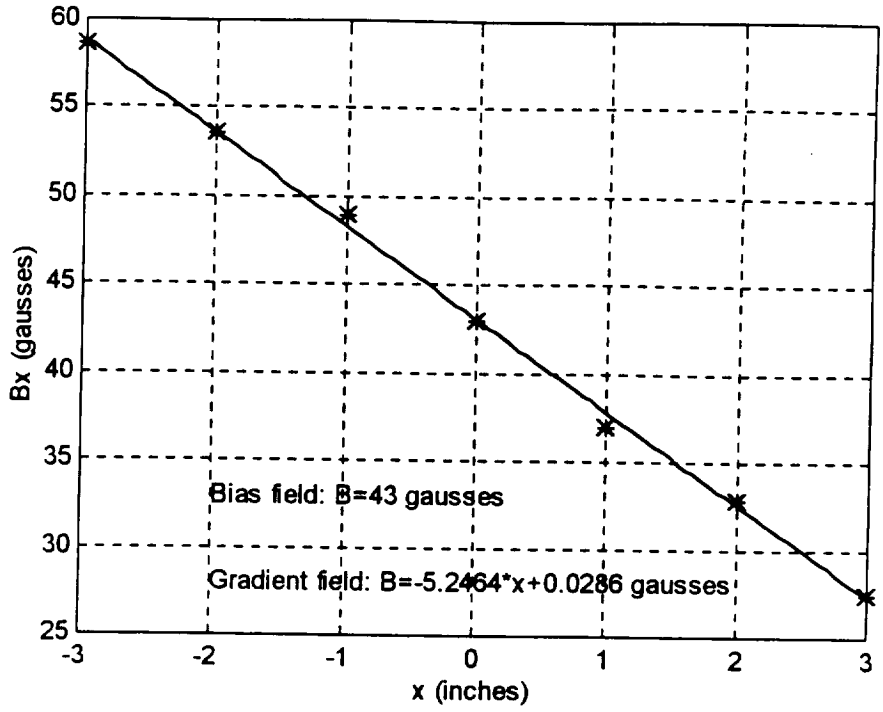

Figure IV.8 Measurement: Magnetic Field by Helmholtz Coil System at I = 3 A

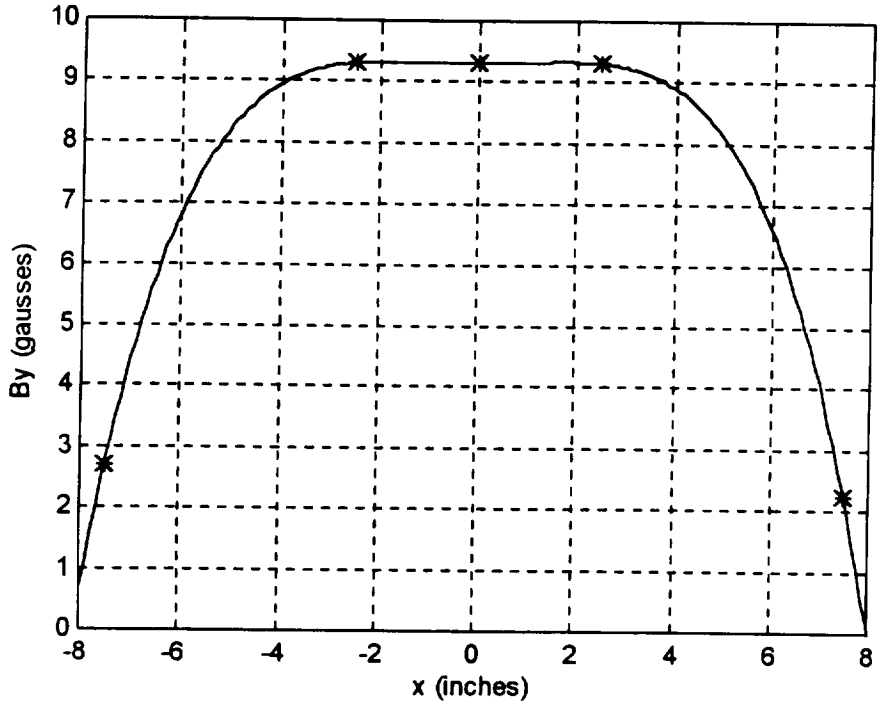

Figure IV.9 Measurement: Magnetic Field by Half Inner Saddle Coil System at I = 3 A

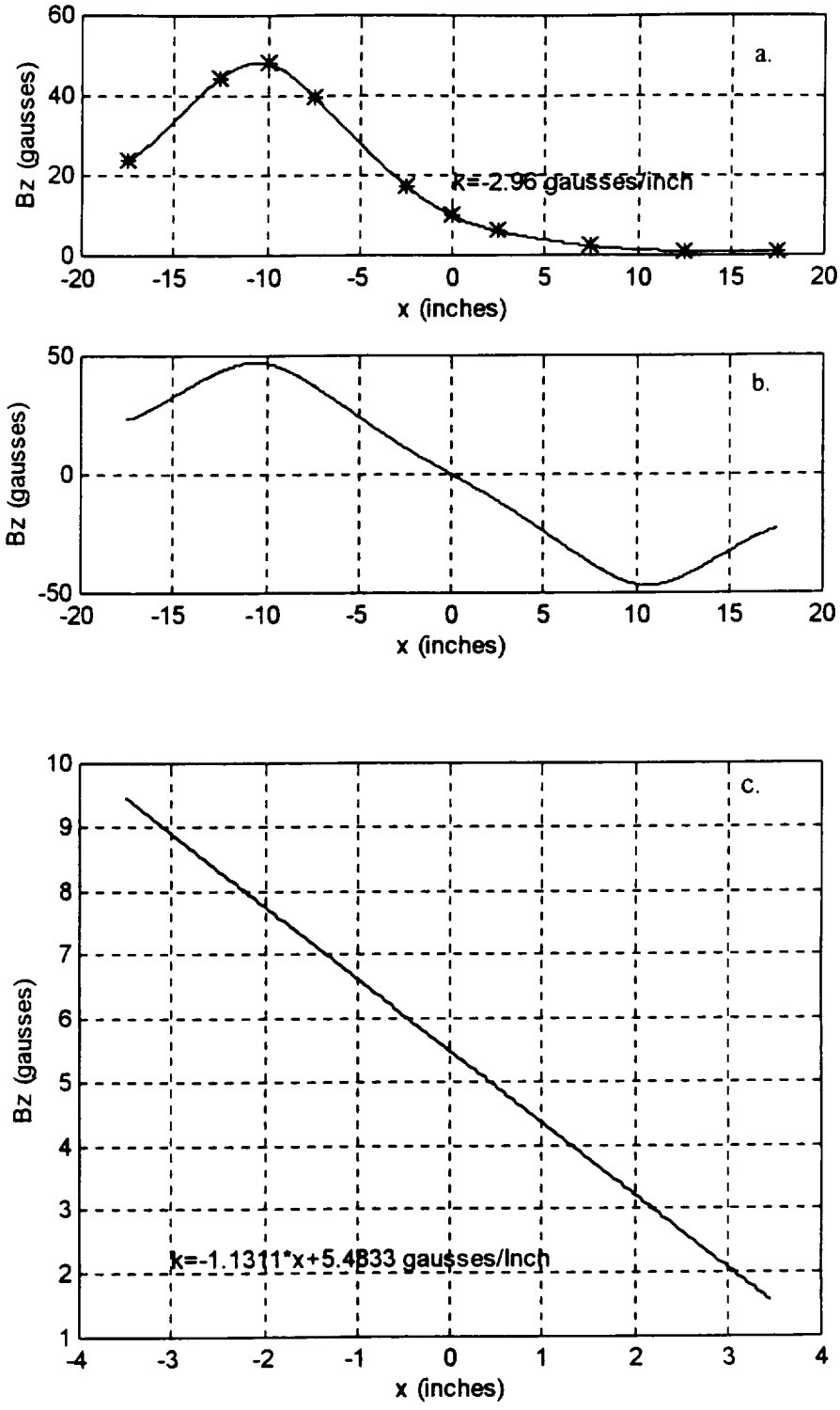

Figure IV.10 Measurement: a. Magnetic Field Along x-axis by a Pair of Coils at I = 3A
b. Magnetic Field Along x-axis by Coil Assembly at I = 3A
c. B_Z or B_Y by Coil Assembly at I = 3A

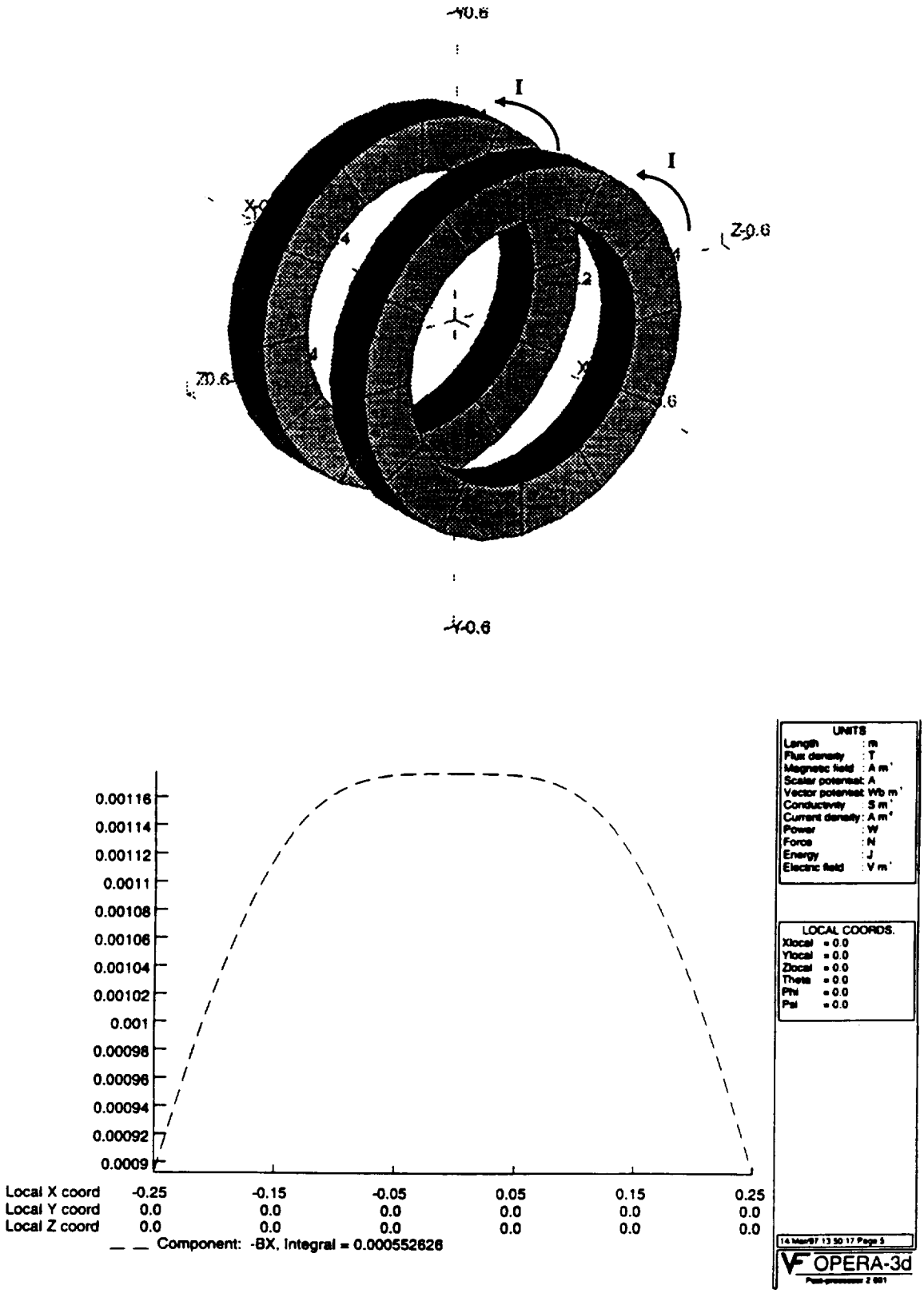

Figure IV.11 Computational Results: Bias Field by Helmholtz Coil System

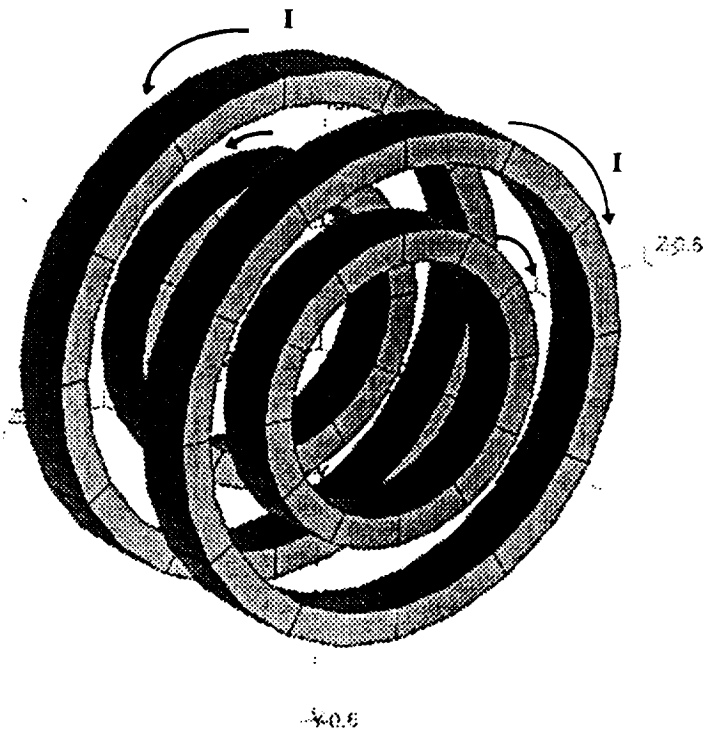

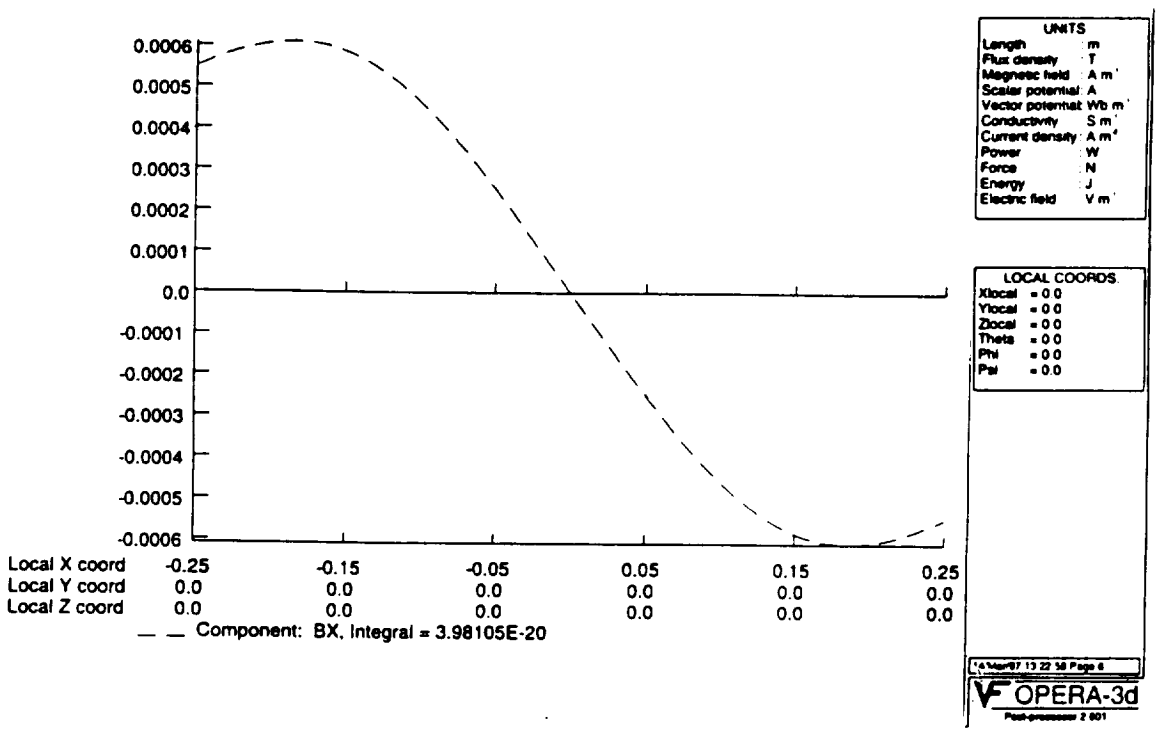

Figure IV.12 Computational Results: Gradient Field by Helmholtz Coil System

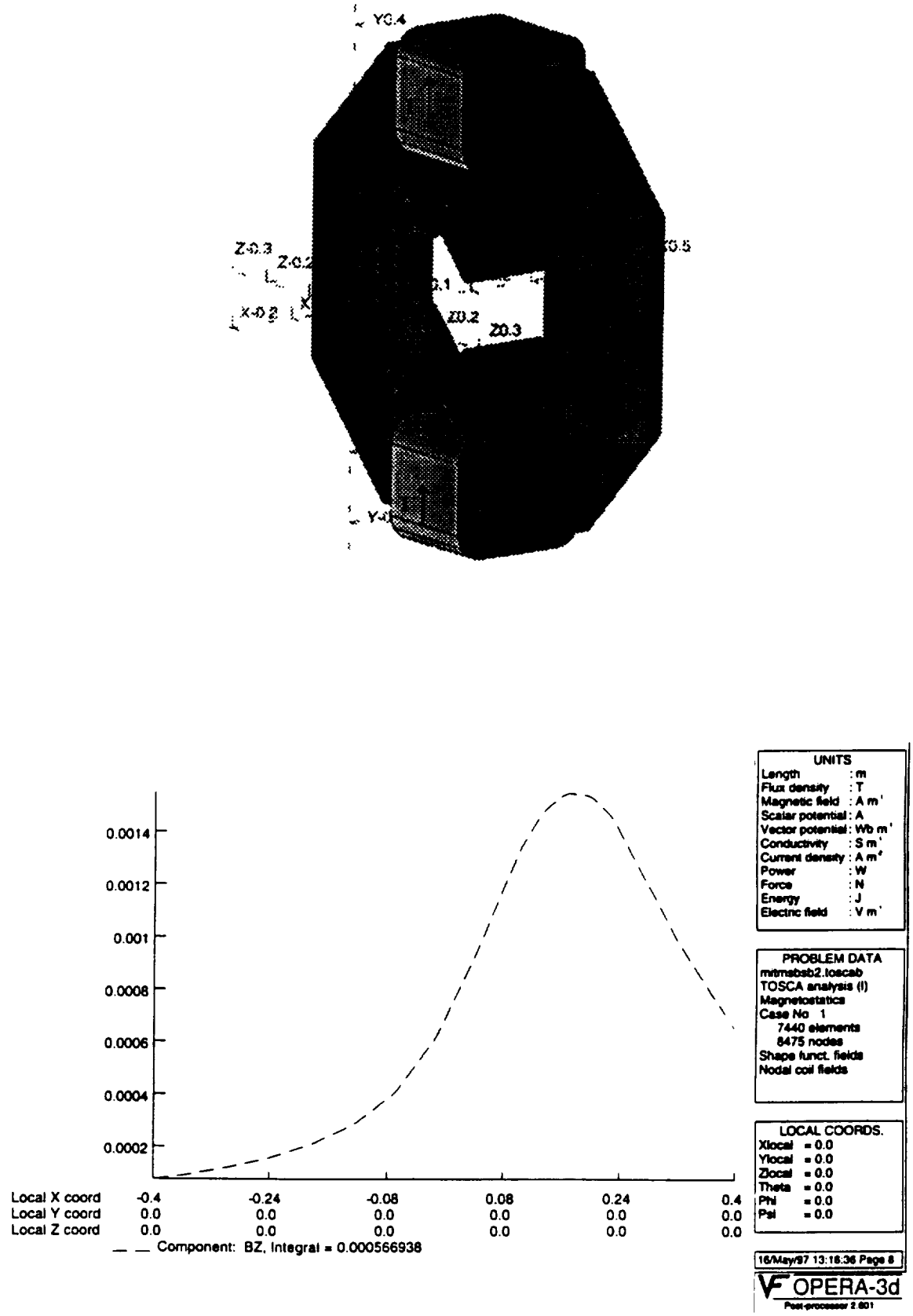

Figure IV.13 Computational Results: Gradients Field by Coil Assembly

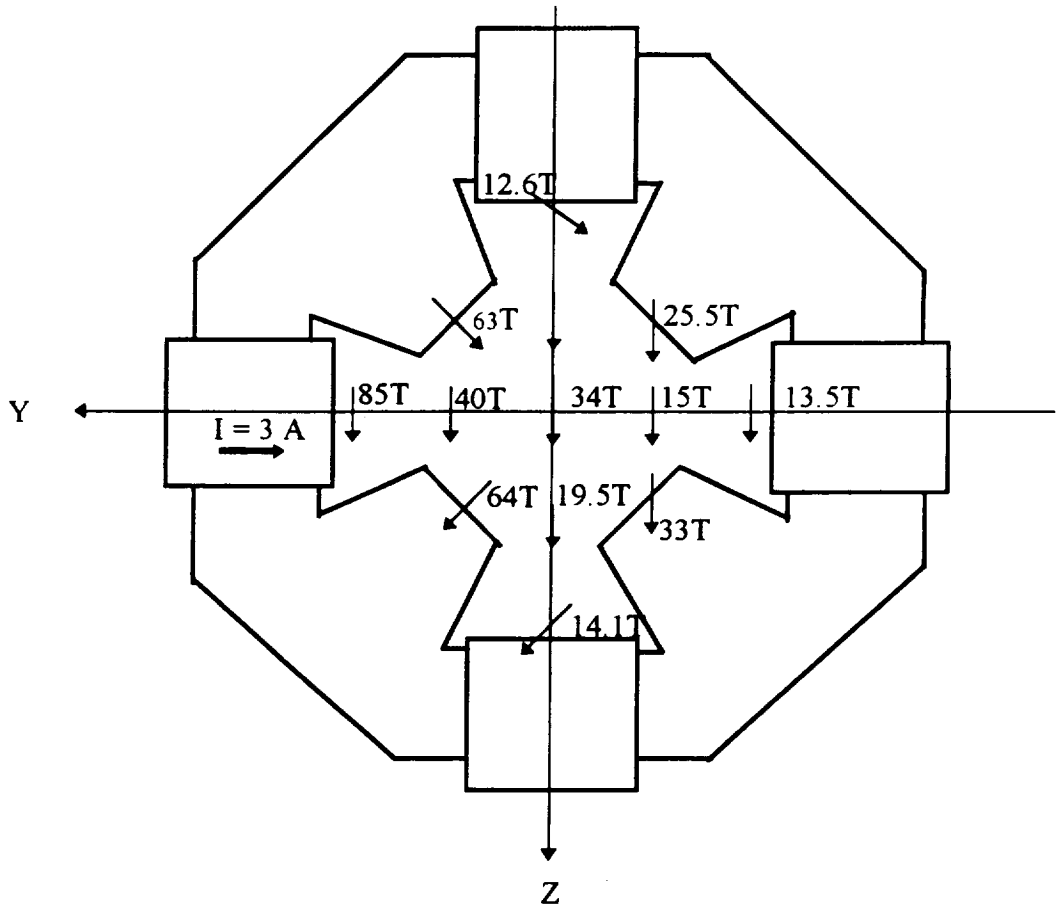

Figure IV.14 Magnetic Flux Path Generated by One Coil

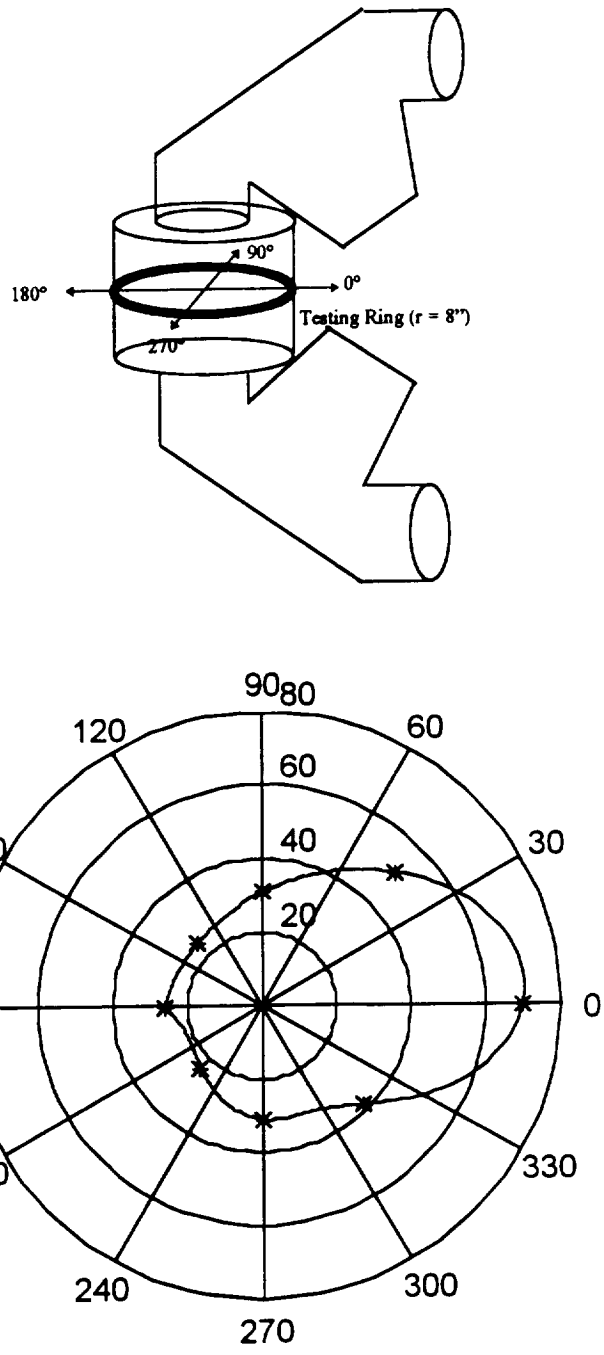

Figure IV.15 Magnetic Field Around One Coil at I = 3 A
(Radial direction is field strength in gausses)

CHAPTER V

CONTROL SYSTEM FOR THE ASPS

The Annular Suspension and Pointing System at the Department of Aerospace Engineering, Old Dominion University, was originally developed by Sperry Flight Systems (now Honeywell Satellite Systems) in the 1970s. Most of the system was loaned to ODU in 1992 by NASA Langley Research Center. The original analog control hardware of this system was replaced by a new digital controller. The hardware status of the Annular Suspension and Pointing System (ASPS) is described in detail by Neff [10] and Neff and Britcher [11]. Most of the modifications to the system since then have been related to the software. A general outline of the system, as well as detailed progress in the controller, is given in this chapter. The intention is that the control software be kept somewhat generic and used as the basis for the 6-inch MSBS controller in the future.

V.1 System Description

The ASPS, shown in Figure V.1, consists of a payload mounting plate, a Vernier Pointing Assembly (VPA), two coarse gimbal assemblies, a mounting and jettison assembly, control electronic rack and balance and testing fixture. The payload mounting plate is a machined aluminum structure with a mass of 12.02 kg, a diameter of 965.2 mm and thickness of 22.2 mm. It can be mounted directly to the gimbal mounting platform in the event that the VPA is not used during the flight.

The Vernier Pointing Assembly, shown in Figure V.2, is the main component of interest here. The VPA includes an annular iron rotor, five Magnetic Bearing Assemblies,

a roll motor, seven pairs of proximity sensors, five vernier latches, a roll resolver, rotary transformer, and battery packs. The suspended model is an annular iron rotor with a mass of 21.6 kg. The system has three axial magnetic bearings, named A, B, and C, spaced 120 degrees apart to levitate this rotor. The lateral position of the payload is controlled by two radial magnetic bearing assemblies, named U and V, which are located 90 degrees apart and ±45 degrees from the axial bearings. The roll motor is on the symmetric axis of the two radial bearings and opposite to one of the axial bearings. The five vernier latches are used to support the iron rotor during launch and recovery maneuvers.

Each magnetic bearing assembly uses a pair of sensors to detect the rotor position. An oscillator provides a 10 MHz, 30 V peak-to-peak signal used by the fourteen proximity sensor coils. The proximity sensors used on the ASPS are model KD-2300-12CU, a product of Kaman Instrumentation Corporation. The electromagnetic field generated by the sensor coils couple with the rotor, and changing gaps cause the impedance of coils to vary. The differential signals from each pair of sensors are then sent to a demodulator card to realize signal processing. The processing includes amplification, filtering, and demodulation and finally gives a linear output voltage.

It is interesting to compare the position sensors used in the two magnetic suspension systems. The proximity sensors used on the ASPS are off-the-shelf products, while the EPS used on the 6-inch MSBS is an experimental device developed specifically for this application. Also, the ASPS sensors can only be used to detect motion in a single degree of freedom, whereas the EPS can resolve motion in five degrees of freedom simultaneously. Both types are non-contacting sensors which use the principle of

impedance variation, where the coupling between a coil in a sensor and a target is dependent upon relative displacement.

The latches can locate the rotor at the center position in case the MBAs fail. To prevent damage to the MBAs, position sensors, and other delicate electronics when not in use, the rotor can be locked in the down position.

The roll resolver and rotary transformer are located at the center of the VPA. These two systems are used to measure the angular rotation and position of the payload. The rotary transformer is used to transfer power between the stationary base of the VPA and the payload. These two parts and the roll motor, which complete the roll control, are not used at the present time.

The control electronics rack is a free standing rack that connects to the VPA via flexible cables. It contains the power supplies and amplifiers to drive the MBAs and sensors. Two Copley Controls Series 661 unregulated D.C. power supplies produce 36 volts D.C. at a rating of 12 A maximum to power the six amplifiers which are needed to control the actuators. A voltage of ±15 volts D.C. is also needed to drive the oscillator card. Copley Controls Corp. 303 series amplifiers are applied in this system.

The controller, which includes data recording, computation and readout functions, is realized by a digital computer, a timer, and two data acquisition boards. Keithley Data Acquisition provides two interface boards to realize A/D and D/A conversions. The DAS-1402 is a multifunction, high-speed, analog-to-digital interface board for IBM and compatible computers. This board offers 8 differential or 16 single-ended analog inputs with 12-bit resolution at 100 k samples/sec. The DAS-1402 can be set for both unipolar

(0-10 V) or bipolar (±10 V) signals. DDA-06 is a digital-to-analog I/O expansion board providing 6 channels of 12 bit analog output and 24 lines of digital I/O. A timer board is also needed to control the sampling rate and handle interrupts. A DT2819 counter/timer board includes an Am9513A System Timing Controller, and provides a software-selectable 5 MHz or 1 MHz base frequency and a single interrupt which is configurable from level 2 to 7.

V.2 Model Establishment

The block diagram in Figure V.3 shows the ASPS control scheme. The position information of the rotor is acquired by proximity sensors. The signals from the sensors are then converted from analog to digital and compared to the commanded position to derive the error signals. Input data are processed via a proportional plus derivative controller. The output signals are then converted back into analog form to drive the actuators. The position of the rotor is sensed continuously and fed back to the computer to maintain system stability.

Each dynamic component in the feedback loop (shown in Figure V.4) has been established discretely either through known physical features of the hardware or by testing [10, 11]. The parameters are listed in Table V.1. Note that, to simplify the system, the transfer functions of the actuators relating the current (i) to the force (F), have been linearized near the steady-state point [10, 11]. The open-loop transfer function of the forward path is:

$$G(s) = (K_p + K_d s)\frac{349.49}{0.0327s^3 + 7.19s^2} \qquad \text{(V-1)}$$

The design process for the PD controller is summarized in Figure V.5. Note that due to unit conversions, the actual values of the gains used in the code differ from those given in the controller transfer functions. In Controller I, the values of the proportional gain K_P and derivative gain K_D were determined by Neff and Britcher [11] using the MATLAB Control System Toolbox. Choosing the ratio $\frac{K_D}{K_P} = 0.1$ yields

$$G(s) = K_p \frac{349.49 + 34.949s}{0.0327s^3 + 7.19s^2} \qquad \text{(V-2)}$$

From the root locus of the system shown in Figure V.6, it can be seen that the closed-loop system will remain stable for a range of K_P from 0 to $+\infty$. The values of K_P and K_D were chosen to be 4.5 and 0.45, respectively, to give a damping ratio of 0.7. However, the real system cannot maintain stability using this design. The actual values used in Neff's code [10] were 403 and 5.5 for K_P and K_D, respectively. These values were determined experimentally, and the new controller using these values is designated Controller II.

Table V.1 Constants Used in Transfer Functions

K_A	τ	μ_0	N	I_0	S	g_0
1.021 A/V	0.00455 sec/rad	$4\pi\times10^{-7}$ H/m	810 turns/coil	1.25 A	1641.7 mm^2	3.41 mm
m	$K_S(A)$	$K_S(B)$	$K_S(C)$	$K_S(U)$	$K_S(V)$	$K_S(W)$
7.19 kg	0.00284 mm/count	0.00308 mm/count	0.00456 mm/count	0.00115 mm/count	0.00111 mm/count	0.00100 mm/count

This work begins with the verification of the transfer functions used by Neff [10]. The model parameters are checked and found correct. The next step is a retuning of the system using an improved code, which is introduced in the next section. The new code

gives values of K_P and K_D of 440 and 4.5, respectively. A new controller is then introduced using these values, designated Controller III. Note that these gains are very close to those in Controller II. It appears that the ratio K_P / K_D should be 0.01, instead of 0.1, to levitate the rotor and maintain system stability. The root locus diagram for Controller III is shown in Figure V.7. The system can also maintain stability for a range of K_P from 0 to $+\infty$. The responses in position of the theoretical controller (Controller I) and the actual working controller (Controller III) to a step input are also given in Figure V.8. By comparing these two responses, it can be seen that while Controller III has a shorter settling time, Controller I has a significantly smaller overshoot. Although Controller I appears in theory to be a better design in some respects, it is based upon simulations for linear systems and does not take into account the aerodynamic damping factor, determined by the physical features of the rotor (large surface areas). Due to these modelling inaccuracies, Controller I does not perform well in reality.

Finally, an integral term is added to the controller to minimize steady-state errors (Controller IV). After running this controller with the integral term turned off and tuning the system to satisfy the stability requirement, integral control is activated by a switch in the software. A suitable value of K_I is determined experimentally to be 3.7.

The actual process of tuning the controller involves experimentally determining the exact values of these gains which yields satisfactory performance. For the axial MBAs, the reference voltage corresponds to a current which will generate enough force to offset gravity. K_P is chosen to provide stiffness, driving the system back to a desired datum, when a disturbance is encountered. The primary role of K_D is to maintain system stability,

while also affecting the rise time and overshoot. The value of K_D should be around one hundredth K_P; an excessive value could cause system vibration. Once the PD controller is working properly, the integral term can be activated to minimize the steady-state error. If the system is moved away from the balance position due to a steady disturbance, in this case a non-conducting weight added to the rotor, the gain K_I performs the function of driving the rotor back to the balance position within a small time period.

V.3 Controller Software

The controller software is written in Microsoft Quick C. The timer board and the associated software driver are supplied by Data Translation, and the data input/output interface and its software driver are supplied by Keithley Data Acquisition. Both software drivers are C-compatible.

A flow chart comparison of the original program and the revised program is given in Figure V.9. In the original code, the controller was included within the main program loop and was executed repeatedly until the exit command was given. Since other functions such as keyboard input and data output must also be accommodated within this main loop, the sampling rate and controller execution were driven by the time required to perform these other functions. The sampling rate was thus chosen to be fairly slow at 100 Hz, and data output could be viewed only after turning off the controller since it takes relatively long time. Although communication between the D/A, A/D, and timer boards was established and the iron rotor was successfully suspended, the system was not sufficiently robust to resist a significant artificial disturbance, in this case, a nudge away from the

commanded position. In real world application, external disturbances might come from vibrations of the base, or disturbance forces on the payload.

The revised program improves the system's performance in several ways. First, a timer board was used to interrupt execution of the main program at the sampling frequency of 200 Hz. When interrupted, program execution jumps to a subroutine which acquires analog position data, performs the A/D translation, data calculation, and D/A translation. This modification was made so that other functions, such as keyboard interrupt and data output which require relatively longer periods of time (e.g. archiving data to disk), would not affect the sampling rate. When the subroutine is completed, execution returns to the main program at the point where it left off. Second, an integral term is added to the controller to achieve zero steady-state error. Third, a screen output table is designed to show the system status while the program is running. All 15 parameters including reference voltage U_{ref}, the proportional gain K_P , the derivative gain K_D and the integral gain K_I for the MBAs can be adjusted in real time, during program execution to determine the optimum value of these constants. These real time inputs are realized by the keyboard subroutine which executes at the end of the data readout loop. Also, the increase in sampling rate from 100 Hz to 200 Hz results in better controller resolution and is helpful for the reduction of noise. The last 10 sets of data which includes all the controller gain and system performance information are saved in array format and written into file DATAOUT.ASC.

The controller tuning process is greatly simplified since real-time data can be read from the screen directly. The axial bearings A, B, and C are tuned before the radial

bearings U and V. Each axial MBA is tuned individually, with the others deactivated, to avoid coupling. When the three axial bearings have been tuned, the rotor is levitated and the radial bearings U and V are tuned.

The test results show that the system's performance has been improved remarkably. The system is now more stable, and due to the increase in sampling rate, is less noisy and has a greater resistance to external disturbances. Figures V.10 and V.11 show the position errors of the five MBAs as a function of time. From the figures it can be seen that the position error of the MBA A is within ±0.2 mm while the original error is about ±0.5 mm [10]. The errors of MBAs B and C have also been reduced. Errors in the radial directions (MBAs U and V) are slightly less, at about ±0.05 mm. Standard deviations (root mean square) for five sets of data (from the 5th second to the 10th second) are listed in Table V.2.

The revised program, as well as a testing program which is used to check if the timer board works properly, is given in Appendix C.

Table V.2 Standard Deviations (STD) of the Position Errors

	A	B	C	U	V
STD (mm)	0.0583	0.0565	0.1138	0.0251	0.0143

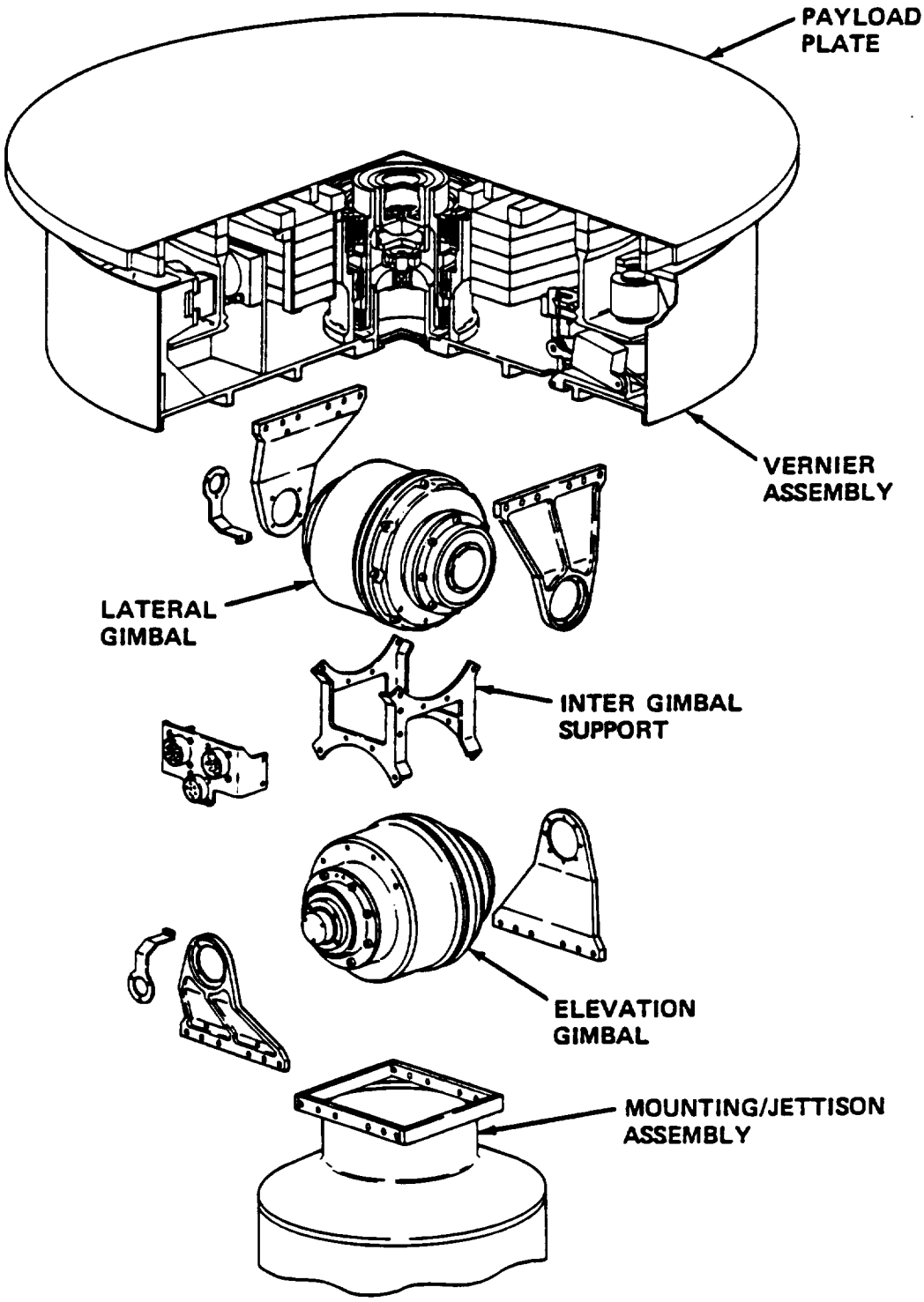

Figure V.1 The ASPS Component Breakdown

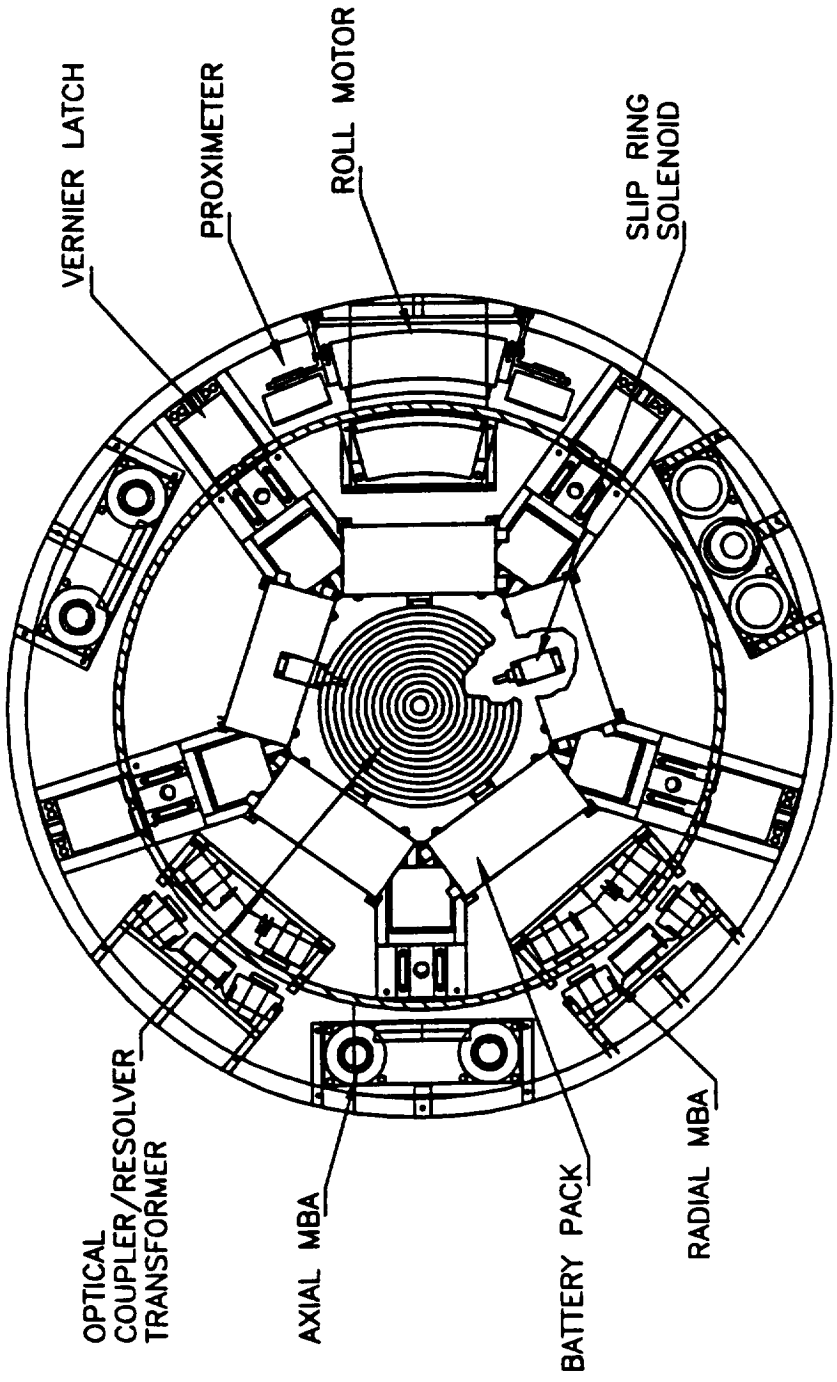

Figure V.2 VPA Layout

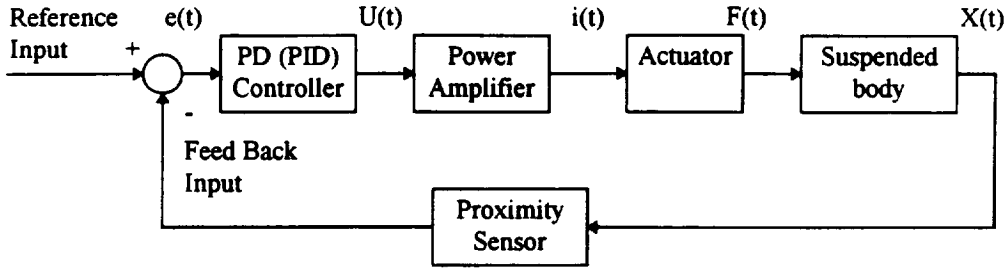

Figure V.3 System Diagram of the ASPS System

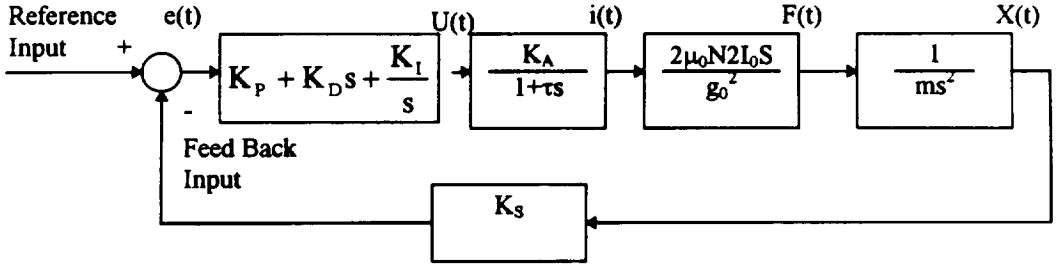

Figure V.4 Transfer Function of ASPS Control System

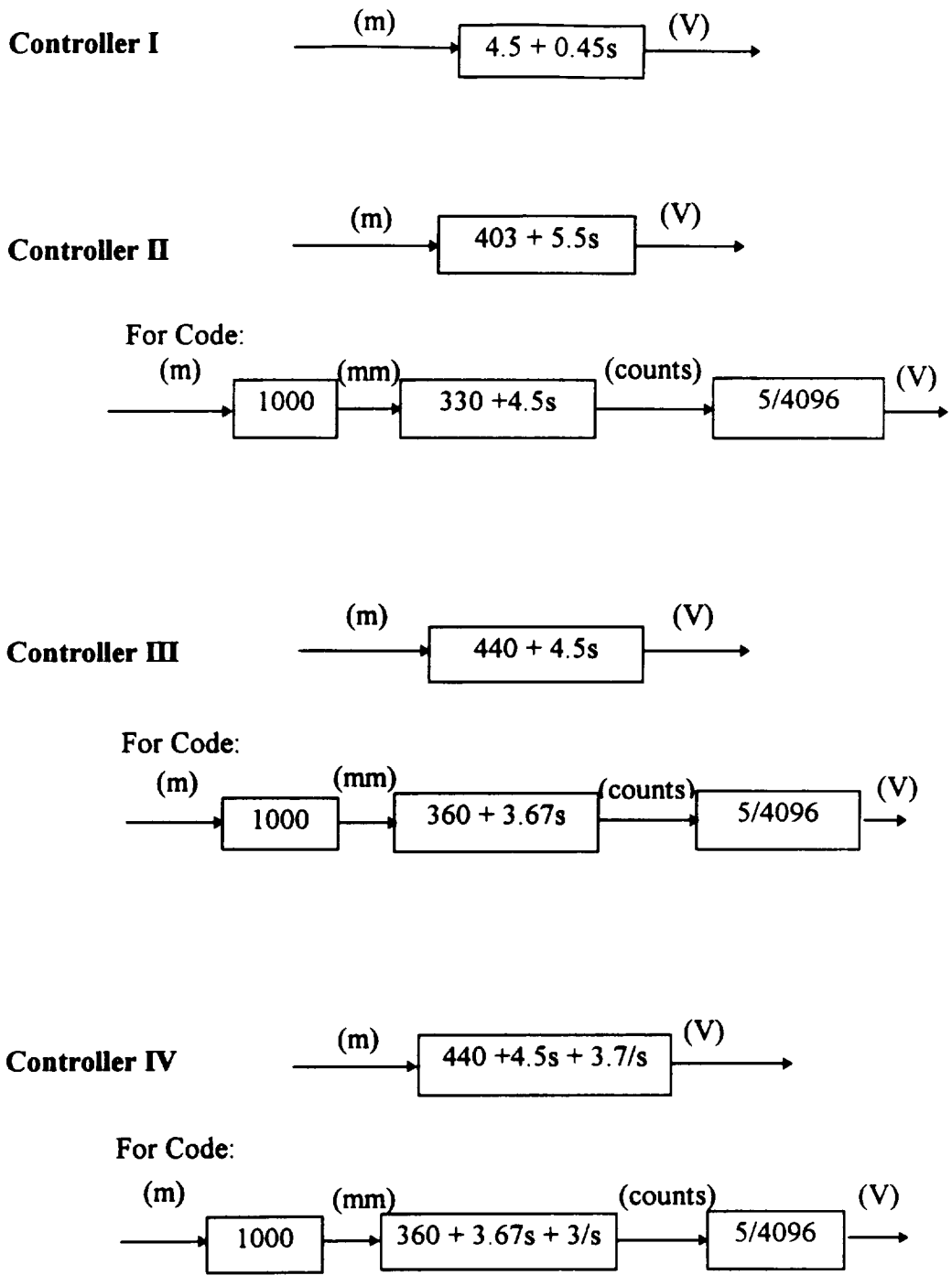

Figure V.5 Controller Design Comparison

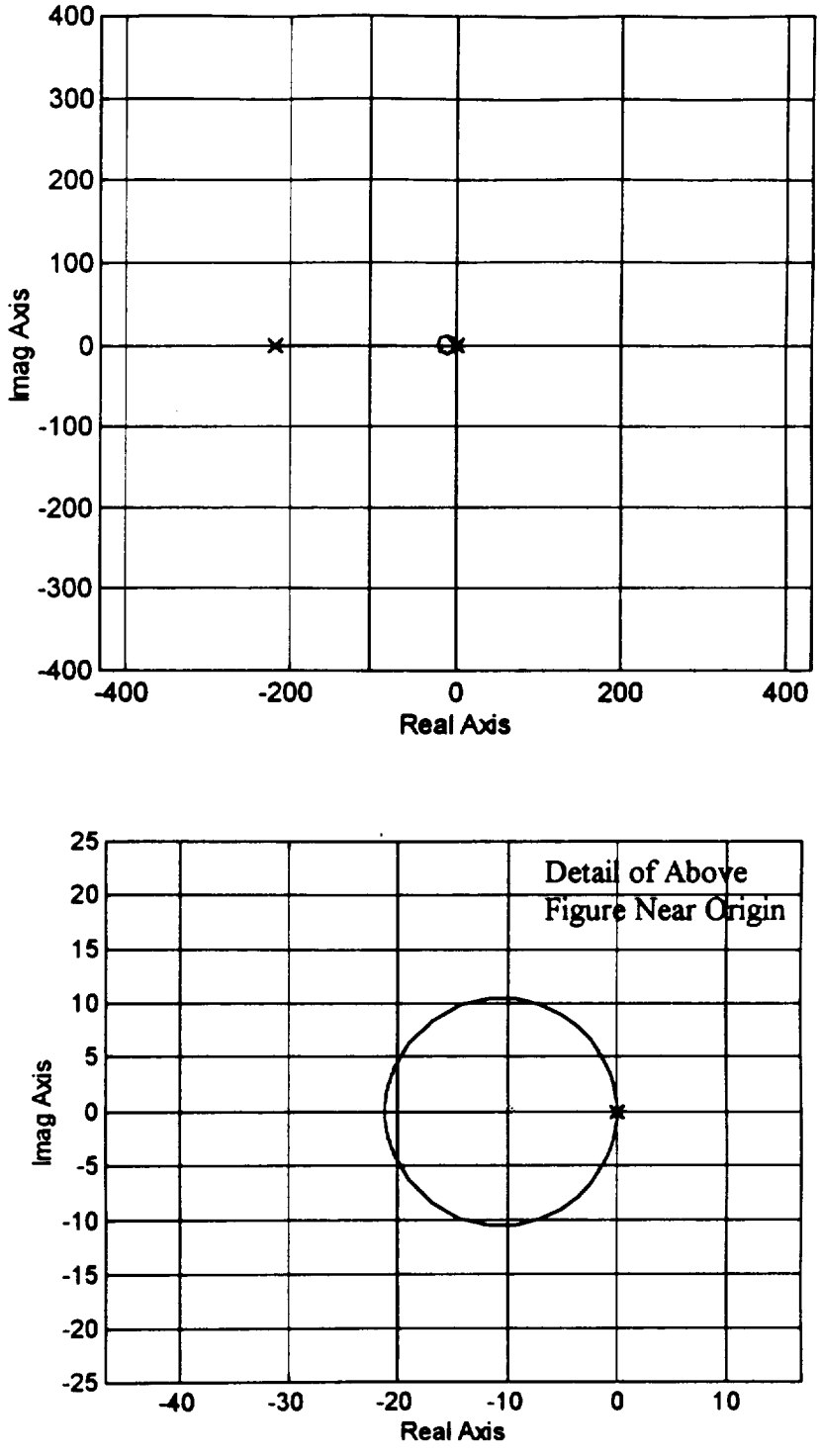

Figure V.6 Root Locus of Controller I (all axes have units of seconds^{-1})

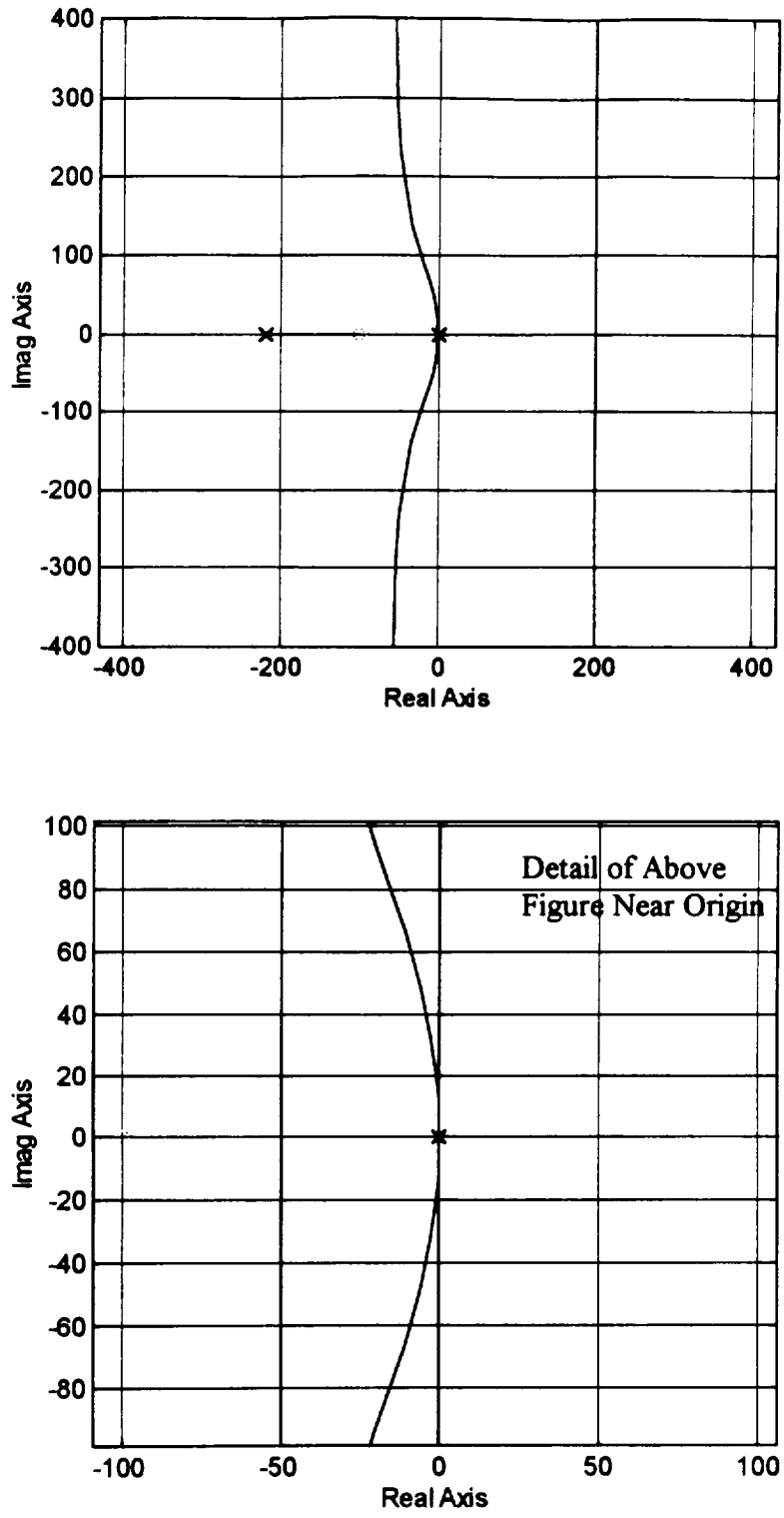

Figure V.7 Root Locus of Controller III (all axes have units of seconds^{-1})

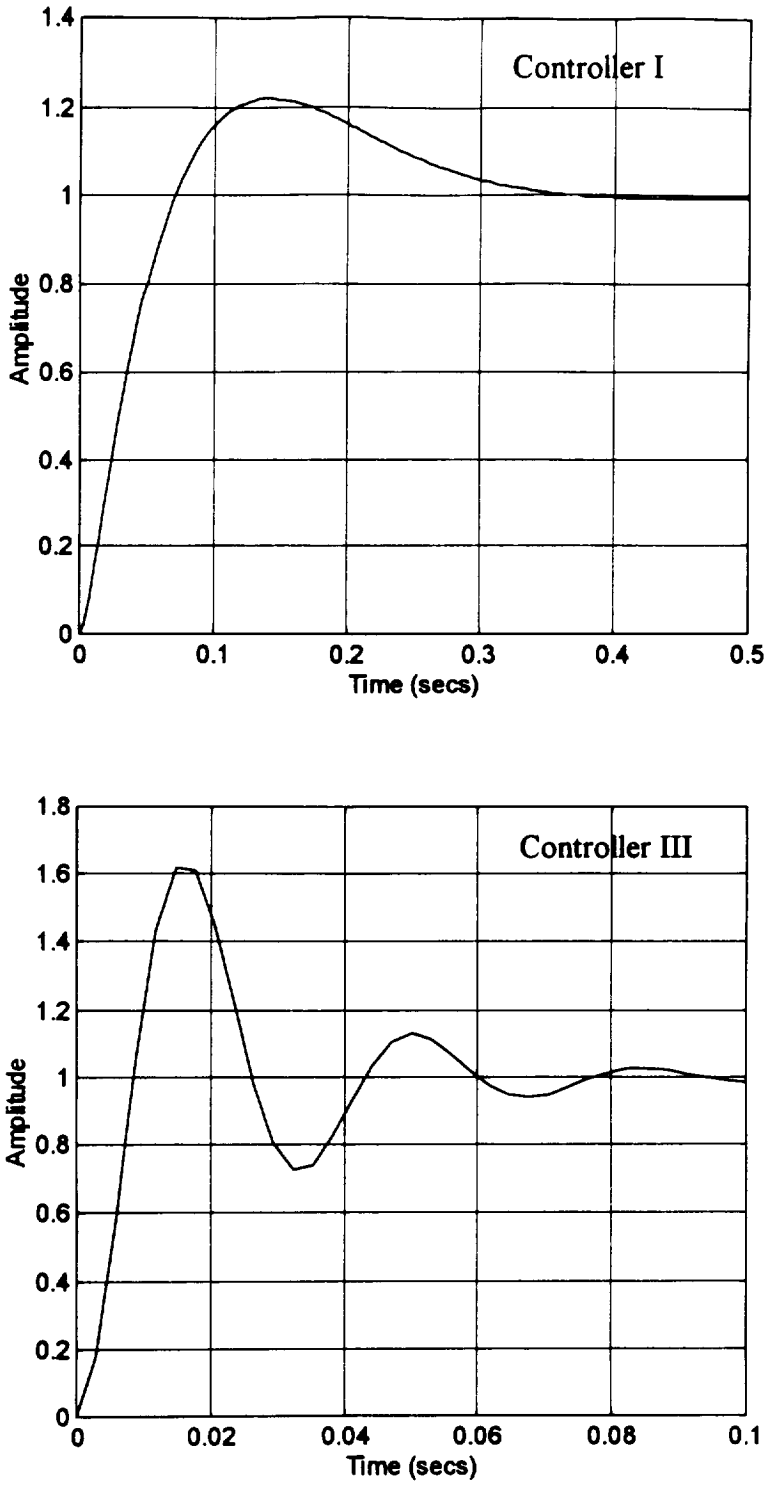

Figure V.8 Unit Step Responses of Controllers I and III (non-dimensional position)

Original Program

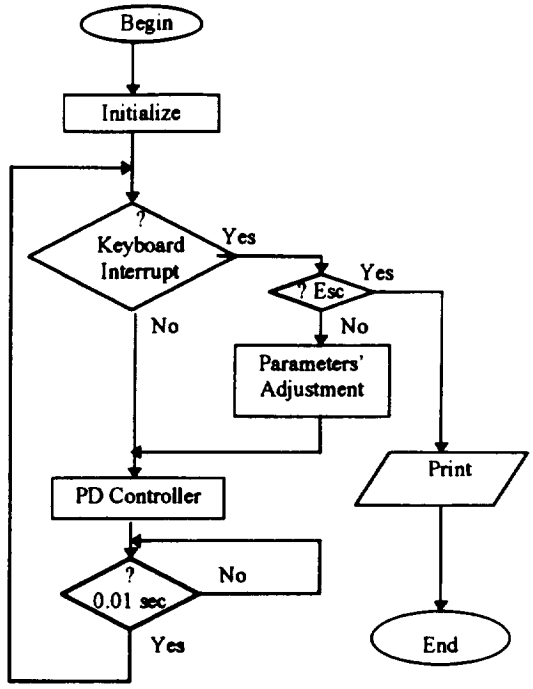

Revised Program

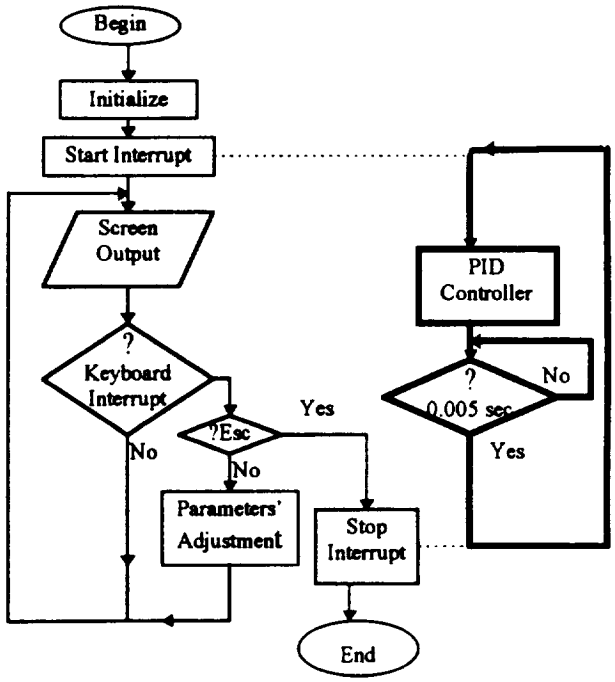

Figure V.9 Flow Chart of Control Program (secondary loop in revised program accessed via timer board interrupt)

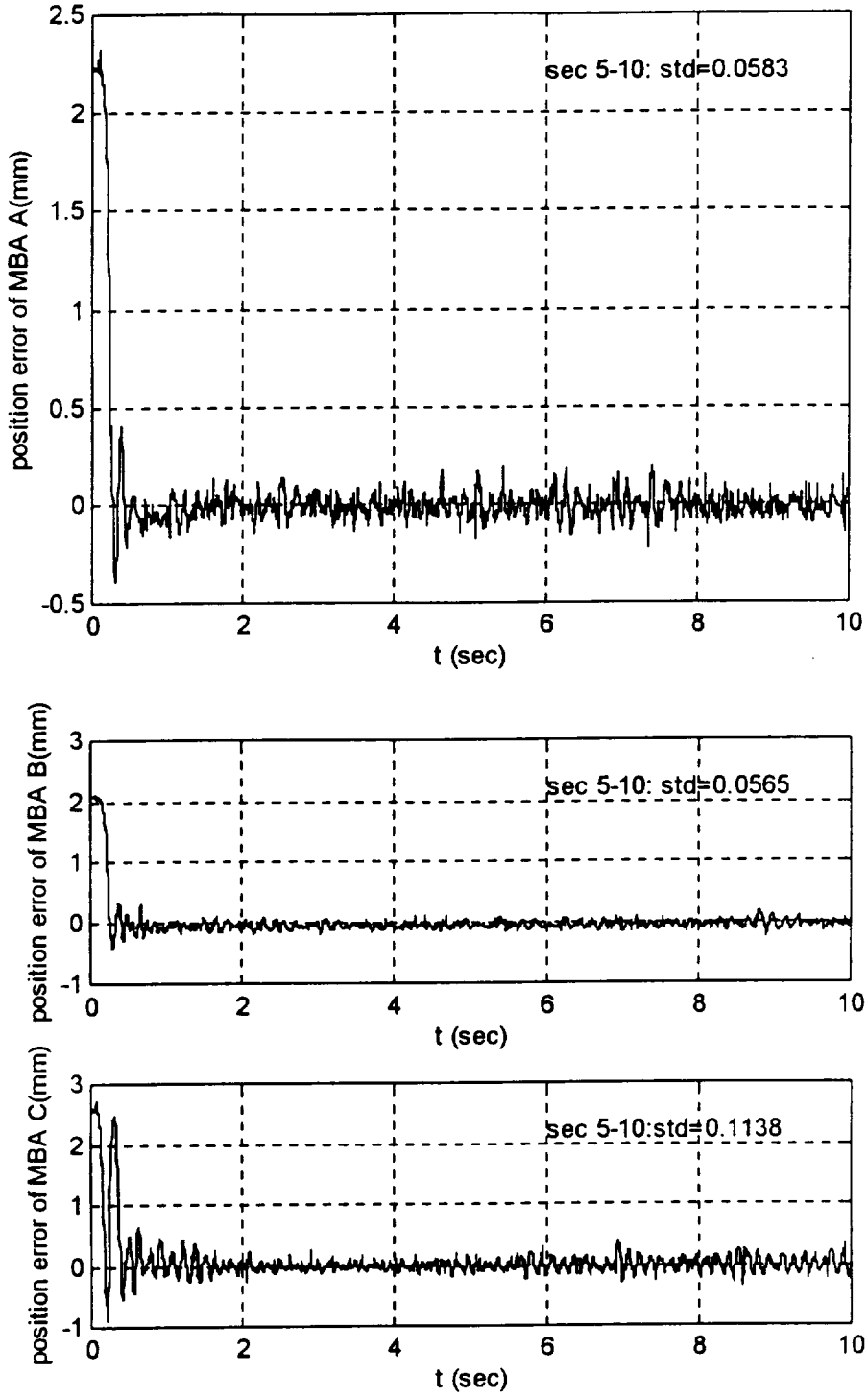

Figure V.10 Time History of Axial MBA

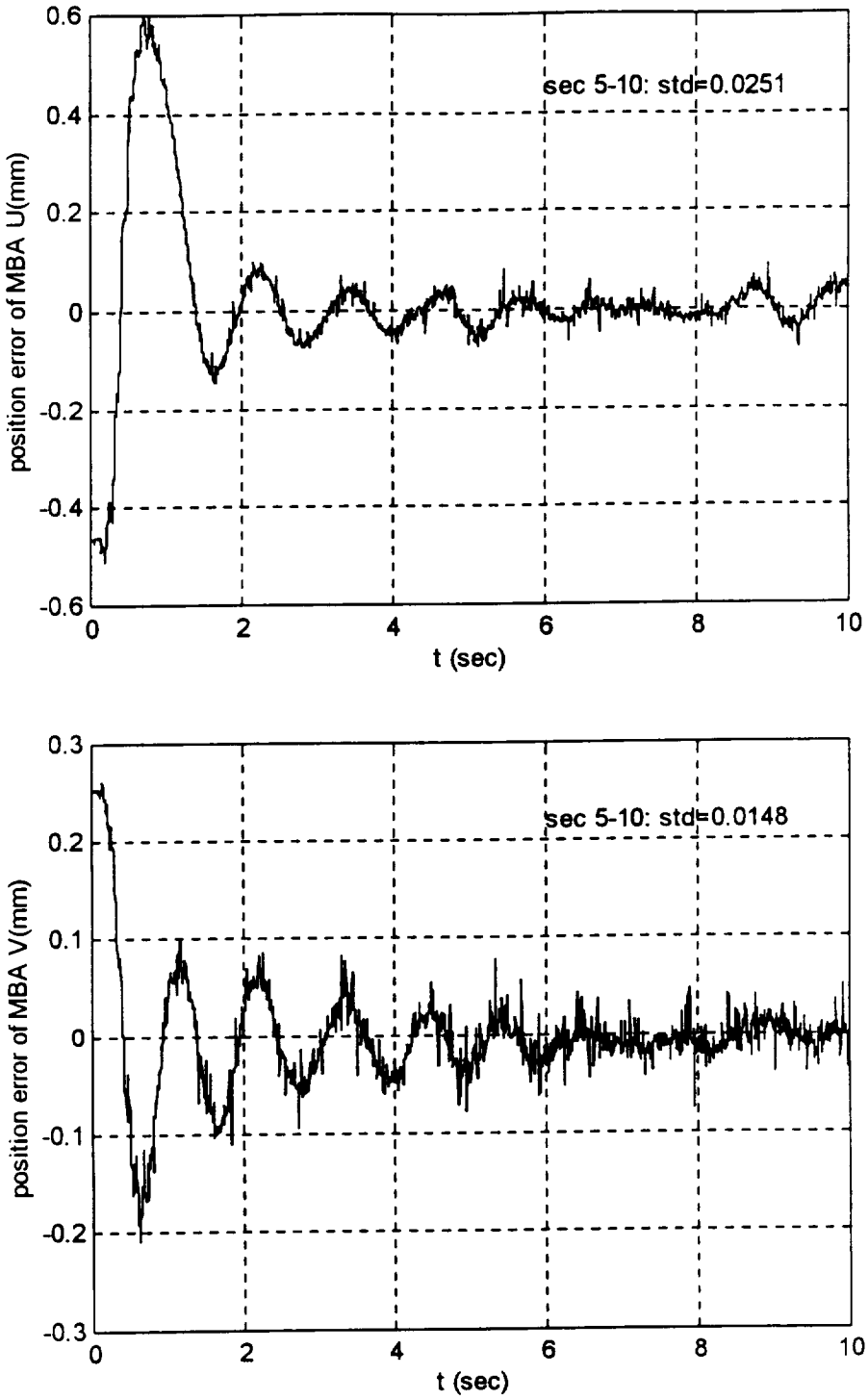

Figure V.11 Time History of Radial MBA

CHAPTER VI

APPLICATIONS OF MSBS

This chapter discusses the application of MSBS as a modern testing facility for use in wind tunnels. Problems in the past which have limited MSBS' applications are also discussed. Further some new technology, which gives the MSBS a promising future, are considered. The role of this research project in the overall program is also discussed briefly.

VI.1 Test Techniques

Advanced airplane designs drive the development of new testing techniques. Advanced testing techniques include the use of adaptive wall test sections, magnetic suspension and balance systems, and non-intrusive laser measurement techniques, all of which improve the quality of tests. The ability to simulate the aerodynamics of flight is therefore constantly improving. The potential of MSBS is valued by scientists due to critical requirements such as data accuracy, elimination of aerodynamic interference, an adequate range of angle of attack, dynamic test capabilities, and wind tunnel productivity.

In the earliest wind tunnels, researchers made corrections for some of the support interference problems to ensure data accuracy. However, it is now known that secondary errors, which are caused by distortion of the flow, still exist and are unpredictable. Errors due to model support systems also increase when large areas of flow separation occur on a solid structure. Thus various support struts were designed with aerodynamic considerations in mind in order to reduce gross errors in static aerodynamic coefficients

such as dynamic pressure, Mach number, and lift coefficient. However, this approach is certainly neither a convenient nor an economical way to solve the problem.

Testing of fighter models usually requires setting the model at high angle of attack. It is difficult to maintain force balance measurement accuracy over a large range of angle of attack since a single balance cannot easily accommodate the widely varying loads. High angles of attack also generate massive separated wakes which can cause excessive support interference, and also decreases in the data accuracy.

MSBS appears to be able to offer a solution to all of the above problems. Additionally, increased experience and improvements in MSBS have led to the capability of performing a variety of dynamic tests without the use of complex mechanical devices. One of the original motivations to generate a magnetic suspension device was to attain more accurate dynamic stability data acquisition [2]. Research on unsteady loads or vibration could be done by combining the magnetic suspension system with advanced sensors and control systems. Applications of MSBS greatly improve the productivity of a wind tunnel by saving time and labor associated with sting and balance set up. Once the system is calibrated, several tests can be done consecutively to acquire fast and reliable data. Table VI.6 gives some information about the worldwide activities on MSBS as of 1996 [21].

VI.2 Problems Arising from MSBS

The research issue of MSBS emerged in the 1940's. In 1957, ONERA in France developed the first wind tunnel magnetic suspension device in the world [22]. After an initial surge of interest, however, research on magnetic suspension technology slowed

Table VI.1 "Operational" MSBSs, 1996

Organization	Apporx. Size[1]	Application	Status
NASA LaRC	13 inch	Low-speed drag, R&D	Inactive
ODU	6 inch	System R&D	Recommissioning
Oxford Univ.	3 inch	Hypersonic aerodynamics	Active
MAI/TsAGI, Moscow	15 inch	System R&D	Inactive
NAL, Japan	4 inch	System R&D	Active
NAL, Japan	23 inch	System R&D	Active
NCKU, Taiwan	6 inch	System R&D	Active
NUDT, P.R. China	6 inch	System R&D	Active

1. Square-root of wind tunnel test section cross-sectional area.

down in the following twenty years. The reasons for its lack of acceptance are various. Although magnetic suspension of models in wind tunnels offers several advantages over conventional mechanical balance systems, such as no physical support affecting flow around the model and capabilities for dynamic testing, a major drawback with magnetic balances is the large amount of power required to operate them, especially for large models at high dynamic pressures. System stability was poor because the sensor and control components were complicated and unreliable at that time. The applications were limited to research and development, since building a large-scale MSBS was considered too expensive. Also, the flow disturbance problems caused by mechanical supports were of relatively minor concern at that time.

Today, innovations in both hardware and software for compensation systems allow optimization and simplification of the whole system, making it more acceptable. The problems associated with attaining flight conditions in a small scale wind tunnel led to the application of MSBS in cryogenic wind tunnels [22].

VI.3 Cryogenic Technology

The use of cryogenic technology with magnetic suspension equipment is strongly linked to high Reynolds number testing. A cryogenic wind tunnel is used to raise the Reynolds number (Re) of an aerodynamic test to more closely match the values in flight. With a decrease in temperature, working gas density ρ increases and viscosity μ decreases which greatly increases the Reynolds number. Cryogenic operation also lowers the velocity for a given Mach number. Taking advantage of MSBS could avoid serious interference effects which may mask the effects of variations of Reynolds number.

The U.S. National Bureau of Standards defines the field of cryogenics to involve temperatures below 123K (-150° F). The boiling points of *"permanent gases"* (helium, hydrogen, neon, nitrogen oxygen and air) all lie below 123K. Nitrogen is often used as the working gas in cryogenic tunnels [23].

VI.4 Applications of 6-Inch MSBS

Following the successful development and demonstration of cryogenic tunnels, research activities relating to the 6-inch MSBS sponsored by the NASA Langley Research Center were resumed in 1976. During the period from 1976 to 1981, research was performed at the Massachusetts Institute of Technology to study the feasibility of using superconductors for magnetic balance coils [24]. A superconductor is one of a series of metals or compounds which, when cooled to cryogenic temperatures, offers no resistance to the flow of electric current. Thus, superconducting magnets have the potential to drastically reduce the power requirements of a Magnetic Suspension and Balance System, possibly making it feasible to use in larger wind tunnels. NASA LaRC spent the period

from January 1977 through August 1980 studying the feasibility of using superconductors for a general-purpose magnetic suspension and balance system [24]. Several designs and specific recommendations were given for the 6-inch MSBS reformation. It soon became obvious that the emergence of new technology in the field of superconductivity, large magnet construction, computers, control techniques, and innovation in MSBS systems made the application of MSBS to large tunnels, not only feasible, but very attractive.

Based on the previous discussion, further development of the 6-inch MSBS will focus on its application to high Reynolds number facilities, either a pressurized tunnel or cryogenic tunnel. This development would lead to the long-term goal of the integration of the 6-inch MSBS into a complete facility. The work which has been done so far involves the initial evaluation of the existing MSBS hardware, and development of a digital controller for the ASPS system, which can later be modified for use in the MSBS.

CHAPTER VII

CONCLUSIONS

Two systems, the 6-inch Magnetic Suspension and Balance System and the Annular Suspension and Pointing System, have been further developed in support of the magnetic suspension research program at ODU. The main focus is on the 6-inch MSBS, which is in the first stage of the recommissioning work.

From the comparison of the estimation, testing, and computation of the magnetic field strength distributions of the 6-inch MSBS, it can be concluded that the magnet system is still working properly. The inclusion of iron cores in the coil assemblies was able to increase the field strength effectively by up to 750 percent. Efforts have been made to reinstate the Electromagnetic Position Sensor; however, further documentation and an amplifier are needed before the system can be reactivated. The circuit diagrams of the EPS have been analyzed and its design has been documented to aid in future work.

A majority of the improvements to the ASPS have been made in the controller software. A timer board has been implemented to enable a higher sampling rate, thus improving system performance. The system now operates with less noise and is more robust. The timer board also allows more flexibility in performing other tasks such as data output and keyboard interruption. The original PD controller has been upgraded to a PID controller to minimize the steady state error. Screen output is now clearer and gives a direct, real-time readout of system performance. This digital controller has successfully replaced the original analog control system and fulfills the iron rotor suspension and

balance task. This revised controller is somewhat generic and will be helpful for the new design of the 6-inch MSBS control system.

The future work on the 6-inch MSBS will focus on the further recommissioning of the hardware. The EPS system must be calibrated after a proper amplifier is installed. The power supply system, cooling system, and control system must also be redesigned to accommodate new applications of the 6-inch MSBS, for example in high Reynolds number wind tunnels. The final step will be reassembly of the wind tunnel components.

Future work on the ASPS system should include the reactivation of the sixth (roll) degree of freedom, as well as a non-linear controller which can take the non-linear characteristics of the actuators into account. Finally, the Balance and Testing Fixture, which enables testing in a simulated zero-g environment, can be included and the entire system calibrated for actual flight conditions.

REFERENCES

[1]. Groom, N. J., "Overview of Magnetic Suspension Research at Langley Research Center", *International Symposium on Magnetic Suspension Technology*, NASA Conference Publication 3152, Part1,1992, pp. 5-11.

[2]. Lawing, P.L., "Magnetic Suspension-Today's Marvel, Tomorrow's Tool", *High Reynolds Number Flows Using Liquid and Gaseous Helium*, Springer-Verlag, 1991, pp.153-164.

[3]. Earnshaw, S., "On the Nature of the Molecular Forces", *Trans. Camb. Phil. Soc.*, Volume 7, 1842, pp. 97-112.

[4]. Stephens, T., "Summary of the Design of a Magnet Suspension and Balance System for the Aerospace Research Laboratories", MIT Aerophysics Laboratory Report 140, 1969.

[5]. Stephens, T., "Design, Construction, and Evaluation of a Magnetic Suspension and Balance System for Wind Tunnels", MIT Aerophysics Laboratory Technical Report 136, 1969.

[6]. Vlajinac, M., "Design, Construction and Evaluation of a Subsonic Wind Tunnel", Master of Science Thesis, Aeronautics and Astronautics, Massachusetts Institute of Technology, Cambridge, June 1970.

[7]. Vlajinac, M., Stephens, T., Gilliam, G., and Pertsas, N., "Subsonic and Supersonic Static Aerodynamic Characteristics of a Family of Bulbous Base Cones Measured with a Magnetic Suspension and Balance System", NASA Contractor Report 1932, January 1972.

[8]. Schott, T., Jordan, T., Daniels, T., and Alcorn, C., "Present Status of the MIT/NASA Langley 6-inch MSBS", *International Symposium on Magnetic Suspension Technology,* Part 2, 1992, pp. 748-749.

[9]. Hamilton, B. J., "Final Report: The Development of The ASPS Vernier System", Sperry Corporation, Flight Systems, June 1983.

[10]. Neff, D. J., "Design and Implementation of a Digital Controller for a Magnetic Suspension and Vernier Pointing System", Master of Science Thesis, Aerospace Engineering, Old Dominion University, Norfolk, August 1995.

[11]. Neff, D. J., and Britcher, C. P., "Design and Implementation of a Digital Controller for a Vibration Isolation and Vernier Pointing System", *Third International Symposium on Magnetic Suspension Technology*, NASA Conference Publication 3336, Part 1, July 1996, pp. 192-206

[12]. Covert, E. E., Vlajinac, M., Stephens, T., and Finston, M., "Magnetic Balance and Suspension Systems for Use with Wind Tunnels", *Progress in Aerospace Sciences*, Volume 14, Pergamon Press, 1973, pp. 27-107.

[13]. Haldeman, C. W., Kramer, R. A., and Way, P., "Developments at M.I.T. Related to Magnetic Model Suspension and Balance Systems for Large Scale Facilities", *First International Symposium on Cryogenic Wind Tunnels*, April 1979, pp. 9.1-9.15

[14]. Way, P., "A Roll Control System for a Magnetic Wind Tunnel Balance and Model Suspension System", Master of Science Thesis, Aeronautics and Astronautics, Massachusetts Institute of Technology, Cambridge, June 1979.

[15]. Covert, E. E., Haldeman, C. W., Ramohalli, G., and Way, P., "Development of Closed Loop Roll Control for Magnetic Balance System", NASA Contractor Report 166017, 1982.

[16]. Stephens, T., "An Electromagnetic Remote Model Position Sensing System for Wind Tunnels with Particular Application to Magnetic Suspension Systems", *Second International Symposium on Electro-Magnetic Suspension*, July 1971, pp. G.1-G.19.

[17]. Daniels, T. S., and Tripp, J. S., "Improvements to an Electromagnetic Position Sensor for a Magnetic Suspension Wind Tunnel", *34th International Instrumentation Symposium*, May 1988, pp. 65-70.

[18]. Luh, P. B., "A Digital Control System for a Wind Tunnel Model Suspension and Balance System", Master of Science Thesis, Aeronautics and Astronautics, Massachusetts Institute of Technology, Cambridge, June 1977.

[19]. Luh, P. B., Covert, E. E., Whitaker, H. P., and Haldeman, C. W., "Application of Digital Control to a Magnetic Model Suspension and Balance System", NASA Contractor Report 145316, December 1977.

[20]. Schott, T., Jordan, T., Daniels, T., and Alcorn, C., "Present Status of the MIT/NASA Langley 6-inch MSBS", *International Symposium on Magnetic Suspension Technology*, August 1991, pp. 745-746.

[21]. Britcher, C. P., "Application of Magnetic Suspension Technology to Large Scale Facilities - Progress, Problems and Promises", AIAA 34th Aerospace Sciences Meeting, Reno, NV, AIAA 97-0346, January 1997.

[22]. Kilgore, R. A., "Cryogenic Wind Tunnels", *High Reynolds Number Flows Using Liguid and Gaseous Helium*, Springer-Verlag, 1991, pp. 53-64.

[23]. Donnelly, R. J., "Liquid and Gaseous Helium as Test Fluids", *High Reynolds Number Flows Using Liguid and Gaseous Helium*, Springer-Verlag, 1991, pp. 3-52.

[24]. Haldeman, C. W., Kraemer, R. A., Prey, S. W., Alishahi, M. M., and Covert, E. E., "Application of Superconducting Coils to the NASA Prototype Magnetic Balance", NASA Contractor Report 165660, January 1981.

[25]. Moschytz, G. S. and Horn, P., "Active Filter Design Handbook", John Wiley & Sons, 1981, p. 40.

[26]. Fredrick, W. H., "Op-Amp Handbook", Second Edition, Prentice-Hall, Englewood Cliffs, New Jersey 07632, 1986, pp. 36, 41.

APPENDIX A

TRANSFORMATION OF AXES

Consider two sets of axes shown in Figure II.1 where a, b, and c are the model's body frame and X, Y, and Z are the wind tunnel frame. The transformation matrix will be given by using Euler angles of "ψ" (yaw angle), "θ" (pitch angle), and "ϕ" (roll angle). The axes X, Y, and Z are rotated with respect to the intermediate axes (X′, Y′, Z′ and X″, Y″, Z″) following the sequence ψ (about Z), θ (about Y′), and ϕ (about X″) to arrive at the body axes a, b, and c.

$$\begin{bmatrix} a \\ b \\ c \end{bmatrix} = \begin{bmatrix} 1 & 0 & 0 \\ 0 & \cos\phi & \sin\phi \\ 0 & -\sin\phi & \cos\phi \end{bmatrix} \begin{bmatrix} \cos\theta & 0 & -\sin\theta \\ 0 & 1 & 0 \\ \sin\theta & 0 & \cos\theta \end{bmatrix} \begin{bmatrix} \cos\psi & \sin\psi & 0 \\ -\sin\psi & \cos\psi & 0 \\ 0 & 0 & 1 \end{bmatrix} \begin{bmatrix} X \\ Y \\ Z \end{bmatrix};$$

$$\begin{bmatrix} a \\ b \\ c \end{bmatrix} = [\mathbf{R}] \begin{bmatrix} X \\ Y \\ Z \end{bmatrix}; \text{ and } \begin{bmatrix} X \\ Y \\ Z \end{bmatrix} = [\mathbf{R}]^{-1} \begin{bmatrix} a \\ b \\ c \end{bmatrix}$$

$$\text{where } [\mathbf{R}] = \begin{bmatrix} \cos\psi\cos\theta & \sin\psi\cos\theta & -\sin\theta \\ -\sin\psi\cos\phi + \sin\phi\cos\psi\sin\theta & \cos\psi\cos\phi + \sin\phi\sin\psi\sin\theta & \sin\phi\cos\theta \\ \sin\psi\sin\phi + \cos\phi\cos\psi\sin\theta & -\sin\phi\cos\psi + \cos\phi\sin\psi\sin\theta & \cos\phi\cos\theta \end{bmatrix}$$

(A1-1)

$$\text{and } [\mathbf{R}]^{-1} = [\mathbf{R}]^{T}. \qquad \text{(A1-2)}$$

APPENDIX B

EPS CIRCUIT DIAGRAMS

The complete circuit diagrams of Electromagnetic Position Sensor (EPS) is shown in this appendix. Blocks are zoomed in to show details. Selected labels are given to indicate certain functions realized by typical elements, such as amplifiers and filters. Footnotes are explained at the end of this section.

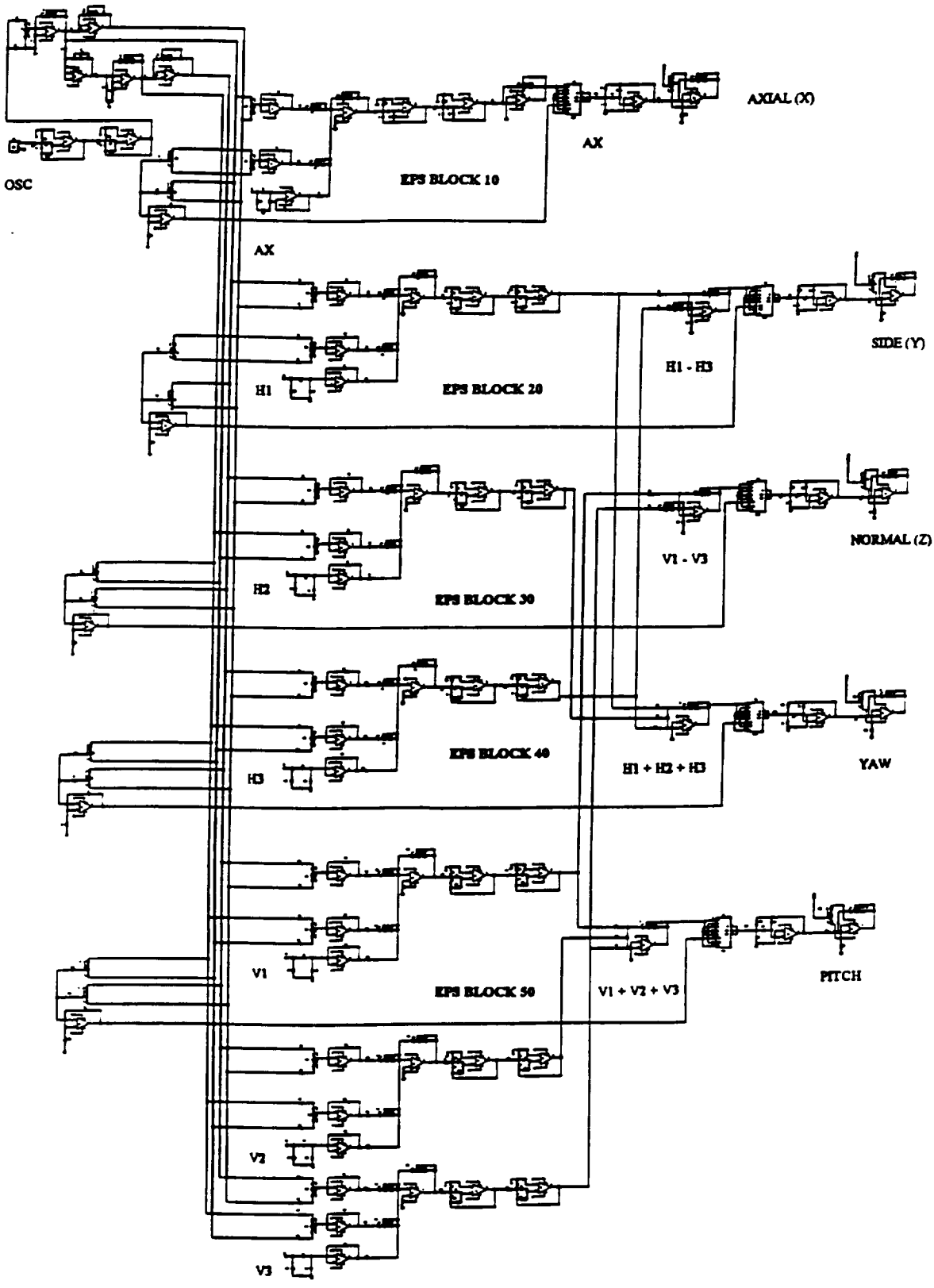

Figure B.1 EPS Circuit Diagram

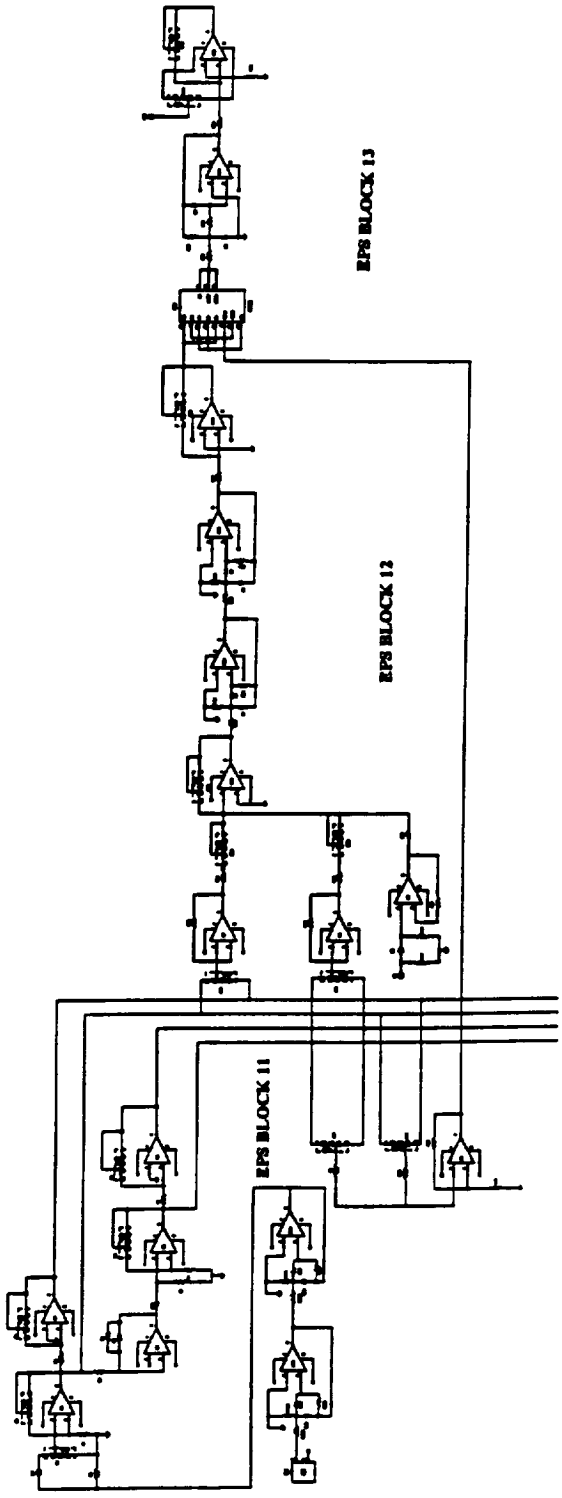

Figure B.2 Circuit Diagram, EPS Block 10

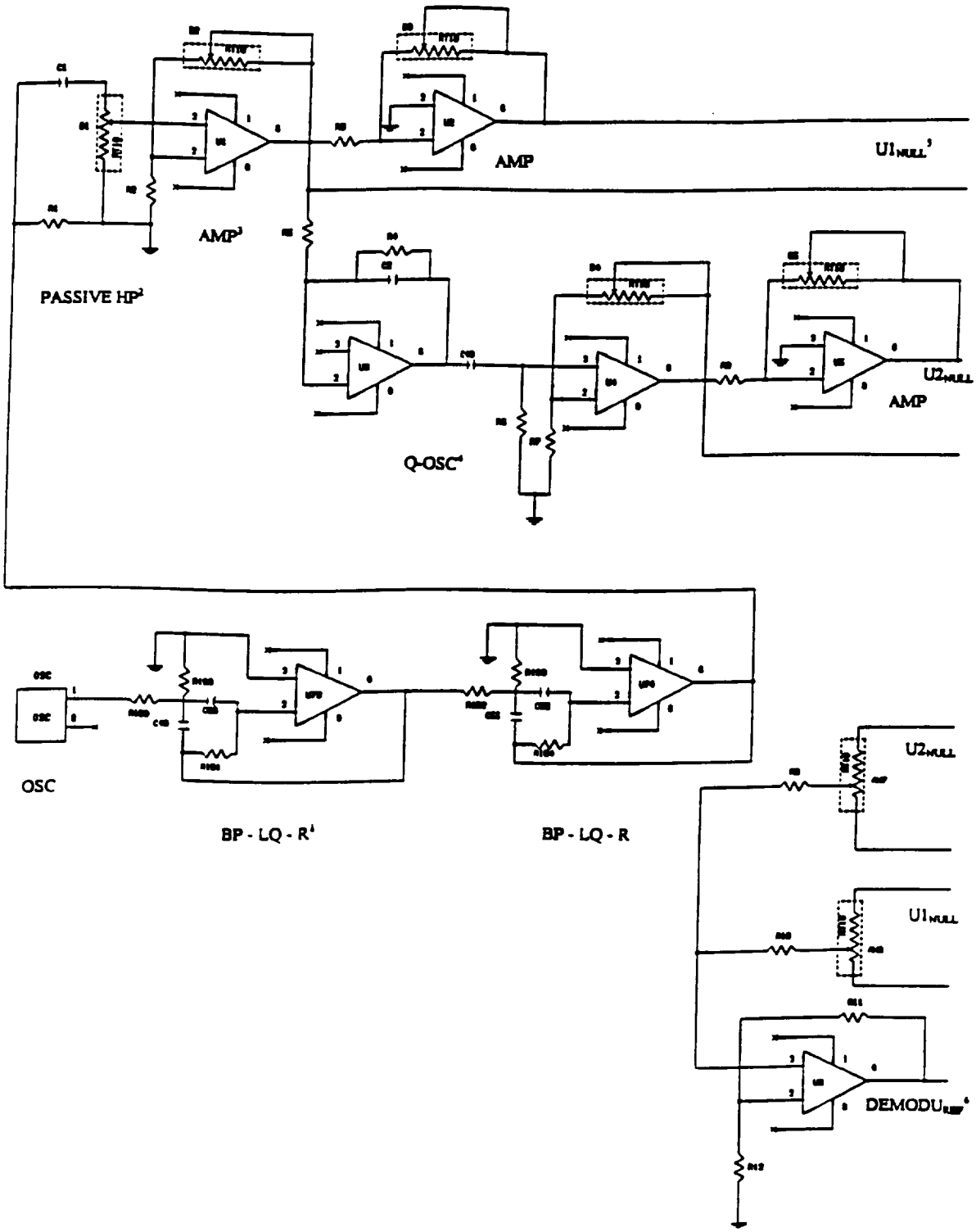

Figure B.3 Circuit Diagram, EPS Block 11

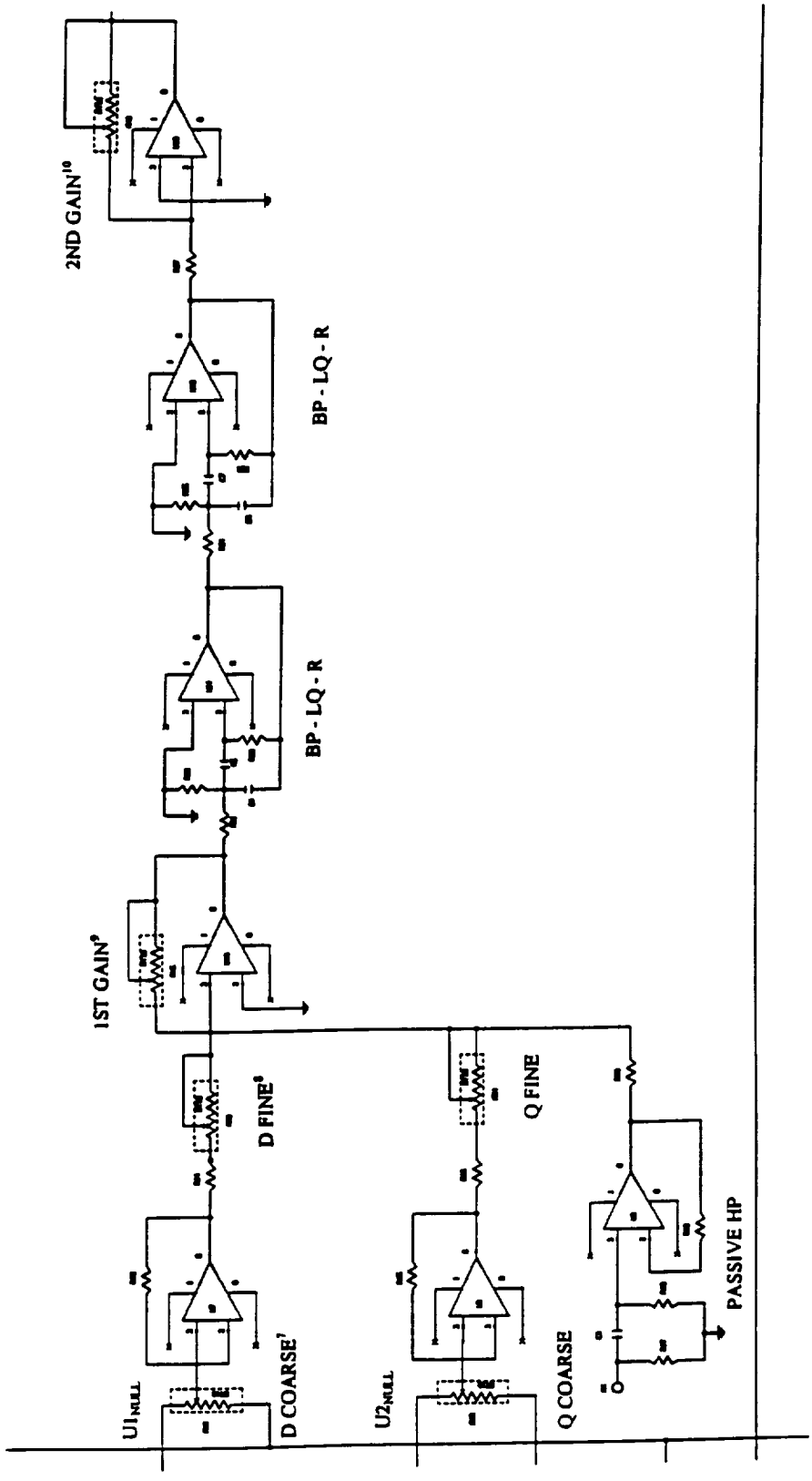

Figure B.4 Circuit Diagram, EPS Block 12

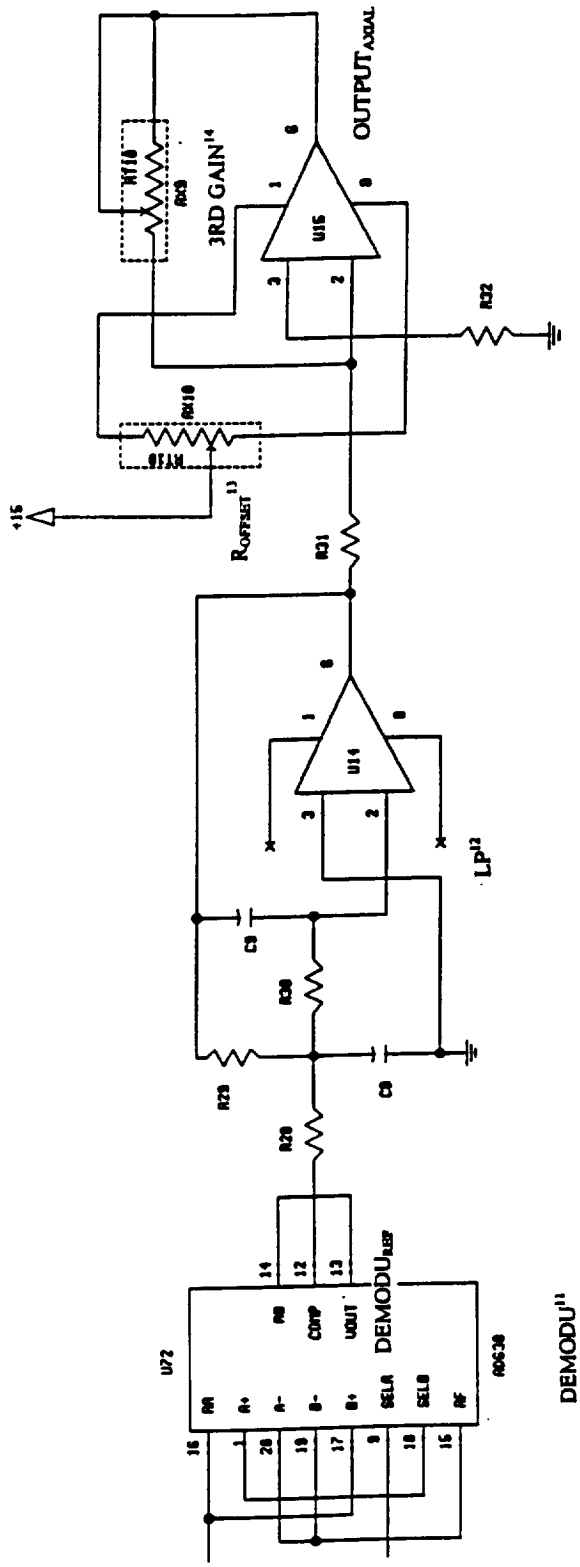

Figure B.5 Circuit Diagram, EPS Block 13

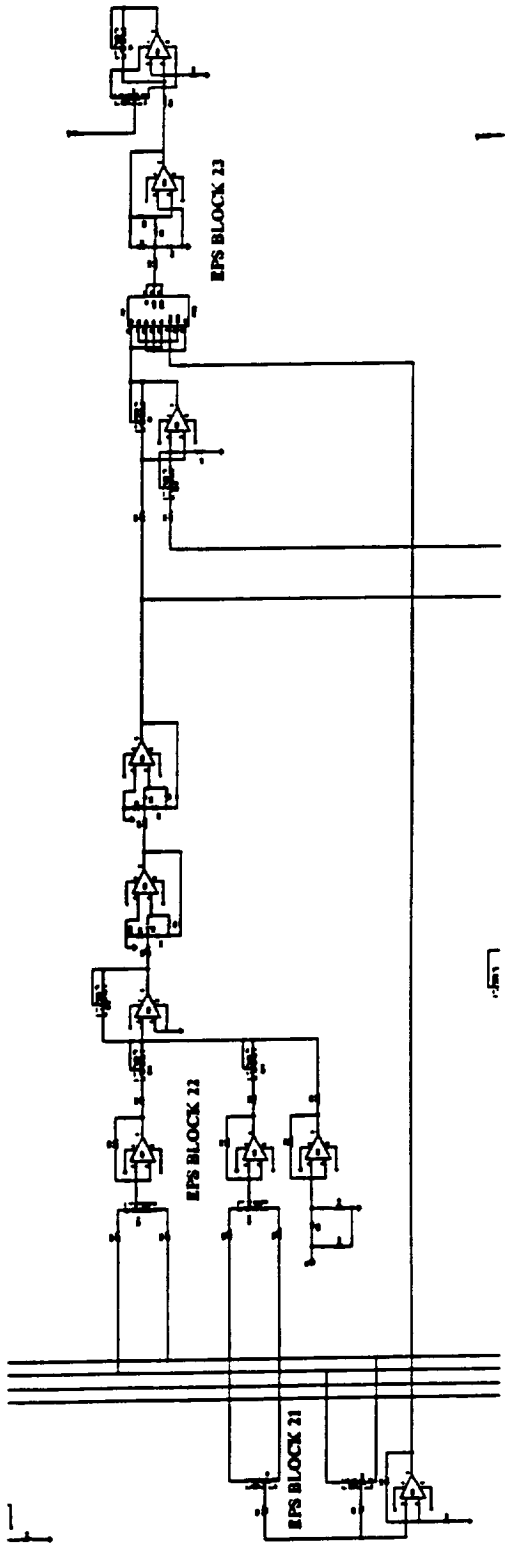

Figure B.6 Circuit Diagram, EPS Block 20

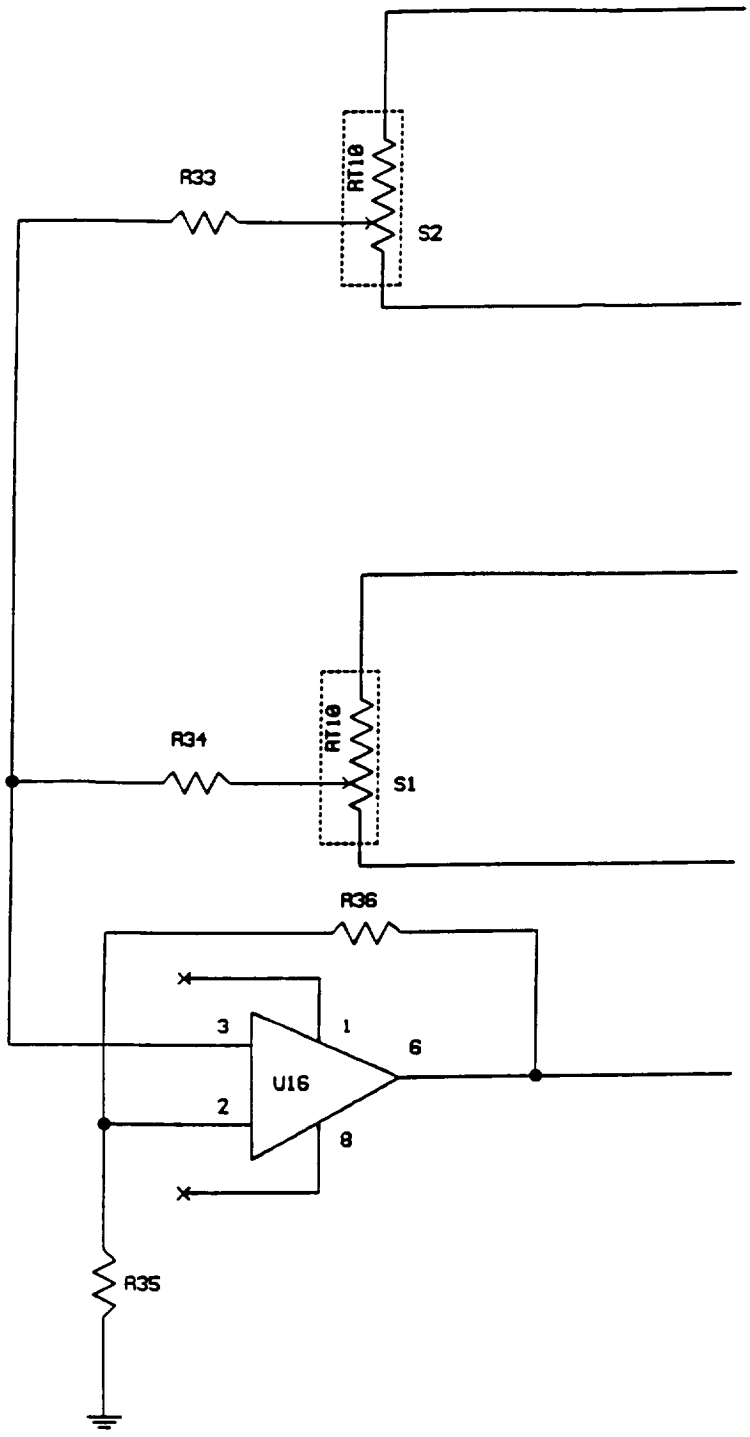

Figure B.7 Circuit Diagram, EPS Block 21

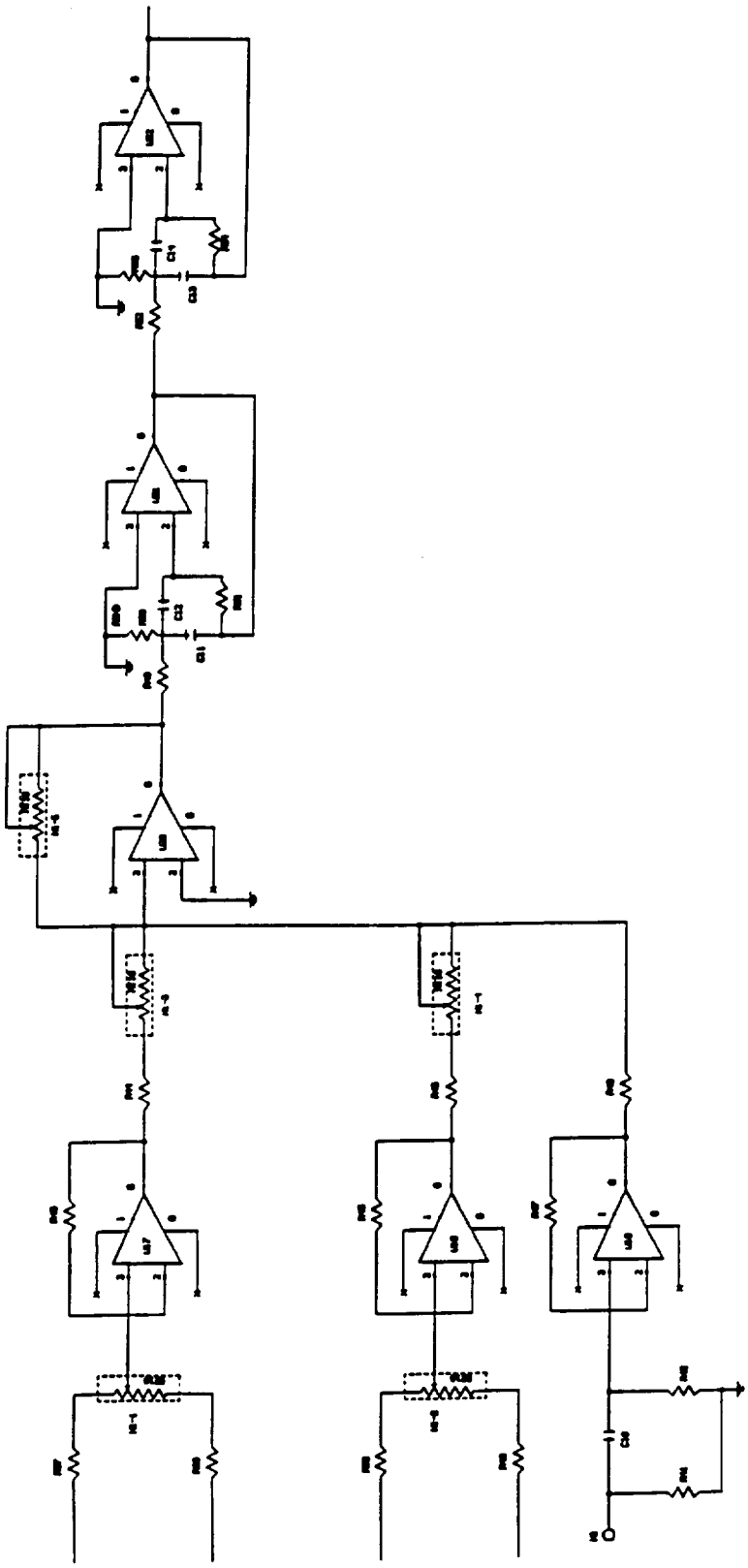

Figure B.8 Circuit Diagram, EPS Block 22

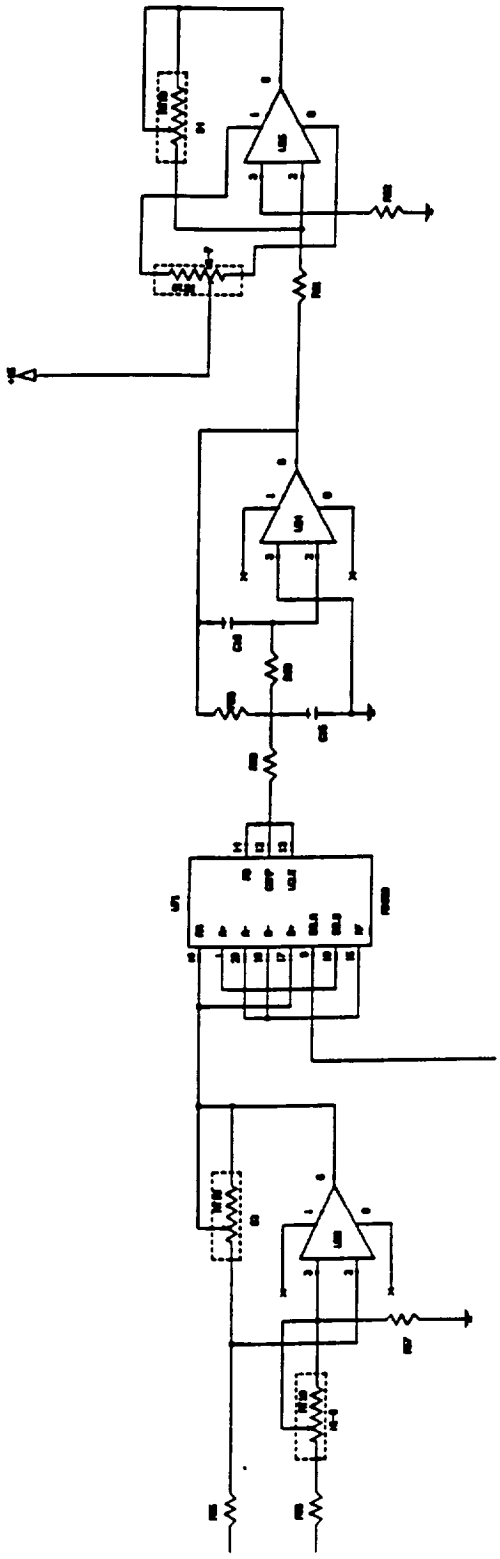

Figure B.9 Circuit Diagram, EPS Block 23

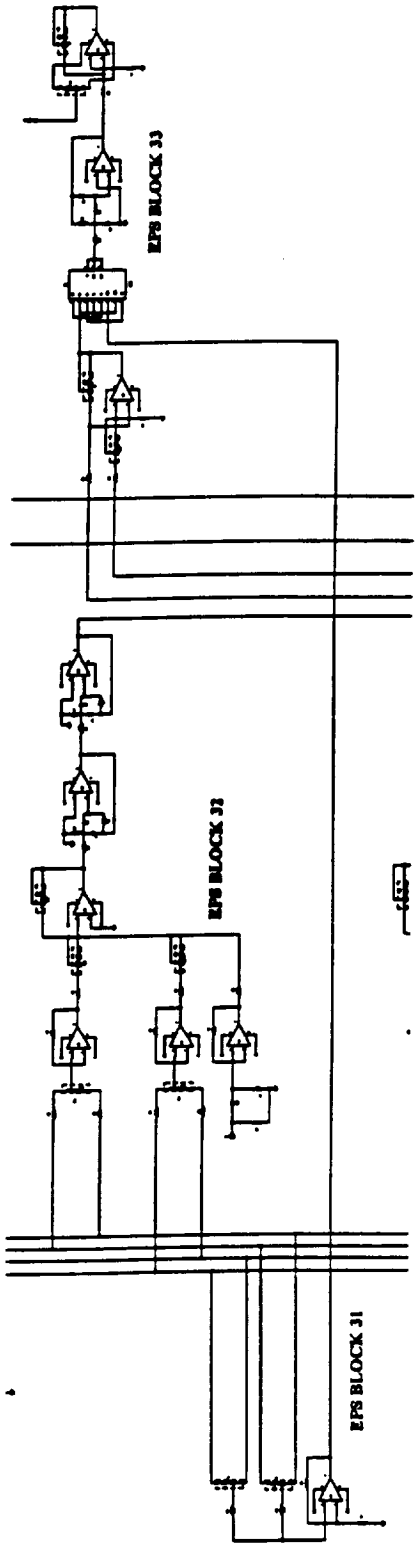

Figure B.10 Circuit Diagram, EPS Block 30

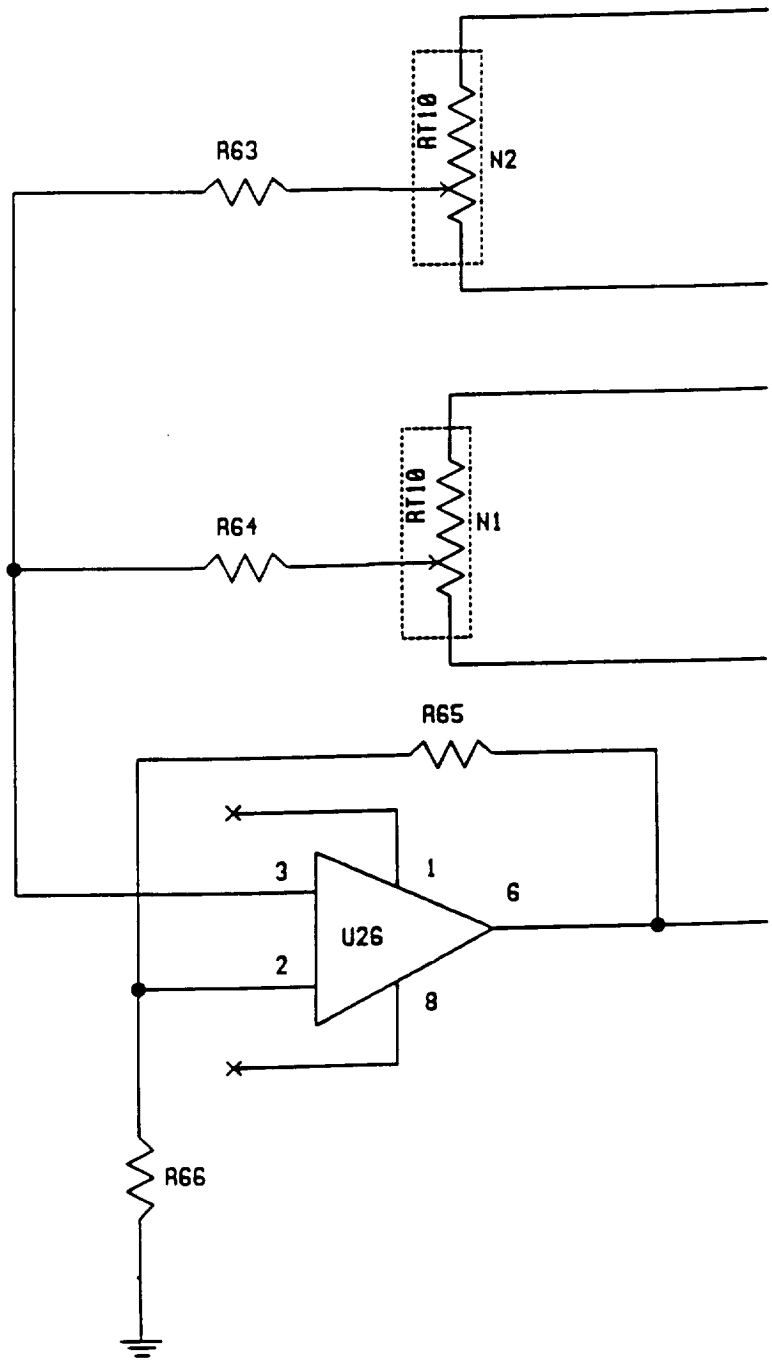

Figure B.11 Circuit Diagram, EPS Block 31

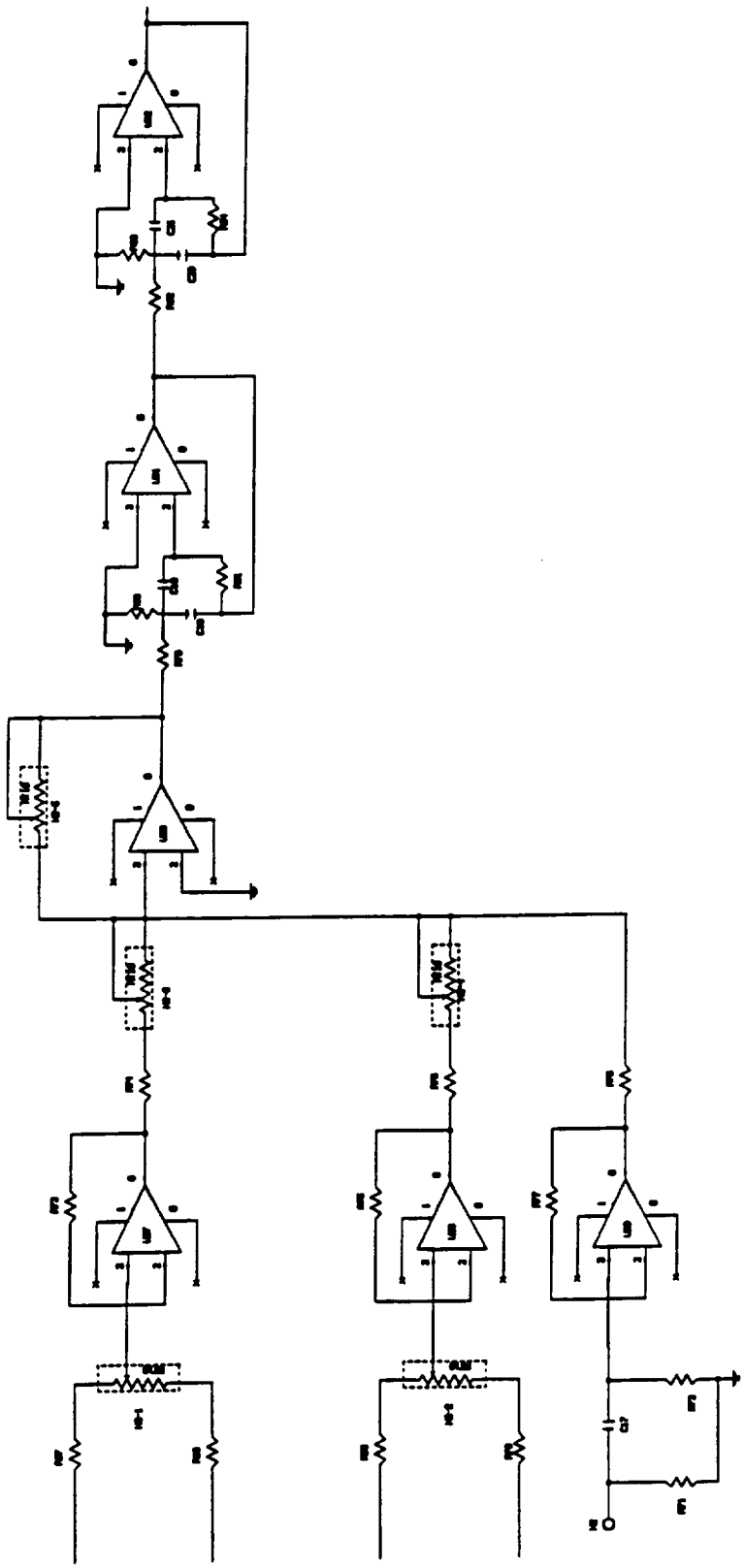

Figure B.12 Circuit Diagram, EPS Block 32

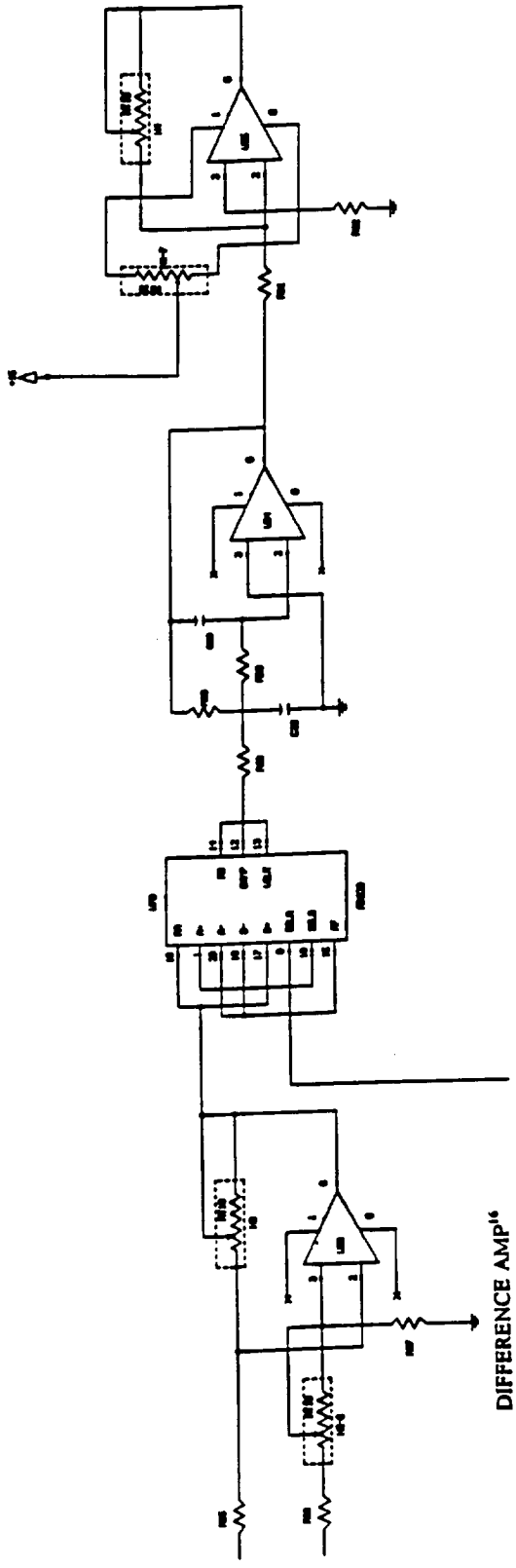

Figure B.13 Circuit Diagram, EPS Block 33

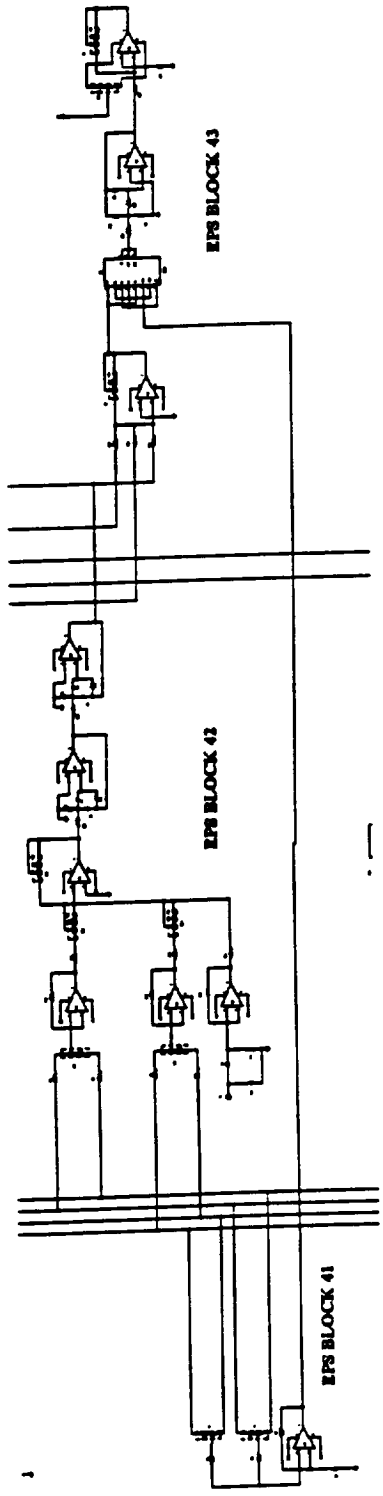

Figure B.14 Circuit Diagram, EPS Block 40

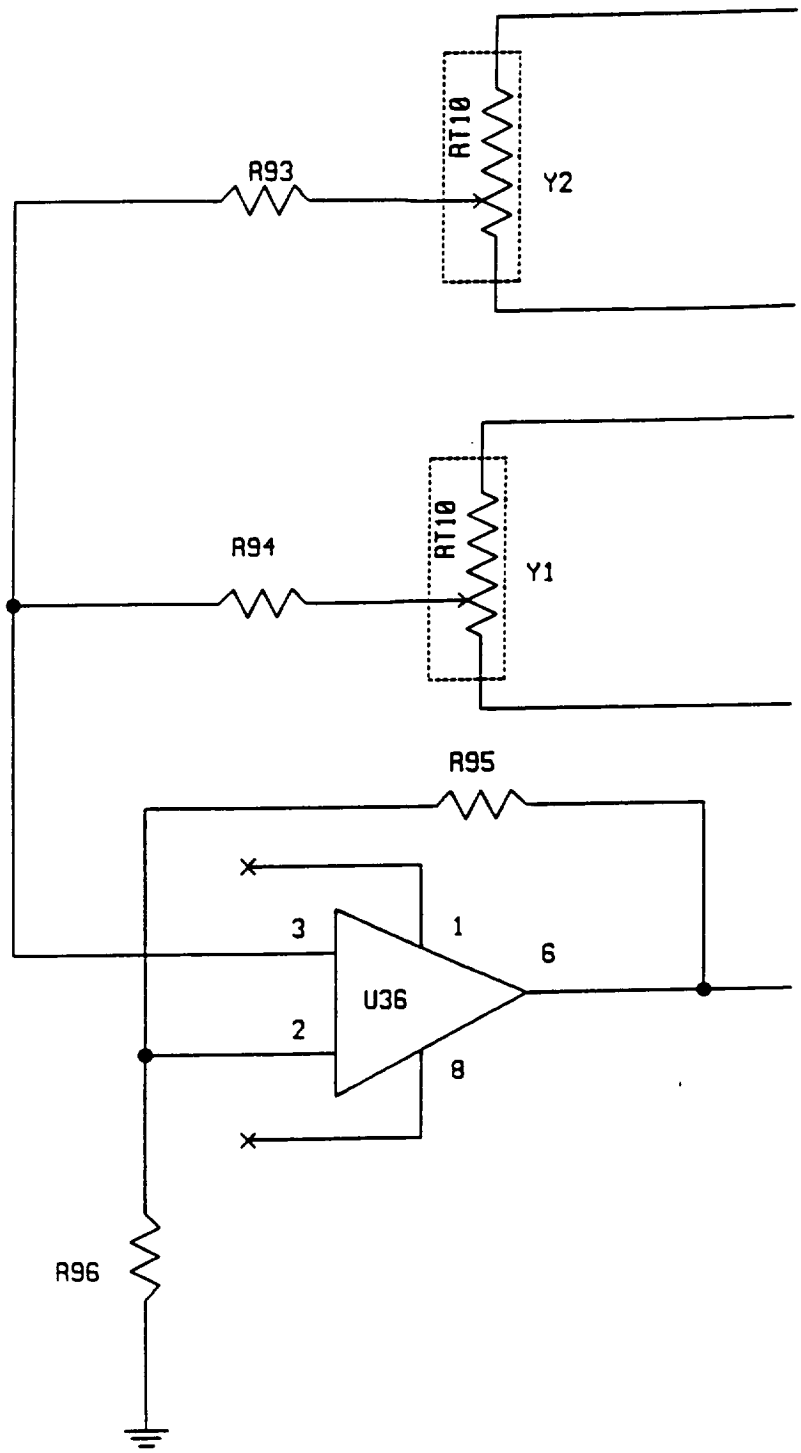

Figure B.15 Circuit Diagram, EPS Block 41

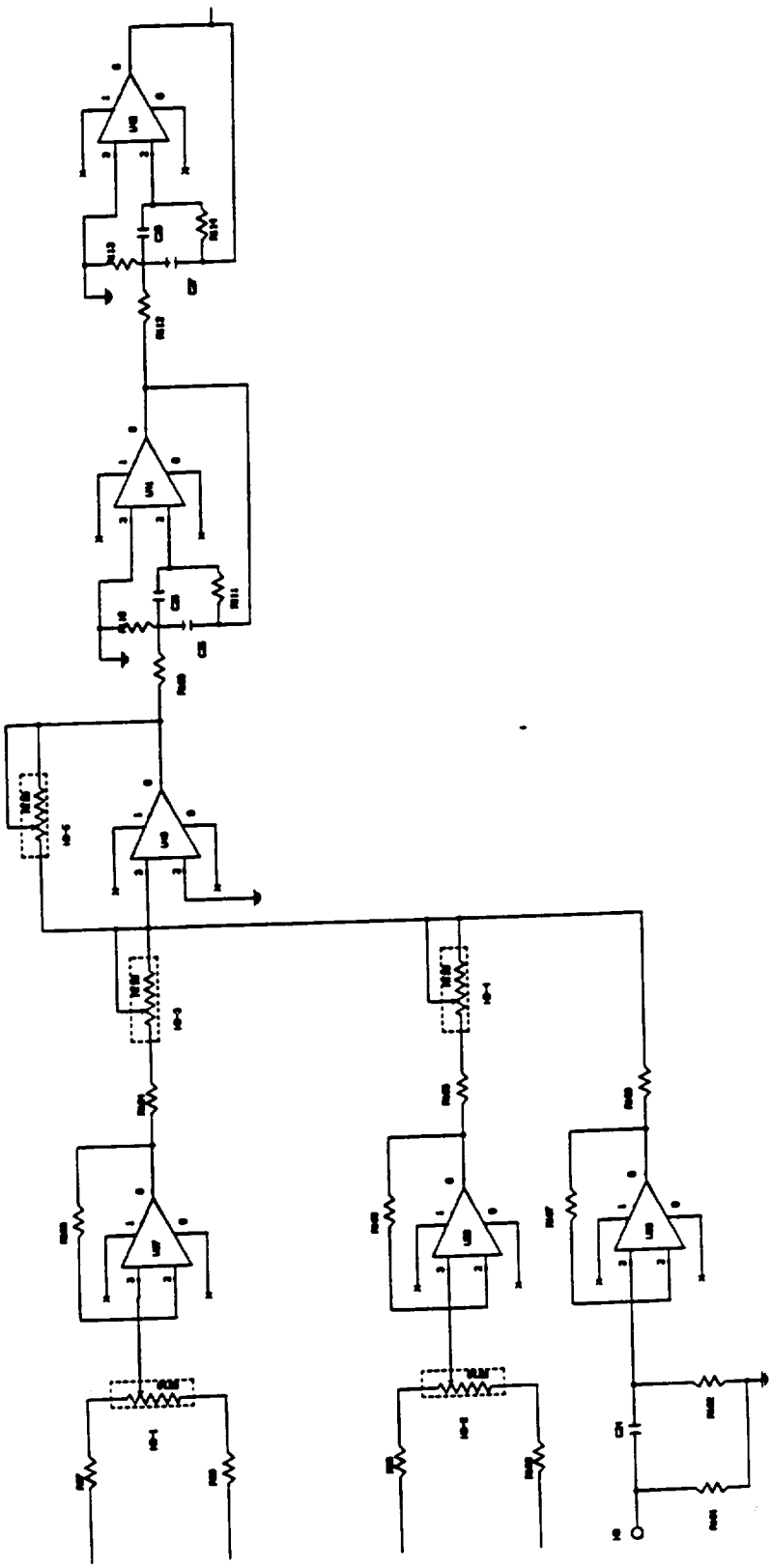

Figure B.16 Circuit Diagram, EPS Block 42

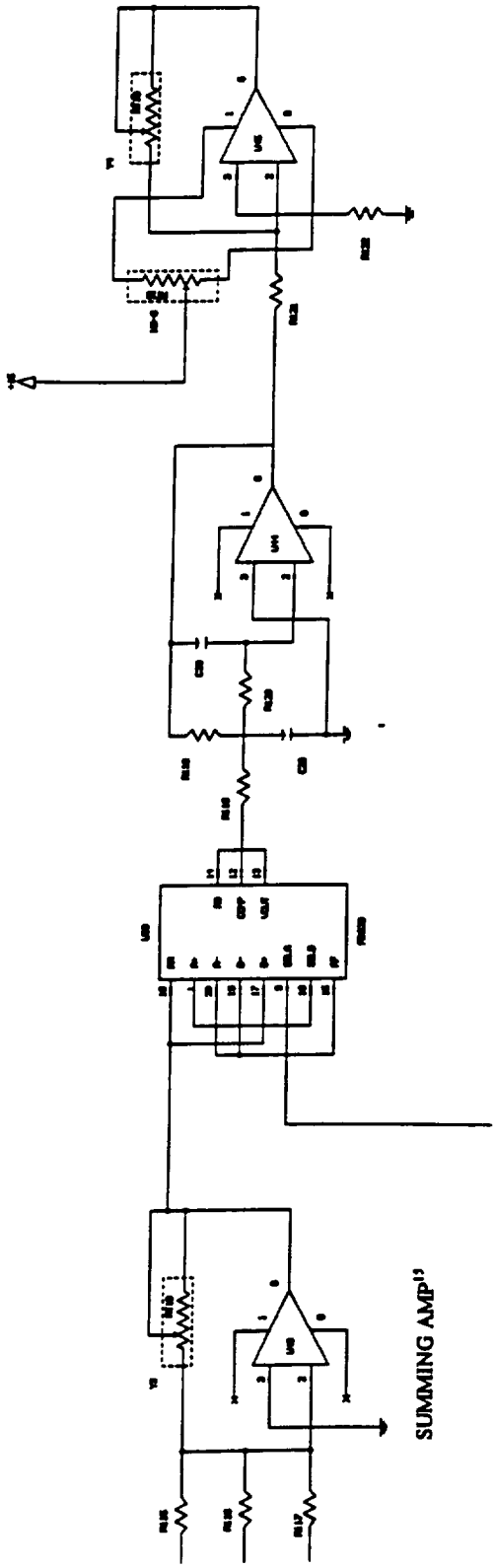

Figure B.17 Circuit Diagram, EPS Block 43

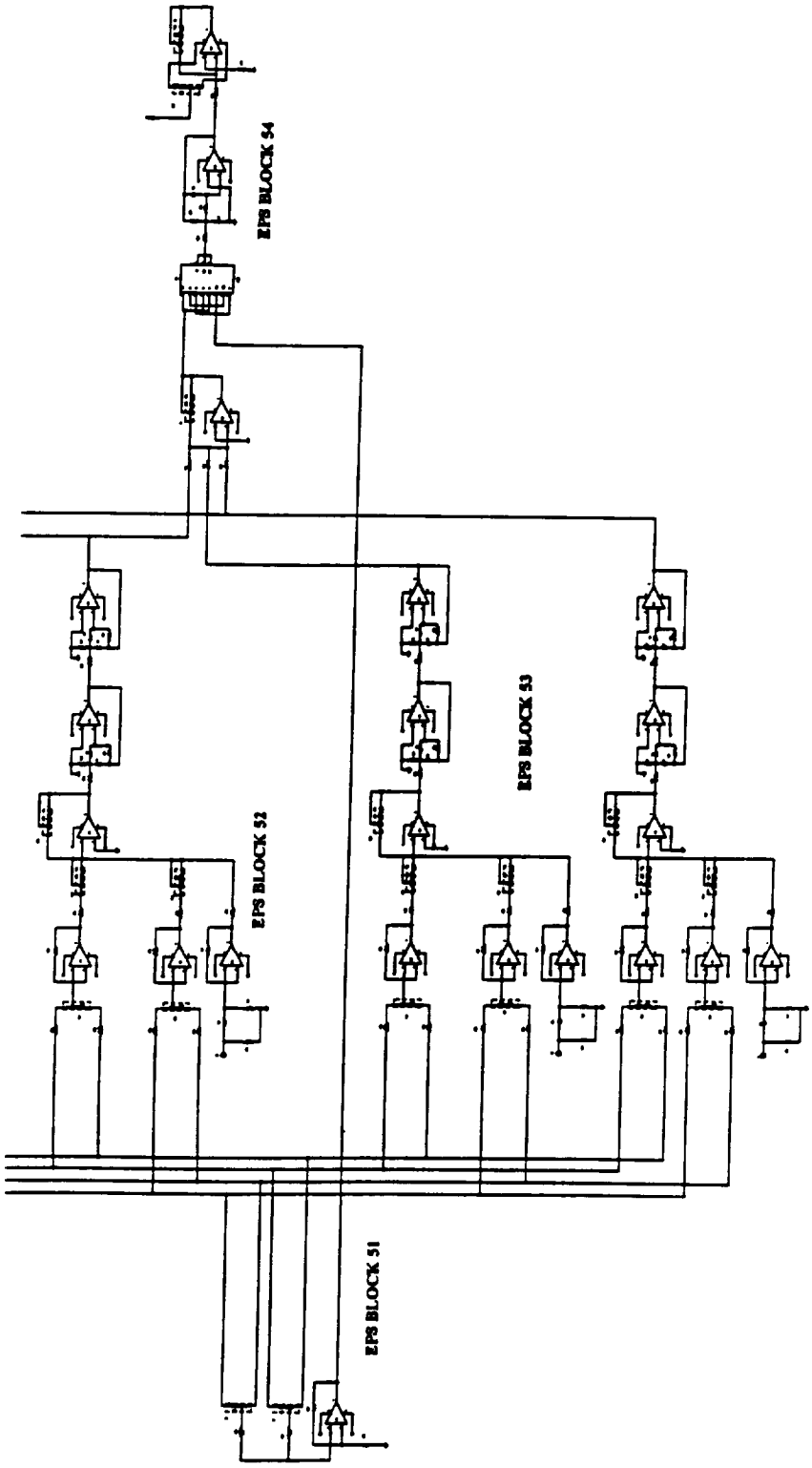

Figure B.18 Circuit Diagram, EPS Block 50

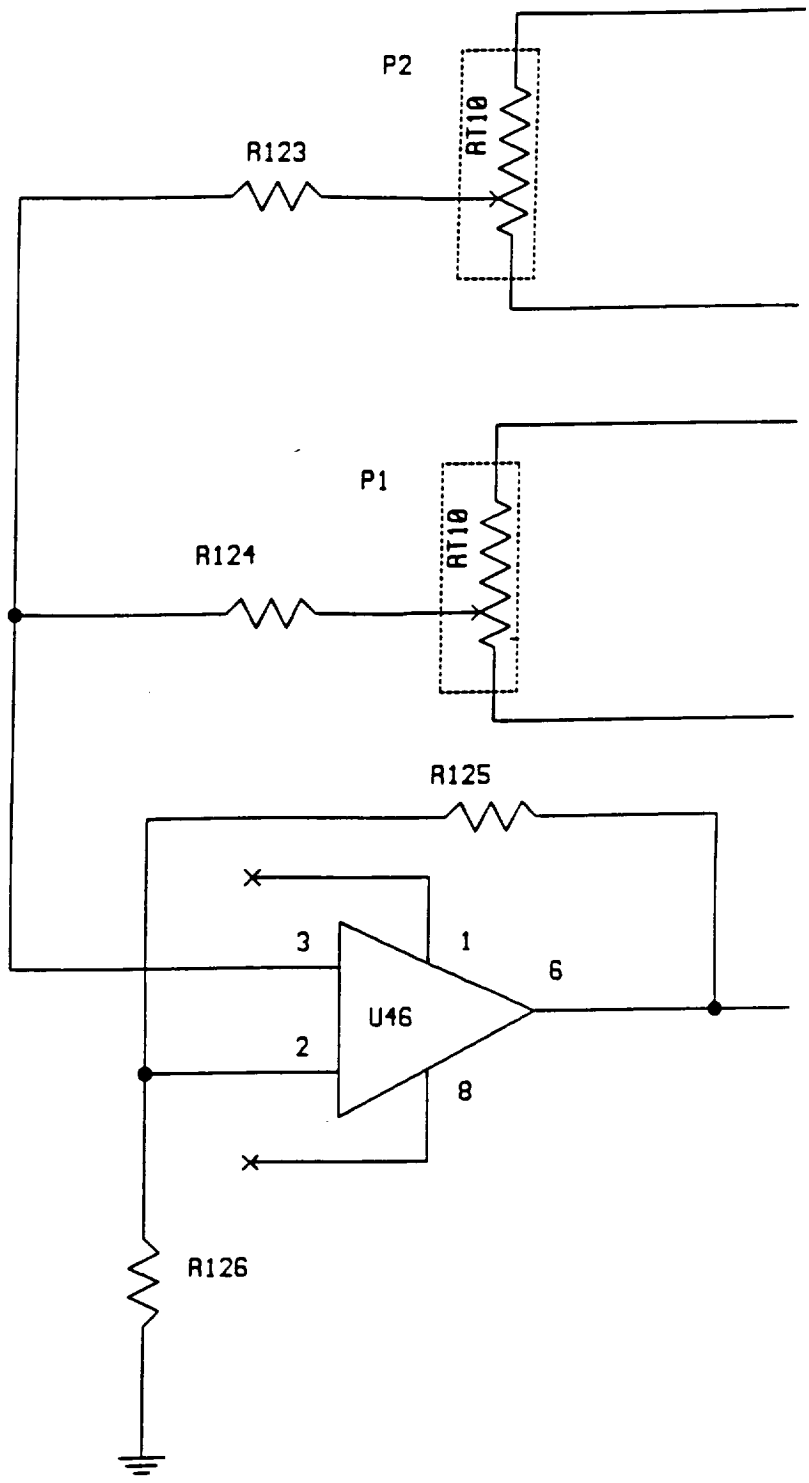

Figure B.19 Circuit Diagram, EPS Block 51

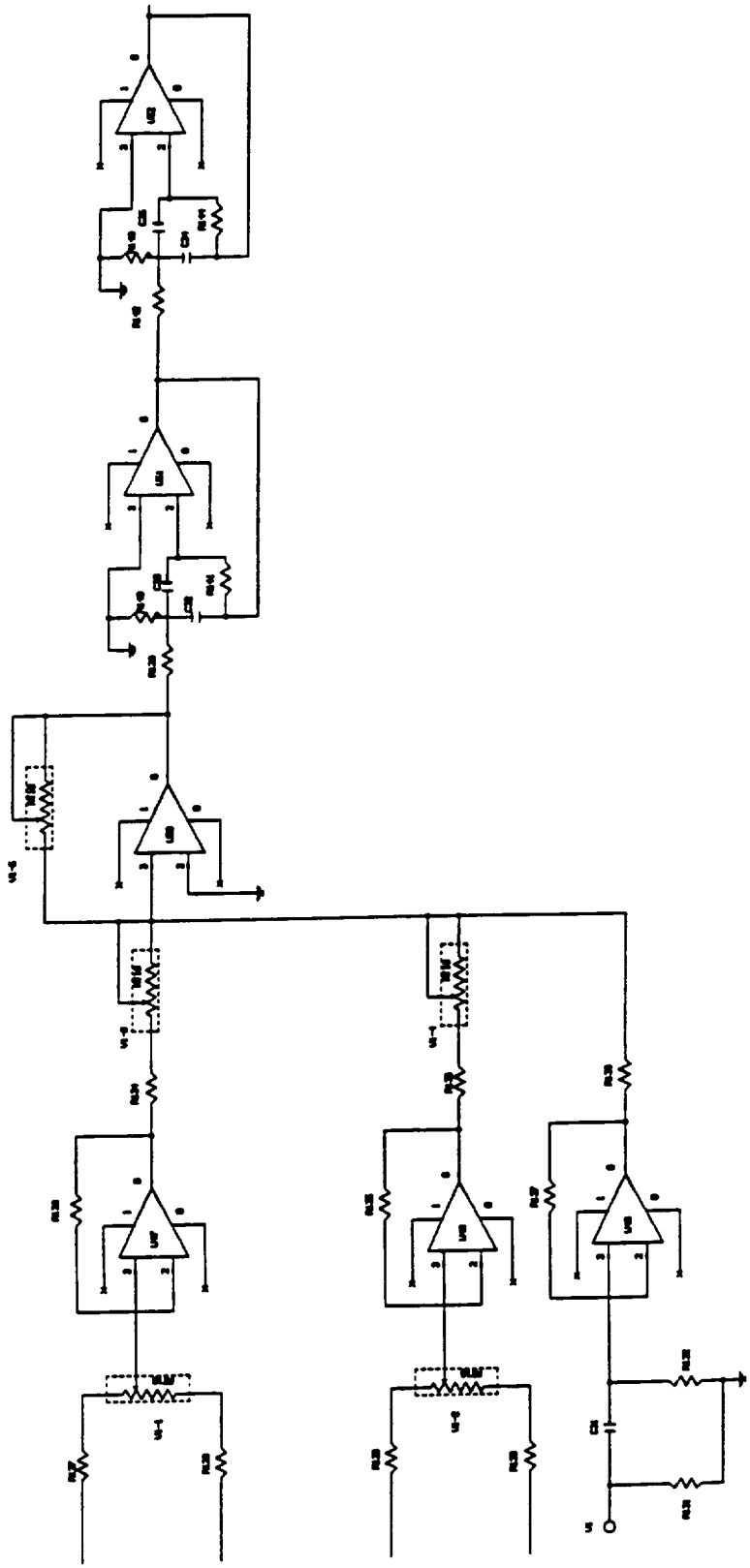

Figure B.20 Circuit Diagram, EPS Block 52

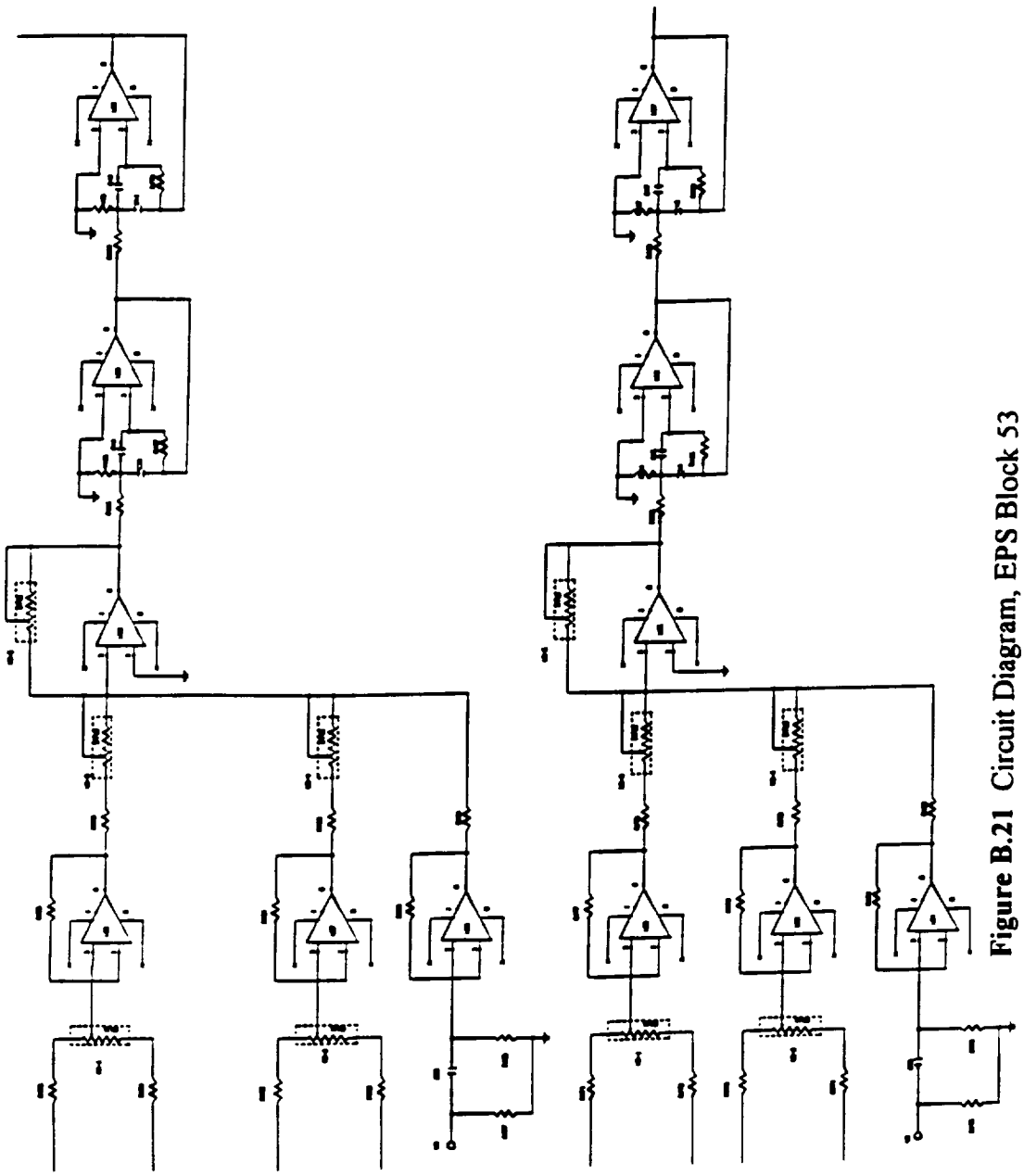

Figure B.21 Circuit Diagram, EPS Block 53

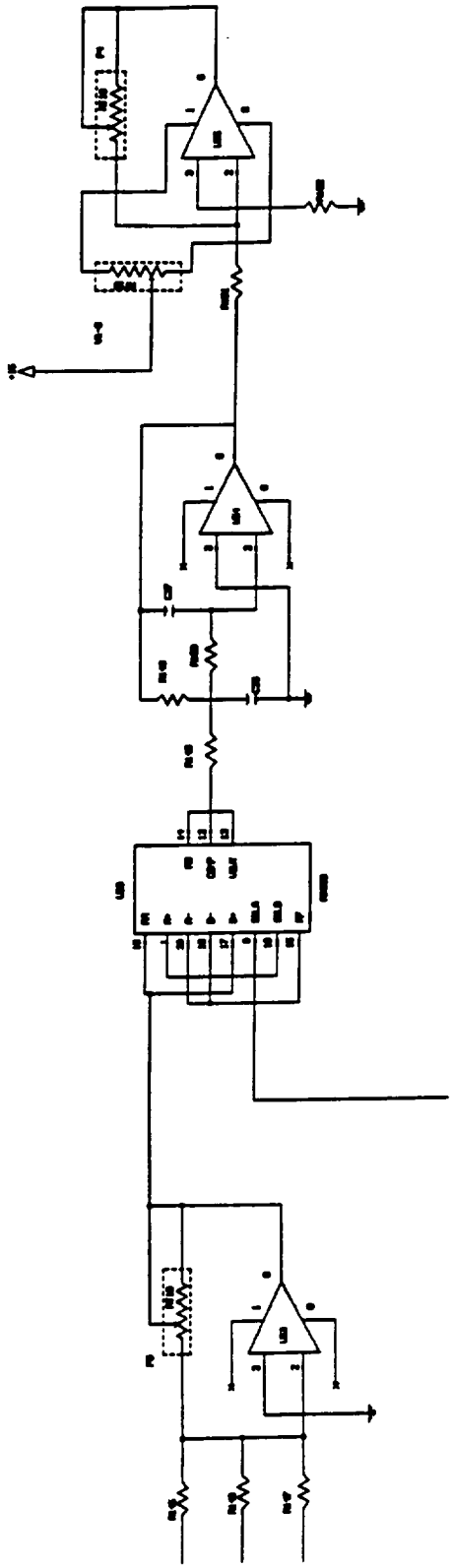

Figure B.22 Circuit Diagram, EPS Block 54

Footnotes for **Figures B.1-B.22**

1. This is a Bandpass-Low Q-Resistive input filter [25]. It is used in serial to eliminate the noise from oscillator.
2. This is a passive high pass filter. It also used for all 7 input signals. (see Block 12, 22, 32, 42 52 and 53)
3. This is a typical inverting amplifier. Some other noninverting amplifiers are also used [26].
4. The quadrature oscillator components are produced by active 90 degree phase lag circuitry, inverters, and summing networks [17]. Vernier adjustments are also available.
5. The demodulator reference and nulling voltages are generated as sums of in-phase U1 and quadrature oscillator components U2.
6. U1 and U2 are added together by a summing circuit to get the demodulator reference signal which will go to AD 630 demodulator (See Block 13).
7. D coarse and Q coarse are adjustable resistors shown on front panel of the electrical box. They can be tuned to get the nulling signals.
8. This is also on the front panel of the electrical box.
9. This is an amplify with adjustable gain show on the panel.
10. The 2nd adjustable gain can be reached inside the electrical box on each function board.
11. This is the AD 630 synchronous demodulator chip [17].
12. After signals are demodulated, a low pass filter is added to eliminate high frequency noise.

13. This adjustable resistor is used to offset the output signal. It can be reached inside the electrical box.

14. Third gain is on the panel too. This is the last and only gain for the D.C. output signal.

APPENDIX C

SOFTWARE

C.1 Program Test1.c

```
/*                    TEST1.C
      This program is developed to test the interrupt ability of
      the Pacer Timer Board. This program will print out "I am
      doing some less important jobs" 80 times in a certain time
      interval. During this period, every two seconds the time
      board sends out a low pulse signal which drive the excution
      to the interrupt subroutine to print out "Do a more important
      job".

      In order for this program to work the Dual Inline Package
      (DIP) switches on the board surface must be set in a proper
      locations such that the I/O base address is 230 hex (default
      vaule) and the interrupt priority level is at level 4 instead
      of default value of level 5. Also, the output of counter 3
      must be connected to the interrupt input pin for the
      measurement routine to work.

      To compile this program correctly it must be linked with
      PACER.LIB. When compiling a user defined subroutine, stack
      checking must be disabled.

                  Written by: Yang Yan
                        May 10, 1997
               Annular Suspension and Pointing System
                  Old Dominion University
               Department of Aerospace Engineering          */


#define INTLEVEL 4

#include <stdio.h>
#include <conio.h>
#include <math.h>

#include "pacerdef.h"
```

```
#pragma check_stack(off)

WORD mode,count;
double counttime;
int far  k,m,n;
unsigned long icount;

void start_measure(int seconds);
int far impt_proc(void);          /* Important job subroutine */

main(void)
{
int   result;
double freq;

PA_INITIALIZE(0x230);       /* Base address set up */
PA_RESET();
PA_SETUP_INTERRUPT(INTLEVEL,impt_proc);

freq=2000;
PA_SET_FOUT(freq);    /* Set Fout to the desired frequency */


start_measure(2);

printf("all jobs are done");
PA_TERMINATE_INTERRUPT();
return(0);
}

void start_measure(int seconds)
{
  WORD mode,count;
  double freq;
  WORD status;
  unsigned long icount;


  /* inititialze the first counter */
PA_BUILD_MODE(MODE_D,SOURCE_F4,GATE_NONE,MODE_OUTPUT_LOW_
PULSE,&mode);
  PA_REPORT_FREQUENCY(3,&freq);
  count=floor(freq*seconds +0.5);
  counttime=count/freq;
  if ( fabs(counttime-seconds)>0.2)
```

```
    printf("\n measure period to long\n");
  PA_INITIALIZE_COUNTER(3,mode,count,0);

  PA_ENABLE_INTERRUPT();
  PA_WRITE_COMMAND(armCounters,0x4);



  m=0;
  do
  {
  m=m+1;
   n=0;
   printf("I am doing some less important jobs\n");
   do
   {
   n=n+1;
   k=0;
   do
    {
    k=k+1;
    }
   while (k <= 30000);
   }
   while(n <=11);
  }
  while(m <=79);




}

int far impt_proc(void)
{

PA_CLEAR_INTERRUPT();
PA_DISABLE_INTERRUPT();
PA_CHECK_INTERRUPT(&icount);
printf("icount=%d, get an interrupt signal\n",icount);
printf("Do a more important job\n");
PA_ENABLE_INTERRUPT();
return(0);
}
```

C.2 Program Testbcd.c

```
/*                    CODE: testbcd.c

This program is developed to use the Pacer Timer Board to perform
a controled loop within a program. A PID controller is designed
and execute as an f=0.005 Hz interruption. The parameters of the
controllers can be changed by keyboard interruption. A colorful
screen output is applied to observe the system performance. The
final report is written into DATAOUT.ASC which includes the last
ten sets of parameters of the controllers and system perfomance
information.

Controller subroutine:
This program will read six channels from the DAS-1401 A/D Data
acquisition board. The input values will be used to calculated the
distance, velocity, and integal of the distance of the iron ring.
Multiply by the gains, the program writes six outputs of controllers
using the DDA-06 D/A data acquisition board.

Keyboard subroutine:
This program will adjust the values of reference voltages to suspend
the ring, proportional gains, integral gains, and derivitive gains
in five degrees of freedom. Also, a integral controller switch is
arranged so that it can be turned on after system is started and
remain stable.

Note:
FOUT pin must be connected to SOURCE 1 in order for this program to
work properly.
To compile this program correctly it must be linked with several
libraries which are: DAS1600.LIB, DASRFACE.LIB, PACER.LIB. The file
my1402.cfg must be in the C:\qc25\bin directory before compiling
this program. This file contains the information about the DAS-1402
configuration.
This program should run from DOS command line.

                    Written by Yan Yang
                      May 31st, 1997
                Annular Suspension and Pointing System□
                   Old Dominion University
                Department of Aerospace Engineering      */
```

```
#define INTLEVEL 4

#include <stdio.h>
#include <conio.h>
#include <graph.h>
#include <math.h>
#include <float.h>
#include <dos.h>
#include "userprot.h"    /*Include file for Keithley DAS-1402 D/A Board*/
#include "pacerdef.h"    /*Include file for Pacer Timer Board */
                         /* Note the order of above Include Files */
#pragma check_stack(off) /* This is necessary for interrupt output */

#define ESC 27
#define UP 72
#define DOWN 80
#define RIGHT 77
#define LEFT 75
#define base 400         /*Base address of DDA-06 D/A Board*/


/* Define data type */
        WORD mode,count;
        double freq,seconds=0.005;      /* This is the testing pace */
        double freq3=50000;    /* Frequence to be set at the FOUT pin */
                               /* This is the frequence used by Counter 3 */
        DDH DAS1402;           /* DevHandle contains base address of DAS1402 */
        FRAMEH frameHandle;
        long far clkTicks;
        int  high,low,i,counter;
        unsigned result,MODE;


        char ch,chin,NumberOfBoards;

        char buffer[80];               /* Output table array */
        float far data[10][6][4];
        char name[10]={"ABCUVW"};
        int pg;

        char  A,AA;
        long  ADvalueA,RefVoltsA,XdemandA,XoldA,ControlA;
        int   highA, lowA;
        float VelocityA,XoffsetA,ControlVoltsA,InVoltsA;
```

```
        float GainControlDA,GainControlPA,GainControlIA;

        char  B,BB;
        long  ADvalueB,RefVoltsB,XdemandB,XoldB,ControlB;
        int   highB,lowB;
        float VelocityB,XoffsetB,ControlVoltsB,InVoltsB;
        float GainControlDB,GainControlPB,GainControlIB;

        char  C,CC;
        long  ADvalueC,RefVoltsC,XdemandC,XoldC,ControlC;
        int   highC,lowC;
        float VelocityC,XoffsetC,ControlVoltsC,InVoltsC;
        float GainControlDC,GainControlPC,GainControlIC;

        char  U,UU;
        long  ADvalueU,RefVoltsU,XdemandU,XoldU,ControlU;
        int   highU,lowU;
        float VelocityU,XoffsetU,ControlVoltsU,InVoltsU;
        float GainControlDU,GainControlPU,GainControlIU;

        char  V,VV;
        long  ADvalueV,RefVoltsV,XdemandV,XoldV,ControlV;
        int   highV,lowV;
        float VelocityV,XoffsetV,ControlVoltsV,InVoltsV;
        float GainControlDV,GainControlPV,GainControlIV;

        char W,WW;
        int highW,lowW;
        int ControlW;

        int m,n,j;

        float dda[2000],ddb[2000],ddc[2000],ddu[2000],ddv[2000];
        int o;

        int IntSwitch=0;
        float IntegratorA,IntegratorB,IntegratorC,IntegratorU,IntegratorV;

        char on[11]="Ki on  :-)";
        char off[11]="Ki off :-(";

        FILE *datao;
        FILE *cond;

void keyboard(void);
```

```
int far ipt_proc(void);

main()
{
/* Note order of initializing boards, Pacer before Keithley */

        WORD result;

/* Initialize DT2819 board */

        PA_INITIALIZE(0x230); /* Set Timer Board at base address 230 hex */
        PA_RESET();         /* Set board to start up conditions */
        PA_SETUP_INTERRUPT(INTLEVEL,ipt_proc);  /* User edit routine */
        PA_SET_FOUT(freq3);   /* Set frequence at FOUT pin to freq3 */
                              /* Base f=5M */
                              /* This will be sent to the Counter 3 */
        PA_BUILD_MODE(MODE_D,SOURCE_SRC1,GATE_NONE,MODE_OUTP
UT_LOW_P
ULSE,&mode);
        freq=freq3;
        count=floor(freq*seconds+0.5);
        PA_INITIALIZE_COUNTER(3,mode,count,count);

/* Initialize DAS-1402 board and reads my1402.cfg and returns Number of Boards */
        DAS1600_DevOpen("my1402.cfg",&NumberOfBoards);
        /* Get Device Handle */
        DAS1600_GetDevHandle(0,&DAS1402);

/* Initial values of variables */
        XdemandA=1960;
        XoldA=XdemandA;
        RefVoltsA=2900;       /* Minumum count value to suspend ring at A */
        GainControlPA=360.7;□
        GainControlDA=3.67;
        GainControlIA=3.00;
        AA=0;                 /* Input Channel for MBA A */
        A=5;                  /* Output Channel for MBA A */

        XdemandB=1951;
        XoldB=XdemandB;
        RefVoltsB=2872;       /* Minumum count value to suspend ring at B */
        GainControlPB=360.7;
        GainControlDB=3.47;
        GainControlIB=3.00;
        BB=1;                 /* Input Channel for MBA B */
```

```
        B=4;            /* Output Channel for MBA B */

        XdemandC=2240;
        XoldC=XdemandC;
        RefVoltsC=2861;     /* Minumum count value to suspend ring at C */
        GainControlPC=360.7;
        GainControlDC=2.97;
        GainControlIC=3.00;
        CC=2;            /* Input Channel for MBA C */
        C=3;             /* Output Channel for MBA C */

        XdemandU=2119;
        XoldU=XdemandU;
        RefVoltsU=2507;     /* Minumum count value to suspend ring at U */
        GainControlPU=447.7;
        GainControlDU=4.47;
        GainControlIU=3.00;
        UU=3;            /* Input Channel for MBA U */
        U=2;             /* Output Channel for MBA U */

        XdemandV=1556;
        XoldV=XdemandV;
        RefVoltsV=2373;     /* Minumum count value to suspend ring at V */
        GainControlPV=447.7;
        GainControlDV=4.47;
        GainControlIV=3.00;
        VV=4;            /* Input Channel for MBA V */
        V=1;             /* Output Channel for MBA V */


        ControlW=2848;

        i=0;

/* Print out some notes on the screen before it starts */
        printf("\n\n\n\t\t\tProgram TESTBCD.C \n");
        printf("\t\tAnnular Suspension and Pointing System\n");
        printf("\t\t\tWritten by: Yan Yang\n");
        printf("\t\t\tOld Dominion University\n");
        printf("\t\tDepartment of Aerospace Engineering\n");
        printf("\t\t\t    MAY, 1997\n\n");
        printf("WARNING This program will not run within WINDOWS");
        printf(" only from the DOS command line.\n");
        printf("\tYou must exit WINDOWS before running this program.\n\n\n");
        printf("\tConnect the FOUT pin to Source 1 on the Timer board.\n\n");
```

```
        printf("\t\tFrequence set at FOUT pin %.2f\n",freq3);
        printf("\t\tTime to exicute  control loop is %1.5f Hz.\n\n",1/freq);
        printf("\t\t\tHit any key to continue\n\n");
        printf("\t\tHit > to turn on the integral gain.\n");
        printf("\t\tHit < to turn off the integral gain.\n");
        printf("\t\tThen Hit ESC to end the program.\n");
        getch();



/* Set up screen */
        _clearscreen( _GCLEARSCREEN );
        _setbkcolor(6);
        _settextcolor(10);□

/* Print the table head */
        _settextposition(1,1);
        sprintf(buffer,"NAME");
        _outtext(buffer);

        _settextposition(1,11);
        sprintf(buffer,"INPUT(V)");
        _outtext(buffer);

        _settextposition(1,21);
        sprintf(buffer,"OUTPUT(V)");
        _outtext(buffer);

        _settextposition(1,31);
        sprintf(buffer,"dX(mm)");
        _outtext(buffer);

        _settextposition(1,41);
        sprintf(buffer,"V(mm/sec)");
        _outtext(buffer);

        for(i=4;i<=12;i+=2)
        {
        _settextposition(i,1);
        sprintf(buffer,"%c",name[(i-4)/2]);
        _outtext(buffer);
        }
```

```
        _settextposition(16,1);
        sprintf(buffer,"Name");
        _outtext(buffer);

        _settextposition(16,11);
        sprintf(buffer,"Ref");
        _outtext(buffer);

        _settextposition(16,21);
        sprintf(buffer,"Kp");
        _outtext(buffer);

        _settextposition(16,31);
        sprintf(buffer,"Kd");
        _outtext(buffer);

        _settextposition(16,41);
        sprintf(buffer,"Ki");
        _outtext(buffer);

        for(i=18;i<=22;i+=1)
        {
        _settextposition(i,1);
        sprintf(buffer,"%c",name[i-18]);
        _outtext(buffer);
        }


pg=0;
o=0;

PA_ENABLE_INTERRUPT();
PA_WRITE_COMMAND(armCounters, 0x4);



while(ch != ESC)
{
/*print the table*/
          pg+=1;
          if(pg==10)
            {pg-=10;}

          for(m=0;m<=5;m++)
           {
```

```
for(n=0;n<=3;n++)
  {
   _settextposition(m*2+4,n*10+11);
   sprintf(buffer,"%2.3f",data[pg][m][n]);
   _outtext(buffer);
  }
 }

_settextposition(18,11);
sprintf(buffer,"%d",RefVoltsA);
_outtext(buffer);

_settextposition(18,21);
sprintf(buffer,"%3.3f",GainControlPA);
_outtext(buffer);

_settextposition(18,31);
sprintf(buffer,"%3.3f",GainControlDA);
_outtext(buffer);

_settextposition(18,41);
sprintf(buffer,"%3.3f",GainControlIA);
_outtext(buffer);


_settextposition(19,11);
sprintf(buffer,"%d",RefVoltsB);
_outtext(buffer);

_settextposition(19,21);
sprintf(buffer,"%3.3f",GainControlPB);
_outtext(buffer);

_settextposition(19,31);
sprintf(buffer,"%3.3f",GainControlDB);
_outtext(buffer);

_settextposition(19,41);
sprintf(buffer,"%3.3f",GainControlIB);
_outtext(buffer);


_settextposition(20,11);
sprintf(buffer,"%d",RefVoltsC);
_outtext(buffer);
```

```
_settextposition(20,21);
sprintf(buffer,"%3.3f",GainControlPC);
_outtext(buffer);

_settextposition(20,31);
sprintf(buffer,"%3.3f",GainControlDC);
_outtext(buffer);

_settextposition(20,41);
sprintf(buffer,"%3.3f",GainControlIC);
_outtext(buffer);


_settextposition(21,11);
sprintf(buffer,"%d",RefVoltsU);
_outtext(buffer);

_settextposition(21,21);
sprintf(buffer,"%3.3f",GainControlPU);
_outtext(buffer);

_settextposition(21,31);
sprintf(buffer,"%3.3f",GainControlDU);
_outtext(buffer);

_settextposition(21,41);
sprintf(buffer,"%3.3f",GainControlIU);
_outtext(buffer);


_settextposition(22,11);
sprintf(buffer,"%d",RefVoltsV);
_outtext(buffer);

_settextposition(22,21);
sprintf(buffer,"%3.3f",GainControlPV);
_outtext(buffer);

_settextposition(22,31);
sprintf(buffer,"%3.3f",GainControlDV);
_outtext(buffer);

_settextposition(22,41);
sprintf(buffer,"%3.3f",GainControlIV);
```

```
        _outtext(buffer);

        _settextposition(30,21);  /* Show integral status */
        if(IntSwitch==1)
        {
        sprintf(buffer,"%s", on);
        _outtext(buffer);
        }
        else
        {
        sprintf(buffer,"%s", off);
        _outtext(buffer);
        }


/* See if get some information from user */
        keyboard();
}
/* At this point the program returns to the top of the loop
        unless the ESC key has been hit.                    */


fclose(cond);
PA_TERMINATE_INTERRUPT();
PA_RESET();
_setvideomode(_DEFAULTMODE);


for(i=0;i<=5;++i)       /* Writes a zero volt command to all amplifiers */
        {               /* to put the amplifies in a no output state.  */
        high=(2047/256);
        low=2047-high*256;
        outp(base+2*i,low);
        outp(base+1+2*i,high);
        }

/* Final report of all the data */
if((datao=fopen("c:\\qc25\\asps\\dataout.asc","w+"))!=NULL)
 {
 for(i=0;i<=9;++i)
  {
  fprintf(datao,"Name\tInV(v)\t\tOutV(v)\t\tX(mm)\t\tV(mm/s)\n");
  for(j=0;j<=4;++j)
   {
```

```
fprintf(datao,"%c\t%2.3f\t\t%2.3f\t\t%2.3f\t\t%2.3f\n",name[j],data[i][j][0],data[i][j][1],d
ata[i][j][2],da
ta[i][j][3]);
  }
 fprintf(datao,"\n\n");
 fprintf(datao,"Name\tRefV(v)\t\tKd\t\tKp\t\tKi\n");
 fprintf(datao,"A\t%d\t\t",RefVoltsA);
 fprintf(datao,"%3.3f\t\t",GainControlPA);
 fprintf(datao,"%3.3f\t\t",GainControlDA);
 fprintf(datao,"%3.3f\n",GainControlIA);
 fprintf(datao,"B\t%d\t\t",RefVoltsB);
 fprintf(datao,"%3.3f\t\t",GainControlPB);
 fprintf(datao,"%3.3f\t\t",GainControlDB);
 fprintf(datao,"%3.3f\n",GainControlIB);
 fprintf(datao,"C\t%d\t\t",RefVoltsC);
 fprintf(datao,"%3.3f\t\t",GainControlPC);
 fprintf(datao,"%3.3f\t\t",GainControlDC);
 fprintf(datao,"%3.3f\n",GainControlIC);
 fprintf(datao,"U\t%d\t\t",RefVoltsU);
 fprintf(datao,"%3.3f\t\t",GainControlPU);
 fprintf(datao,"%3.3f\t\t",GainControlDU);
 fprintf(datao,"%3.3f\n",GainControlIU);
 fprintf(datao,"V\t%d\t\t",RefVoltsV);
 fprintf(datao,"%3.3f\t\t",GainControlPV);
 fprintf(datao,"%3.3f\t\t",GainControlDV);
 fprintf(datao,"%3.3f\n\n",GainControlIV);

 }
fclose(datao);
}
else
{
printf("Error:Couldn't create file.\n");
}

/* NOISE.ASC is the first 10 secs record of the system postion error */
cond=fopen("c:\\qc25\\asps\\noise.asc","w+");
for(o=0;o<1999;o++)
   fprintf(cond,"%3.3f %3.3f %3.3f %3.3f %3.3f\n",dda[o],ddb[o],ddc[o],ddu[o],ddv[o]);
fclose(cond);
}
/* end of the main*/


/************** Keyboard subroutine ***************************/
```

```
void keyboard(void)
{
    if(kbhit() !=0)
    {
    chin=getch();

                switch(chin)
                {
                case ESC:ch=ESC;
                        break;


                case'q':case'Q':RefVoltsA=RefVoltsA+1;
                        break;
                case'w':case'W':RefVoltsA=RefVoltsA-1;
                        break;
                case'e':case'E':GainControlPA=GainControlPA+1;
                        break;
                case'r':case'R':GainControlPA=GainControlPA-1;
                        break;
                case't':case'T':GainControlDA=GainControlDA+0.1;
                        break;
                case'y':case'Y':GainControlDA=GainControlDA-0.1;
                        break;

                case'a':case'A':RefVoltsB=RefVoltsB+1;
                        break;
                case's':case'S':RefVoltsB=RefVoltsB-1;
                        break;
                case'd':case'D':GainControlPB=GainControlPB+1;
                        break;
                case'f':case'F':GainControlPB=GainControlPB-1;
                        break;
                case'g':case'G':GainControlDB=GainControlDB+0.1;
                        break;
                case'h':case'H':GainControlDB=GainControlDB-0.1;
                        break;

                case'z':case'Z':RefVoltsC=RefVoltsC+1;
                        break;
                case'x':case'X':RefVoltsC=RefVoltsC-1;
                        break;
                case'c':case'C':GainControlPC=GainControlPC+1;
                        break;
                case'v':case'V':GainControlPC=GainControlPC-1;
```

```
        break;
case'b':case'B':GainControlDC=GainControlDC+0.1;
        break;
case'n':case'N':GainControlDC=GainControlDC-0.1;
        break;

case'1':case'!':RefVoltsU=RefVoltsU+1;
        break;
case'2':case'@':RefVoltsU=RefVoltsU-1;
        break;
case'3':case'#':GainControlPU=GainControlPU+1;
        break;
case'4':case'$':GainControlPU=GainControlPU-1;
        break;
case'5':case'%':GainControlDU=GainControlDU+0.1;
        break;
case'6':case'^':GainControlDU=GainControlDU-0.1;
        break;

case'=':case'+':RefVoltsV=RefVoltsV+1;
        break;
case'-':case'_':RefVoltsV=RefVoltsV-1;
        break;
case'0':case')':GainControlPV=GainControlPV+1;
        break;
case'9':case'(':GainControlPV=GainControlPV-1;
        break;
case'8':case'*':GainControlDV=GainControlDV+0.1;
        break;
case'7':case'&':GainControlDV=GainControlDV-0.1;
        break;

case']':case'}':GainControlIA=GainControlIA+0.1;
        break;
case'[':case'{':GainControlIA=GainControlIA-0.1;
        break;
case'p':case'P':GainControlIB=GainControlIB+0.1;
        break;
case'o':case'O':GainControlIB=GainControlIB-0.1;
        break;
case'i':case'I':GainControlIC=GainControlIC+0.1;
        break;
case'u':case'U':GainControlIC=GainControlIC-0.1;
        break;
case';':case':':GainControlIU=GainControlIU+0.1;
```

```
                    break;
                case'l':case'L':GainControlIU=GainControlIU-0.1;
                    break;
                case'k':case'K':GainControlIV=GainControlIV+0.1;
                    break;
                case'j':case'J':GainControlIV=GainControlIV-0.1;
                    break;

                case'>':case'.':IntSwitch=1;
                    break;
                case'<':case',':IntSwitch=0;
                    break;


                }
        }
}




/***************** Interrupt routine ***********************************/
int far ipt_proc(void)
{
PA_CLEAR_INTERRUPT();
PA_DISABLE_INTERRUPT();

/* Read the sensor signal: A-D */
        K_ADRead(DAS1402,AA,2,&ADvalueA);
        K_ADRead(DAS1402,BB,2,&ADvalueB);
        K_ADRead(DAS1402,CC,2,&ADvalueC);
        K_ADRead(DAS1402,UU,2,&ADvalueU);
        K_ADRead(DAS1402,VV,2,&ADvalueV);

/* Transfer input counts to the voltage value */
        data[pg][0][0]=((ADvalueA>>4)-2047)*20/4096.0;    /*InVoltsA*/
        data[pg][1][0]=((ADvalueB>>4)-2047)*20/4096.0;    /*InVoltsB*/
        data[pg][2][0]=((ADvalueC>>4)-2047)*20/4096.0;    /*InVoltsC*/
        data[pg][3][0]=((ADvalueU>>4)-2047)*20/4096.0;    /*InVoltsU*/
        data[pg][4][0]=((ADvalueV>>4)-2047)*20/4096.0;    /*InVoltsV*/

/* Calculate the displacement, velocity and control values */
        data[pg][0][2]=((ADvalueA>>4)-XdemandA)*.00284;  /* XoffsetA in mm */
```

```
        data[pg][0][3]=(((ADvalueA>>4)-XoldA)*.00284)/(count/freq); /* VelocityA in
mm/sec */
        IntegratorA=IntSwitch*GainControlIA*data[pg][0][2]*(count/freq)+IntegratorA;

ControlA=(GainControlPA*data[pg][0][2]+GainControlDA*data[pg][0][3]+IntegratorA
+RefVoltsA);
/*in counts */

        data[pg][1][2]=((ADvalueB>>4)-XdemandB)*.00308;
        data[pg][1][3]=(((ADvalueB>>4)-XoldB)*.00308)/(count/freq);
        IntegratorB=IntSwitch*GainControlIB*data[pg][1][2]*(count/freq)+IntegratorB;

ControlB=(GainControlPB*data[pg][1][2]+GainControlDB*data[pg][1][3]+IntegratorB+
RefVoltsB);

        data[pg][2][2]=((ADvalueC>>4)-XdemandC)*.00419;
        data[pg][2][3]=(((ADvalueC>>4)-XoldC)*.00419)/(count/freq);
        IntegratorC=IntSwitch*GainControlIC*data[pg][2][2]*(count/freq)+IntegratorC;

ControlC=(GainControlPC*data[pg][2][2]+GainControlDC*data[pg][2][3]+IntegratorC+
RefVoltsC);

        data[pg][3][2]=((ADvalueU>>4)-XdemandU)*.00115;
        data[pg][3][3]=(((ADvalueU>>4)-XoldU)*.00115)/(count/freq);
        IntegratorU=IntSwitch*GainControlIU*data[pg][3][2]*(count/freq)+IntegratorU;

ControlU=(GainControlPU*data[pg][3][2]+GainControlDU*data[pg][3][3]+IntegratorU
+RefVoltsU);

        data[pg][4][2]=((ADvalueV>>4)-XdemandV)*.00111;
        data[pg][4][3]=(((ADvalueV>>4)-XoldV)*.00111)/(count/freq);
        IntegratorV=IntSwitch*GainControlIV*data[pg][4][2]*(count/freq)+IntegratorV;

ControlV=(GainControlPV*data[pg][4][2]+GainControlDV*data[pg][4][3]+IntegratorV
+RefVoltsV);


if(o<=1999)
{
dda[o]=data[pg][0][2];
ddb[o]=data[pg][1][2];
ddc[o]=data[pg][2][2];
ddu[o]=data[pg][3][2];
ddv[o]=data[pg][4][2];
o=o+1;
```

```
}
else
{
dda[1999]=data[pg][0][2];
ddb[1999]=data[pg][1][2];
ddc[1999]=data[pg][2][2];
ddu[1999]=data[pg][3][2];
ddv[1999]=data[pg][4][2];
}


/*Convert the output counts to the volts */
        data[pg][0][1]=(ControlA-2047)*5/4096.0;
        data[pg][1][1]=(ControlB-2047)*5/4096.0;
        data[pg][2][1]=(ControlC-2047)*5/4096.0;
        data[pg][3][1]=(ControlU-2047)*5/4096.0;
        data[pg][4][1]=(ControlV-2047)*5/4096.0;

/* Write the output to the amplify: D-A */
        highA=(ControlA/256);
        lowA=ControlA-high*256;
        outp(base+2*A,lowA);     /* Writes control output to Amplifier A*/
        outp(base+1+2*A,highA);  /* Using DDA-06 D/A Data acquisition Board*/
        XoldA=ADvalueA>>4;       /* saves old distance for velocity */


        highB=(ControlB/256);    /* same as above */
        lowB=ControlB-highB*256;
        outp(base+2*B,lowB);
        outp(base+1+2*B,highB);
        XoldB=ADvalueB>>4;

        highC=(ControlC/256);
        lowC=ControlC-highC*256;
        outp(base+2*C,lowC);
        outp(base+1+2*C,highC);
        XoldC=ADvalueC>>4;

        highU=(ControlU/256);
        lowU=ControlU-highU*256;
        outp(base+2*U,lowU);
        outp(base+1+2*U,highU);
        XoldU=ADvalueU>>4;

        highV=(ControlV/256);
```

```
        lowV=ControlV-highV*256;
        outp(base+2*V,lowV);
        outp(base+1+2*V,highV);
        XoldV=ADvalueV>>4;

        highW=(ControlW/256);
        lowW=ControlW-highW*256;
        outp(base+2*W,lowW);
        outp(base+1+2*W,highW);□


PA_ENABLE_INTERRUPT();
return(0);
}
```

VITA

Yan Yang received her elementary and secondary education in Nanjing, P.R. China, graduating from Nanjing Jinling High School in 1990. She attended Nanjing University of Aeronautics and Astronautics and received her Bachelor of Science Degree in Testing and Measurement Engineering in 1994. After working at Nanjing International Airport for one year, she came to the United States to pursue a Master of Science degree. She has been involved in various projects related the magnetic suspension research program at Old Dominion University during her two year stay.